

NRL Report 6221

Diffusion in Columbium Rich Columbium-Titanium Alloys with Consideration of the Possibility that the Diffusion Coefficient is Time Dependent

T. C. REUTHER, JR.

High Temperature Alloys Branch

Metallurgy Division

December 14, 1964



U.S. NAVAL RESEARCH LABORATORY
Washington, D.C.

Copies available from Office of Technical Services
Department of Commerce, Washington, D.C. 20230 - \$3.00

CONFIDENTIAL

ABSTRACT

Interdiffusion has been studied in Cb vs. Cb 8.5 atom percent Ti and Cb vs. Cb 35 a/o Ti couples at temperatures of 1300° to 2000°C and for times of 0.1 to 1000 hours. The electron microprobe has been used to obtain the penetration curves.

Marker displacement toward and the development of porosity within the alloy at 1800° and 2000°C demonstrate that a vacancy mechanism is operative in this b.c.c. alloy system. Porosity was also observed at 1500°C. At 1500°C for anneal times extending from 10 to 1000 hours for the more dilute alloy and from 10 to 120 hours for the 35 a/o Ti alloy, the interdiffusion coefficient D computed by the Boltzmann-Matano analysis is determined to be independent of time.

The Arrhenius plot for results extrapolated to 100 a/o Cb is a straight line and yields an activation energy of 110 k cal/g-atom. However, as composition is increased to 30 a/o Ti, an increase in the concentration dependence of D is observed with decreasing temperature. This is manifest by curvature of the $\log D$ vs. $\frac{1}{T}$ plots with increasing titanium content.

PROBLEM STATUS

This report completes one phase of the problem; work on other aspects of the problem is continuing.

AUTHORIZATION

NRL Problem M01-09
Project RR 007-01-46-5407

This Naval Research Laboratory Report was submitted to the faculty of the School of Engineering and Architecture of the Catholic University of America in partial fulfillment of the requirements for the degree of Doctor of Engineering.

ACKNOWLEDGEMENT

The author wishes to acknowledge the guidance and support given by Dr. E. P. Klier, Research Professor of Metallurgy at the Catholic University of America and by Dr. M. R. Achter, Head, High Temperature Alloys Branch, in their roles as dissertation adviser and supervisor, respectively.

The electron microprobe analyses were performed by Mr. E. J. Brooks of the Analytical Chemistry Branch, Metallurgy Division, and the instrument of the Electron Optics Branch, Optics Division, was used. Acknowledgement is gratefully made to those support personnel in the Metallurgy Division and in the general support organizations of NRL who aided in this research. Particular thanks are due Mr. A. R. Donaldson for metallographic preparation of the diffusion couples; to Mr. W. A. Fraser for gas analysis; and to Mr. Owen R. Gates and Mr. Brooks for analysis of microprobe standards.

TABLE OF CONTENTS

	Page
ABSTRACT	ii
ACKNOWLEDGEMENTS	iii
Chapter 1 INTRODUCTION	1
1.1 The Diffusion Equations	1
1.2 Critical Examination of the Diffusion Equations	3
1.3 Objectives and Design of the Problem	7
1.3.1 Time Dependency of D	7
1.3.2 Diffusion in b.c.c. Alloys	8
1.4 Selection of Alloy System	9
1.5 Experimental Plan	10
1.6 Solutions to the Diffusion Equations	11
1.6.1 Boltzmann-Matano Solution	12
1.6.2 Grube Solution	13
Chapter 2 EXPERIMENTAL	14
2.1 Materials	14
2.2 Welding of Diffusion Couples	16
2.3 Marker Measurements, As Welded	19
2.4 Diffusion Anneals, Equipment	19
2.4.1 1000° and 1300°C Anneals > 1 Hr.	20
2.4.2 1500° 1800° and 2000°C Anneals > 1 Hr.	21
2.4.3 1300° and 1500°C Anneals for 0.1 Hr.	22
2.5 Diffusion Anneals, Procedure	23
2.6 Final Marker Measurements	24
2.7 Microprobe Procedure	25
2.7.1 Preparation	25
2.7.2 Standards	26
2.7.3 Microprobe Operation	27
Chapter 3 RESULTS	29
3.1 Marker Data	29
3.2 Concentration - Penetration Data	33
3.3 Results of the Grube Analysis	36
3.4 Results of the Boltzmann-Matano Analysis	39

	Page
3.5 Activation Energy and Frequency Factor	45
Chapter 4 DISCUSSION	47
4.1 Marker Measurements	47
4.2 Limits on the Penetration Data	47
4.2.1 Short-time limits; the microprobe	47
4.2.2 Long-time limits; contamination	49
4.3 Time Dependence of D	50
4.4 Concentration Dependence of D	51
4.5 Curvature of the Arrhenius Plot	52
Chapter 5 SUMMARY AND CONCLUSIONS	55
ILLUSTRATIONS TO MAIN TEXT	57
Appendix 1 DEVELOPMENT OF THE DIFFUSION EQUATIONS AND THE REQUIRED SOLUTIONS	89
A.1-1 Fick's Laws	89
A.1-2 Grube Solution	91
A.1-3 Boltzmann-Matano Solution	94
Appendix 2 EXPERIMENTAL DATA	97
A.2-1 C/Co versus Distance, Probability Plots	97
A.2-2 Concentration vs Distance, Linear Plots	99
Appendix 3 SAMPLE CALCULATIONS	148
A.3-1 Grube Solution	148
A.3-2 Boltzmann-Matano Method	150
A.3-3 Effective Penetration During Welding	152
Appendix 4 CONTAMINATION PROBLEM	153
A.4-1 Source of Contamination	154
A.4-2 Identity of Precipitate	155
LIST OF REFERENCES	161

LIST OF TABLES

<u>Table</u>	<u>Subject</u>	<u>Page</u>
1	Anneal Schedule	10
2	Analysis of Materials, As Received	15
3	Marker Data	30
4	Example of Penetration Data	34
5	Results of Grube Analysis as 'Dt' and 'D'	36
6	Results of Matano Analysis 'D' vs. 'C' at 1300°, 1500°, 1800° and 2000°C.	40
7	Diffusion Coefficient vs. Temperature at 0, 10, 20 and 30 a/o Ti.	44
8	Activation Energy and Frequency Factor	46
9	Hardness of Alloy after Diffusion Anneal	50

LIST OF FIGURES*

<u>Figure</u>	<u>Subject</u>	<u>Page</u>
1	Arrangement for welding diffusion couples.	57
2	Photomicrograph of as-welded diffusion couple showing marker material, X50.	58
3	Photomicrograph of as-welded diffusion couple showing marker material, X250.	59
4	Sketch indicating initial marker measurement face.	60
5	Arrangement for induction heating for 0.1-hour diffusion anneals.	61
6	Reproduction of temperature record, 0.1-hour anneal.	62
7	Macro-photo of mounted and polished pair of couples along with standards ready for insertion into electron microprobe. X5.	63
8	Sketch showing the sectioning of a diffusion couple for microprobe analysis.	64
9	Arrangement of specimen in microprobe.	65
10	Photomicrograph of voids in the diffusion zone of a Cb-Cb.35 a/o Ti couple after 10 hours at 2000°C. X200.	66
11	Photomicrograph showing voids adjacent to marker material. Cb-Cb 35 a/o Ti couple after 1000 hours at 1500°C. X200.	67
12	Example of calibration curve. #33, 35 a/o Ti, 1500°C, 10 hours.	68

* The figures relating to the main text are grouped together beginning on page 57.

	FIGURES (Continued)	<u>Page</u>
13(a)	Probability plot for Grube solution, C/C ₀ (probability scale) vs. distance (linear). [Example, see Appendix 2, for complete plots.]	69
(b)	Concentration (linear) vs. distance (linear) for Boltzmann-Matano solution. [Example, see Appendix 2 for complete plots.]	70
14(a)	Photomicrograph of contamination trace from microprobe. [Cb-Cb 35 a/o Ti, 1500°C, 10 hours] X100.	71
(b)	Photomicrograph of contamination trace from microprobe. [Cb-Cb 35 a/o Ti, 1500°C, 10 hours] X500.	72
15(a)	Photomicrograph of contamination trace from microprobe. [Cb-Cb 8.5 a/o Ti, 1500°C, 120 hours] X100.	73
(b)	Photomicrograph of contamination trace from microprobe. [Cb-Cb 8.5 a/o Ti, 1500°C, 120 hours] X500.	74
16	Diffusion coefficient, D vs. composition, 1300°C.	75
17	Diffusion coefficient, D vs. composition, 1500°C.	76
18	Diffusion coefficient, D vs. composition, 1800°C.	77
19	Diffusion coefficient, D vs. composition, 2000°C.	78
20	Arrhenius plot, log D vs. $\frac{1}{T}$, 0 a/o Ti.	79
21	Arrhenius plot, log D vs. $\frac{1}{T}$, 10 a/o Ti.	80

FIGURES (Continued)		<u>Page</u>
22	Arrhenius plot, log D vs. $\frac{1}{T}$, 20 a/o Ti.	81
23	Arrhenius plot, log D vs. $\frac{1}{T}$, 30 a/o Ti.	82
24	Arrhenius plot, log D vs. $\frac{1}{T}$ for Fig. 20 to 23, superimposed.	83
25	Hypothetical specimen profile.	84
26(a)	Photomicrograph of alloy section of Cb/Cb 35 a/o Ti/Cb diffusion couple [1500°C, 100 hours] Widmanstätten "hydride" precipitates. X20.	85
(b)	Photomicrograph of alloy section of Cb/Cb 35 a/o Ti/Cb diffusion couple [1500°C, 1000 hours] Widmanstätten "hydride" precipitates. X100.	86
27(a)	Arrhenius plot, log D vs. $\frac{1}{T}$ for results of Grube solution, Cb/Cb 35 a/o Ti couples.	87
(b)	Arrhenius plot, log D vs. $\frac{1}{T}$ for results of Grube solution, Cb/Cb 8.5 a/o Ti couples.	88

Chapter 1

INTRODUCTION

1.1 The Diffusion Equations

The differential equations which describe the diffusion process in an isotropic medium due to the random molecular motion within the medium are based upon the concept of Adolph Fick (1) that the flux is proportional to the gradient of the concentration. Using vector notation these differential equations may be written as follows:

For steady state conditions this is

$$\vec{F} = -D\nabla C \quad [1]$$

where \vec{F} is the flux per unit

area per unit time ($\text{g/cm}^2/\text{sec}$)

C is the concentration (g/cm^3)

and D is the constant of proportionality (cm^2/sec).

For non-steady conditions the rate of accumulation at any point will be given by the divergence of the flux at that point,

$$\frac{\partial C}{\partial t} = \nabla \cdot (D\nabla C) \quad [2]$$

For diffusion in one dimension which is the condition usually applied to experimental investigations,

UNCLASSIFIED

Equations [1] and [2] reduce to

$$F = -D \frac{\partial C}{\partial x} \quad [3]$$

and to
$$\frac{\partial C}{\partial t} = \frac{\partial}{\partial x} \left(D \frac{\partial C}{\partial x} \right). \quad [4]$$

The gradient in all cases is taken along the diffusion path.

If the condition obtains that D is constant, Equation [2] and Equation [4] become

$$\frac{\partial C}{\partial t} = D \nabla^2 C \quad [5]$$

and

$$\frac{\partial C}{\partial t} = D \frac{\partial^2 C}{\partial x^2}. \quad [6]$$

The relationships [1] and [3] are called Fick's First Law and [2], [4], [5] and [6] are called Fick's Second Law. If strict historical credit is observed only Equations [1], [3], [5] and [6] would be so named, for Fick took D to be constant. However, it is common practice also to name the more general forms, Equation [2] and Equation [4] after him. This usage is followed in this dissertation.

Many authors have published the development of these equations and selected solutions to them. The most complete and very useful mathematical treatment is that of Crank (2). A readily available and tersely

written one is that of Darken (3). A development which generally follows Crank is presented in Appendix I.

In the general form of Fick's second law, Equation [4], the diffusion coefficient, D, is taken implicitly to be a function of only the variables of state: temperature, pressure (stress) and composition. It is assumed to be independent of the concentration gradient, or for the infinite and semi-infinite boundary conditions which are defined by Equation [7], p. 11, independent of time.

In applying this differential equation to diffusion in metal systems at a given temperature, the diffusion coefficient has universally been taken as a single valued function of composition. For this reason, metallurgists have in general taken the relationship

$$\frac{\partial C}{\partial t} = \frac{\partial}{\partial x} \left(D(C) \frac{\partial C}{\partial x} \right)$$

to be inviolate.

1.2 Critical Examination of Equations [2] and [4]

While critically examining the limitations on Fick's law, Darken, in a "Formal Basis for Diffusion

Theory", (3) brought to the attention of the metallurgical world the observation of Hartley (4) which was probably the first reported failure of the general form of Fick's law, Equations [2] and [4], for diffusion in a binary system. Hartley, in studying diffusion of organic solvents into a polymer (cellulose acetate) observed "Not only is D not constant, ... but it is no longer a single valued function of C . D depends not only on C , but also on the history of the particular diffusion process." Hartley attributed this effect to swelling which took place during the diffusion processes leading to anisotropy. Darken (3) continued "Although the small size and approximate spherical symmetry of the atoms in metals might predispose us to think we are unlikely to encounter related phenomena here, I doubt that we should feel too certain If the diffusion process itself creates lattice imperfections then we may anticipate a failure of Fick's law analogous to that found by Hartley -- that is D will no longer be a single valued function of composition."

In the published metallurgical literature one such example was noted in 1957. Reynolds, Averbach and Cohen (5) in their exhaustive study of self-diffusion and interdiffusion in the gold-nickel system report an effect of the time of anneal on the diffusion

coefficient at the nickel rich end of pure-metal couples as measured by the Boltzmann-Matano (6) method. They observed (i) a greater D in pure-metal couples at a given composition as compared to incremental couples after a 25 hour anneal, and (ii) an even further enhancement after a shorter (11 hour) diffusion anneal. Corrections made for the effects of volume change and porosity were minor. Reynolds et al. suggest that the steep concentration gradients in the pure-metal couples and the correspondingly large initial differences in molar volume in the diffusion zone may produce non-steady structural effects in the shorter diffusion anneals. They further suggest that such conditions could probably lead to the generation of excess vacancies or short circuiting paths, thus to enhanced diffusion. Aside from this observation which Reynolds et al. considered as a spurious situation to be alleviated, no further observations on a time dependency of D have been reported until just recently.

In work reported to the AIME New York meeting, February 19, 1964, but not yet published, Hartley and Steedly (7,8) observed an effect similar to that of Reynolds et al. They made diffusion measurements on Cu vs. Pt and Cu vs. Pt60 atom percent (a/o) Cu.

diffusion couples over the temperature range 794° to 1021°C. They used the electron microprobe for analysis and applied the Boltzmann-Matano analysis to the concentration penetration data. At 1021°C they observed an increase in D of about two times in going from an annealing time of 64 hours to 15 hours. Their explanation of the observation (if, they point out, it be true) follows that of Reynolds et al.

Even more recently Woodbury (9) in reporting on the diffusion of cadmium in cadmium sulfide noted in a footnote "...since the experimentally calculated diffusion rate depends strongly on the firing time" (diffusion anneal time???)... "the time dependence of Fick's law does not hold." No further explanation or discussion is contained in the paper.

From these observations, prophetically noted by Darken, it is evident that for diffusion in binary metal systems Fick's law in its general case, as usually applied, is not necessarily inviolate. Actually it is not the law (or differential equation) which does not hold, but rather it is the boundary condition that D is single valued that does not hold. For diffusion in a solid metal no rigorous experimental test has been made of the assumption that D is independent of the concentration gradient which in effect means for the semi-infinite

and infinite boundary conditions, the time of diffusion. And except for the three observations noted above-- two of which are at best, cursory -- no exceptions have been noted. This is not too surprising for the time of the diffusion anneal at a given temperature is usually selected in accord with the smallest zone which can be accurately analyzed on one hand, and by reasonable allocation of furnace time on the other. In substitutional diffusion the time span selected for annealing seldom has been changed by more than a factor of ten. Thus experimental conditions have seldom been favorable for the observation of a time dependency, if indeed it exists.

1.3 Objectives and Design of the Problem

1.3.1 Time Dependency of D

The present work was undertaken to examine experimentally in a rigorous manner the question of a time dependency of the diffusion coefficient, D, in a substitutional alloy metal system. Limits on the available range of annealing times may conveniently be extended to four orders of magnitude if the electron microprobe is used for analysis: For a semi-infinite slab with a diffusivity of $10^{-9} \text{ cm}^2/\text{sec}$, an initial

concentration of 5% and an analytical end point of 0.5%, a penetration distance of 10 microns would require about two minutes. At the other extreme, an anneal of say 30 days would give a time variation of 10^4 . For this broad range of time intervals, a time dependent diffusion coefficient may be observable.

1.3.1 Diffusion in b.c.c. Alloys

A controversy exists concerning the mechanism of diffusion in some b.e.e. alloy systems (12), and while it is not the prime objective of this investigation, diffusion data on an additional b.c.c. alloy system may help to clarify the present controversy. The inclusion of markers in the diffusion couples of the present investigation might contribute to this discussion for a Kirkendall shift is positive evidence that the diffusion process follows a vacancy mechanism (13). While the converse is not true, it is felt that additional marker data on a b.c.c. system would be of value. Activation energy (Q) and frequency factor (D_0) determinations might also contribute to this question.

1.4 Selection of Alloy System

The columbium-titanium alloy system was selected for several reasons:

(a) At the time of the initiation of the problem no diffusion data were available for it, and alloys of the system were of potential technological interest.

(b) The x-ray spectra of titanium and columbium are mutually amenable to resolution in the microprobe.

(c) The alloy system is represented by a continuous b.c.c. solid solution above the transformation temperature (885°C) of titanium, and this b.c.c. structure is continuous to below room temperature in alloys >50 w/o columbium (10,11). This voids any question of precipitation during cooling which might adversely affect probe analysis.

Based on these considerations alloys of Cb 8.5 a/o Ti and Cb 35 a/o Ti were selected. The more dilute alloy was chosen because it was felt that for a limited concentration range D might be independent of concentration and therefore consideration of concentration effects might be eliminated from part of the data. The 35% alloy was chosen for marker measurement and to extend activation energy and frequency factor data further into the alloy system.

1.5 Experimental Plan

Briefly, the experimental program is as follows: Experiments are performed with three layer sandwich couples of the type Cb/Alloy/Cb which satisfy the infinite boundary conditions of Fick's law. The alloys and pure columbium are first stabilized against structural change by annealing at a temperature in excess of the highest diffusion anneal temperature prior to welding. The diffusion anneal schedule is given in Table 1.

Table 1

The Compositions of Diffusion Couples
and the Temperature and Time of the Anneals

Temp (°C)	Alloy Ti, (a/o)	Time (hr.)	Purpose
1000	35	120	Q, D ₀
1300	8.5	.1, 1.0, 10, 120, 480, 1000	D = f (t) ?
	35	120	Q, D ₀
1500	8.5	.1, 1.0, 10, 120, 480, 1000	D = f (c, t) ?
	35		Q, D ₀
1800	35	10	Q, D ₀
2000	35	10	Q, D ₀

Thus the question of D as a function of time is examined at two temperatures and two compositions at

one temperature for times ranging from 0.1 hour to 1000 hours. Anneals for the purpose of determining activation energy and frequency factor extend from 1000° to 2000°C.

Concentration-penetration contours are measured by the electron microprobe and are analyzed by the Boltzmann-Matano method or by that of Grube, as applicable. Granular thoria is used for markers and marker measurements are made from interface to interface in the three-layer sandwich couples.

1.6 Solutions to the Diffusion Equations*

The experiments in this investigation are designed for the infinite boundary conditions of the diffusion equation. These conditions are

$$\begin{aligned} t = 0, x < 0, C &= 0 \text{ (100\% Cb)} \\ t = 0, x < 0, C &= C_0 \text{ (Alloy)} \\ \text{all } t, x = \pm\infty, \frac{\partial C}{\partial x} &= 0 \end{aligned} \quad [7]$$

* Only the boundary conditions and the final solutions are given here. A development of these may be found in Appendix I.

1.6.1 Boltzmann-Matano Solution

For the general problem in one dimension where D is a function of composition only, Equation [4], the Boltzmann-Matano solution applies. This is

$$D_{C_1} = -\frac{1}{2t} \left. \frac{dx}{dC} \right|_{C_1} \cdot \int_{C_0}^{C_1} x dC \quad [8]$$

where $D(C_1)$ is the diffusion coefficient at some composition C_1 . The slope of the concentration penetration curve $\frac{dx}{dC}$ is evaluated at C_1 and the integral is evaluated to C_1 . The time of diffusion is t .

Matano (6) showed that to apply Equation [8], the origin of the distance ordinate must be selected so that

$$\int_0^{C_0} x dC = 0.$$

This is equivalent to

$$\int_{C(x=-\infty)}^{C(x=0)} x dC = \int_{C(x=0)}^{C(x=\infty)} x dC \quad [9]$$

Expression [9] defines the so-called "Matano Interface" (see Appendix 1)

1.6.2 Grube Solutions

If D is not a function of concentration, the solution to the diffusion equation, Equation [6], of Grube (14) may be used:

$$C(x,t) = \frac{C_0}{2} \left(1 - \operatorname{erf} \frac{x}{2\sqrt{Dt}} \right) = \frac{C_0}{2} \operatorname{erfc} \frac{x}{2\sqrt{Dt}} \quad [10]$$

Johnson (15) pointed out that if this solution holds (as it does if D is constant with composition) a plot of $C(x)/C_0$ vs. x on probability paper will plot as a straight line. He also pointed out that such a plot is a convenient measure of whether D is or is not a function of composition. Data in this study are thus examined first by the Grube solution in the manner of Johnson and if this fails, then by the method of Matano (6) using the Boltzmann solution to Equation [4].

Chapter 2

EXPERIMENTAL

2.1 Materials

The alloys and columbium were obtained from The Stauffer Chemical Company. The columbium was in the form of an electron-beam melted ingot, two inches in diameter. This was hammered and swaged to 1/2 inch diameter rod. The alloys were produced by alloying electron-beam melted columbium with high purity titanium by double arc melting. The alloys were forged into rod form by the supplier. Unfortunately this was done hot (1500 - 2100°F) and in air. Contamination by oxygen and nitrogen is evident in the analysis given in Table 2.

The alloys, after a recrystallization anneal were found to be two phase. A vacuum anneal at 1900°C removed the precipitate phase; however, during diffusion anneals at 1300° and 1500°C in the presence of alumina, it reformed. This was resolved by performing all 1500°C and higher anneals in an all metal furnace and by wrapping the specimen in columbium foil. At 1300°C in the first furnace, wrapping prevented

Table 2
Supplier's Material Analysis,
As Received

Element	Electron Beam Melted Columbium (ppm)	Columbium- 8.5a/oTitanium (ppm)	Columbium- 35a/oTitanium (ppm)
C	19	47	62
Fe	< 20	< 20	< 20
H			
Mo	< 50	< 50	50
N	40	57	65
O	60	130	453
Ta	150	< 150	< 150
Ti	< 20	4.3 w/o	21.1 w/o
W	<150	<150	< 150
Zr	< 20	< 20	< 20

All other metallic impurities were reported as < 50 ppm.

formation of the precipitate in all but the 1000 hour anneal. The precipitate was identified as a ternary oxide very rich in titanium, probably of the form $Ti(Cb)_0$. Details of the resolution of this contamination problem are included in Appendix 4.

2.2 Welding of Diffusion Couples

The as-received rods were annealed in a vacuum of 10^{-5} torr at 1900°C by passing them through a 1 1/2-inch long induction coil at a rate of 1.5-inch per hour. This gave a net time at temperature of about one hour. The resultant grain size was the order of one millimeter for the alloys and several millimeters and occasionally as much as one centimeter for the columbium.

Vacuum fusion and Kjeldahl analysis gave

<u>Material</u>	<u>Oxygen</u>	<u>Nitrogen</u>
8.5 a/o Alloy	50 ppm	20 ppm
35 a/o Alloy	60	70
Columbium	28	15

Disks for welding were cut from the annealed rod by a water-cooled abrasive wheel. They were ground to size, 0.500-inch for the alloy and 0.250-inch for the columbium with the ends held parallel to ± 0.0005 -inch. After grinding, the ends (or faces) of the weld disks were lapped with a slurry of 600 grit silicon carbide in oil. A commercial lapping machine, "Lapmaster 12", with a 12-inch diameter slotted steel lap was used. All trace of grinding was removed in about 0.005-inch. If

thermally insulated by Mullite ceramic disks (C). Loading is applied to this assembly through the Mo-0.5Ti alloy compression rods (D). The fixed top rod contains a thermocouple well. Loading is applied to the bottom one through a bellows seal by a hydraulic jack. The mechanical support arrangement for the loading system maintains the faces of the compression rods parallel within 0.0005in. The sandwich is heated inductively with power supplied by a 10 kw, 450 kc rf generator.

The assembly consisting of the specimen, the ceramic disks, the compression rods, and the induction coil is contained in a cold-wall, stainless-steel vacuum chamber. The associated pumping system is capable of maintaining a vacuum of less than 10^{-6} torr at the temperature of welding.

Welding was done at a brightness temperature of 1100-1125°C. Taking the emissivity of Columbium to be 0.35 (16) this gives a true temperature of 1195° to 1220°C. A load of 2000-2400 psi was applied and maintained after the assembly reached temperature. Loading was maintained for five to seven minutes while deformation was followed with a dial gage indicator. A total deformation of 0.010 to 0.020-inch was achieved. Most of this deformation took place upon initial loading and would be due to (i) embedding of thoria marker material into the metal

(ii) take up of looseness in the loading system and
(iii) compression of high points on the surface of the
weld disks or of the weld disk and the alumina insula-
tor. Figures 2 and 3 show the interface of a Cb/Cb35Ti
diffusion couple as welded.

2.3 Marker Measurements, As-Welded

The as-welded three layer sandwiches contain-
ing thoria marker material had a face machined and
ground parallel to their longitudinal axis as shown in
Fig. 4. This face was given a metallographic polish,
was etched and measurements of the marker spacing were
made. This was done on a Leitz micro-hardness tester
at a magnification of 200X using the machinist-type
stage micrometer which could be read to 0.0002-in. The
markers were lined up parallel to one of the micrometer
travel directions and a series of five measurement
traces was made perpendicular to the markers. Fig-
ures 2 and 3 also show the appearance of the thoria
markers in an as-welded couple.

2.4 Diffusion Anneals, Equipment

Diffusion anneals were carried out in three

different furnaces. Anneals of one hour or more were done in resistance furnaces and those at 0.1 hour were done by induction heating. In this investigation the furnaces used for the different kinds of anneals were as follows:

2.4.1 1000 and 1300°C Anneals >1 hour:

Materials Research Corporation Model VF 92

Heater: Molybdenum wire wound on an alumina core (Marshall Furnace Company)

Max. Temp: 1500°C (5 KVA)

Temp. Measurement: Pt6%RH vs Pt 30%Rh thermocouple calibrated against a standard Pt vs. Pt10Rh couple. Thermocouple accuracy, ± 1 °C.

Temp. Control: Current proportioning millivolt meter type sensitive to ± 1 °C. For long time anneals the control was accurate to at least ± 3 °C at 1300°C.

Vacuum System: Water cooled stainless steel furnace chamber, liquid nitrogen cold trap, optical baffle, oil diffusion pump and mechanical vacuum pump. With liquid nitrogen, vacuum was 2×10^{-6} torr at temperature.

Specimen Placement: The foil wrapped diffusion couple is supported in a tantalum 'can' which is suspended from radiation shields inside the alumina core. The tantalum sheathed measuring thermocouple extended inside the 'can' with the bead adjacent to the foil wrapped sample.

2.4.2 1500°, 1800° and 2000°C Anneals >1 Hour:

R. D. Brew, Model 424B

Heater: Self supporting tantalum sheet resistor

Max. Temp: 2400°C (35KW)

Temp Measurement: W3Re vs. W25Re thermocouple calibrated to 1450°C against a standard Pt-Pt10Rh couple ($\pm 2^\circ\text{C}$) and to 2400°C by calibrated optical pyrometer ($\pm 10^\circ$ at 1800°C, $\pm 20^\circ\text{C}$ at 2400°C).

Calibration is for the lot of wire.

All 1500°C anneals were made before the 1800° and 2000°C anneals to eliminate any change in calibration which the higher temperatures might produce.

Temp Control: Position-adjusting-type proportional control by a potentiometric circuit. The controller operated

a variable transformer which supplied the primary power. Sensitivity: $\pm 3.5^{\circ}\text{C}$. Charts indicate the sensitivity to be better, but accuracy over long times was usually $\pm 4^{\circ}\text{C}$ at 1500°C .

Vacuum System: Stainless steel plumbing, Freon chilled (30°F) optical baffle, oil diffusion pump and mechanical vacuum pump. Pressure at temperature: $<10^{-5}$ torr.

Specimen Placement: Foil wrapped specimen is supported in hot zones in Ta 'can' suspended from radiation shields. Thermocouple extends into 'can' adjacent to specimen.

2.4.3 1300° and 1500°C for 0.1 hour:

Heater: Direct heating of specimen by induction at a frequency of 10,000 cps.

Power Supply: 30 KW, 10,000 cycle motor-generator set.

The relationship of the specimen, radiation shield, induction coil, support system and thermocouple is shown

in Figure 5. The bare W3Re vs. W26Re thermocouple is held firmly by spring pressure against the end of the hole which is drilled to the weld interface. Sections for probe analysis were taken adjacent to this hole.

Temp. Control: Temperature control was obtained by manual adjustment of the generator field current while observing temperature on an extended range (6 in. = 100°C) recorder. Control was good to ±5°C. Figure 6 is a reproduction of a typical recorder chart for a 0.1 hr anneal.

2.5 Diffusion Anneals, Procedure

After the initial marker measurements, the couples were given a light pickle (H₂O-HNO₃-HF) to remove any surface contamination. They were wrapped in clean columbium foil and placed in the furnace. The furnace was evacuated to <10⁻⁵ torr and outgassed at 500° to 600°C for times ranging from a couple of hours to 24 hours. This thorough outgassing, of the furnace more than the

specimen, was necessary to permit rapid heating to the diffusion anneal temperature. Heating rates were such that the interior of the 'can' reached the diffusion anneal temperature in five minutes or less. Because of the nature of vacuum furnaces and the radiative heat transfer inherent in them, the closer the temperature to the anneal temperature, the more rapid the heating rate. Thus heating rates in excess of $200^{\circ}/\text{minute}$ prevailed as ^{the} anneal temperature was approached, except for ^{the} final $5-10^{\circ}$ when the controller takes effect.

2.6 Final Marker Measurements

Following diffusion, couples containing markers were prepared for measurement by milling and grinding a second longitudinal face parallel to that on which initial marker measurements had been made. This second face was made near the axis of the $1/2$ -inch diameter diffusion couple. The surface was prepared by conventional metallographic polishing techniques, was etched, and measured using the stage of a micro-hardness tester as in the initial measurements.

Location of the marker interface was not always easy, for a given plane often only passed through two or three thoria granules, and these were sometimes

partially or completely pulled out of the surface by the polishing procedure. It was then necessary to distinguish between holes remaining from pulled out thoria granules, holes due to random pitting during polishing and porosity due to the diffusion process. If doubt existed, the couple was reground and a second set of measurements was obtained. These characteristics are noted in the tabulation of the marker data.

2.7 Microprobe Procedure

2.7.1 Preparation

The sample holder of the electron microprobe used for analysis in this investigation (17) is one centimeter in diameter and about 5/16-inch deep, Figure 7. To accommodate this configuration, a slice approximately 0.1-inch x 0.35-inch x 0.185-inch is cut from one diffusion zone of the three layer sandwich, Figure 8.

The procedure usually followed was to mount two such slices and five standards in each mount prepared for the probe, Figure 7. These were contained in a stainless steel ring of appropriate size and mounted in bakelite in a standard 1-1/8-inch diameter

mount. The mounted couples and standards were lightly ground by hand through 3/0 silicon carbide paper and hand polished with 3 to 5 micron diamond paste carried on fine silk cloth backed by plate glass on a rotating metallographic polishing wheel. Every effort was made to prevent contouring of the surface. The polished array was broken from the large mount by splitting the ring from it and was prepared for insertion into the probe as shown in Figure 7. Conducting silver paint was used to achieve grounding and a patch of fluorescent material was included to permit focusing of the electron beam.

2.7.2 Standards:

The standards included in the mount were prepared from the Cb8.5 a/o Ti, the Cb35 a/o Ti, and the columbium rods and from a Cb17 a/o Ti alloy. Pieces of these were swaged to approximately 0.1 inch diameter. Short pieces were cut from these and mounted with each pair of diffusion couples. Samples of these standards were analyzed by x-ray fluorescence. The mean values and 90% confidence limits based upon three samplings (adjacent to those pieces actually used) are:

- (a) Cb- 8.5 ± 0.5 a/o Ti
- (b) Cb- 17.0 ± 0.0 a/o Ti
- (c) Cb- 34.6 ± 1.8 a/o Ti.

Pure metal columbium and titanium standards were also included in each mount.

2.7.3 Microprobe Operation

The instrument of the Optics Division of the United States Naval Research Laboratory described by Birks and Brooks (17) was used. The slices cut from the diffusion couples were oriented in the specimen chamber of the probe as shown schematically in Figure 9. Initial plans called for motor driven scanning of the sample across the electron beam. Of the two translation screws, only B can be used with the motor drive. The weld interface orientation with respect to emergent x-rays (actually the spectrometer) was then fixed. The motor drive failed to operate properly and it became necessary to do point by point measuring, advancing the specimen manually. However, the same sample to instrument orientation as in Figure 9 was used.

The emergent x-radiation is analyzed by a curved crystal spectrometer for the K radiation. A

helium path is used for the titanium spectrometer path.
Counting is by Geiger-Müller tube.

The electron gun was operated at 30 kv. Intensities from the pure metals were approximately 1500 cps for titanium and 700 cps for columbium.

In the measurement of diffusion penetration, the standards were examined before and after each scan. Instrument drift occurs but this procedure permits a correction to be applied via the calibration curves.

Chapter 3

RESULTS

3.1 Marker Data

Marker data are presented in Table 3. The initial values of marker position listed represent the mean of five measurements along the length of the couple between the weld interfaces of the three layer sandwich. The stage micrometer could be read to an accuracy of 0.0002-inch. Standard deviations (σ) computed for several sets of measurement values ranged from 0.0005 to 0.0010-inch. The lower figure corresponds to approximately the summation of the reading accuracies.

For the final position, the values in the table represents the mean of three or more sets of measurements. Standard deviations computed from several sets of final marker position measurements range from 0.0008-inch to 0.0015-inch. The final marker position values are measurements of actual thoria marker material except for #47 (10 hr. at 2000°C). In this couple no markers could be found, but porosity stringers, shown in Figure 10, were used.

The column headed ' ΔW ' is the maximum difference in thickness between the initial measurement face and the final measurement face, i.e., $\Delta W = W_2 - W_1$ in Figure 8. The measurements are taken on the one-inch length of the entire three layer couple. Over the 1/2-inch 'gage' of the marker measurements, differences in parallelism of the two faces would be at least half the listed values (and probably less).

Table 3
Marker Data

Couple No.	Anneal Time(hr)	Marker Spacing			ΔW (in)
		Initial (in)	Final (in)	Shift (in, X10,000)	
<u>1000°C</u>					
53 (35a/oTi)	120	.4902	.4909	+7	
54 (8.5a/oTi)	120	.4975	.4976	+1	
<u>1300°C (8.5a/oTi)</u>					
50	1	.4998	.4992	-6	.003
36	10	.4986	.4992	+6	.0001
40	120	.4981	.4960	-19	.0001
<u>1300°C (35a/oTi)</u>					
39	120	.4886	.4874	-12	.004

Table 3 Continued

Couple No.	Anneal Time (hr)	Marker Spacing			ΔW (in)
		Initial (in)	Final (in)	Shift (in, X10,000)	
<u>1500°C(8.5a/oTi)</u>					
42	1	.5000	.4963	-27	.0015
34	10	.4989	.4997	+8	.0018
31	48	.4989	.4990	+1	--
38	120	.4982	.4967	-15	.005
25	480	.4914	.4914	0	--
49	1000	.4995	.4999	+4	
<u>1500°C(35a/oTi)</u>					
41	1	.4904	.4917	+12	.0045
33	10	.4931	.4926	-5	.0028
32	48	.4887	.4875	-12	--
37	120	.4919	.4905	-14	.0001
26	480	.4897	.4987	+40	--
48	1000	.4912	.4905	-7	.0004
<u>1800°C</u>					
44 (8.5a/oTi)	10	.4999	.4990	-8	.003
43 (35a/oTi)	10	.4873	.4809	-64	.0001
<u>2000°C</u>					
46 (8.5a/oTi)	10	.4961	.4969	+8	.003
47 (35a/oTi)	10	.4951	.4873	-78	.0002

For all the data except that of the 35 a/o alloy at 1800° and 2000°C, the precision is insufficient to resolve any shift in the marker position. The sum of the standard deviations for the initial and final values exceed the difference between them. However, the 1800° and 2000°C anneals of the 35 a/o couples clearly produced a Kirkendall shift. The direction is toward the alloy indicating that titanium is moving from the alloy faster than columbium is into it. This leads to a net vacancy flux from the columbium to the alloy.

The 2000°C anneal also produced considerable porosity as is evident in Figure 10. Porosity was also found in couples which did not indicate a marker shift. These voids usually were adjacent to the marker material as in Figure 11. It was found predominantly on the alloy side of the marker at both interfaces. This observation identifies the porosity as originating from the diffusion process and may be taken as evidence that the voids observed are not simply thoria which has been pulled out. This phenomenon is similar to observations on porosity formation noted by da Silva (18) and others (19).

3.2 Concentration-Penetration Data

The output of the x-ray spectrometer of the micro-probe was obtained at a chart recording of count rate vs. time (=distance). From the chart of each couple, a table of count rate data for both the standards and for the diffusion couple was obtained. A calibration curve, Figure 12, was plotted for each couple. From these, concentration vs. distance data were obtained and finally, relative concentration, C/C_0 was computed. These data were tabulated as in Table 4 for each couple.

The complete data from the couples annealed according to Table 1 are presented in Appendix 2 as $C/C_0 \times 100$ on a probability scale vs. penetration distance on a linear scale. Also included in Appendix 2 are linear concentration, C , vs. penetration distance plate for those couples to which the Boltzmann-Matano analysis was applied. For convenience, an example of each type of curve is included in the main text, Figures 13(a) and 13(b).

Photomicrographs of the contamination trace were made of each scan of the probe across the diffusion zone to assure that the count rate data did not represent structure irregularities such as marker material, voids, or large scratches. Figures 14(a), (b) and 15(a), (b) show typical contamination traces.

Table 4

An Example of the Microprobe DataCouple #33: Cb/Cb35Ti - 1500°C - 10 hr

Calibration Data						
a/o Ti	Titanium			Columbium		
	1*	2	3	1	2	3
100	870	780	730	35	3	32
35	82	90	80	305	290	280
17	46	41	41	360	335	320
85	25	25	23	380	355	340
0	7	7	8	400	380	355

* 1 - Before Scan 1

2 - Between Scans

3 - After Scan 2

Penetration Data - Scan #1						
Position	Titanium			Columbium		
	Probe Units	c/s	a/o	C/Co	c/s	a/o
1-5	10	1.6	4.5	385		
6	11	2.0	5.6	385		
7	16	4.4	12.4	375		
8	28	10.3	28.9	365		
9	34	13.3	37.1	355		
10	40	16.2	45.5	350		
11	48	20.0	56.2	340		

Table 4 Continued

Position	Titanium			Columbium		
	Probe Units	c/s	a/o	C/Co	c/s	a/o
12	54	23.0	64.6	335		
13	56	24.0	67.4	335		
14	58	25.0	70.2	335		
15	60	26.0	73.0	335		
16	63	27.3	76.6	335		
17	65	28.3	79.5	330		
18	67	29.3	82.4	325		
19	69	30.2	84.9	320		
20	70	30.8	86.5	315		
21	71	31.2	87.6	315		
22	72	31.7	89.0	312		
23	74	32.7	91.9	312		
24	75	33.1	93.0	310		
25	76	33.6	94.4	310		
26	76	33.6	94.4	310		
27	77	34.1	96.0	310		
28	78	34.6	97.2	310		
29	78	34.6	97.2	310		
30-42	80	35.6	97.2	310		

3.3 Results of the Grube Analysis

For the purpose of testing the applicability of the Grube solution Equation [10], the data are plotted as C/C_0 vs. X on probability paper. As noted above, these data are contained in Appendix 2. The Grube solution was applied to the 'straight line' portion of these plots as in the sample calculation, Appendix 3, p. 148. The resultant interdiffusion coefficients, D , and the parameter, Dt , where t is the time of diffusion are given in Table 5. Also included are ' Dt ' data from undiffused couples and a computed value for the welded couple based upon the time and temperature of welding.

Table 5

Diffusion Results ' Dt ' and ' D ' by the Grube Solution

Time (hr)	Dt (cm ²)		D (cm ² /sec)	
	Scan 1	Scan 2	Scan 1	Scan 2
<u>Undiffused - 8.5 a/o Ti:</u>				
0	39.8×10^{-8}	22.7×10^{-8}		
<u>Undiffused - 35 a/o Ti:</u>				
	80.0×10^{-8}	76.3×10^{-8}		
<u>1300°C - 8.5 a/o Ti:</u>				
0.1	6.2×10^{-8}	3.74×10^{-8}	17.0×10^{-11}	10.6×10^{-11}
1.0	12.8×10^{-8}	616×10^{-8}	3.6×10^{-11}	171×10^{-11}
10.0	88.0×10^{-8}	144×10^{-8}	2.5×10^{-11}	4.1×10^{-11}
120.0	339×10^{-8}	225×10^{-8}	0.8×10^{-11}	0.5×10^{-11}

Table 5 Continued)

Time (hr)	Scan 1	Scan 2	Scan 1	Scan 2
<u>1300°C - 35 a/o Ti:</u>				
120	405x10 ⁻⁸	400x10 ⁻⁸	0.95x10 ⁻¹¹	0.94x10 ⁻¹¹
<u>1500°C - 8.5 a/o Ti:</u>				
0.1	139x10 ⁻⁸	56x10 ⁻⁸	3.9x10 ⁻⁹	16.4x10 ⁻¹⁰
1.0	47.7x10 ⁻⁸	16x10 ⁻⁸	14x10 ⁻¹¹	4.6x10 ⁻¹¹
10	80x10 ⁻⁸	56x10 ⁻⁸	2.2x10 ⁻¹¹	1.6x10 ⁻¹¹
120	373x10 ⁻⁸	321x10 ⁻⁸	0.88x10 ⁻¹¹	0.80x10 ⁻¹¹
480	2680x10 ⁻⁸		1.6x10 ⁻¹¹	
1000	8810x10 ⁻⁸	5150x10 ⁻⁸	2.5x10 ⁻¹¹	1.5x10 ⁻¹¹
<u>1500°C - 35 a/o Ti:</u>				
0.1	838x10 ⁻⁸	210x10 ⁻⁸	2.4x10 ⁻¹²	5.9x10 ⁻¹¹
1.0	137x10 ⁻⁸		3.9x10 ⁻¹⁰	
10	377x10 ⁻⁸	309x10 ⁻⁸	1.05x10 ⁻¹⁰	0.87x10 ⁻¹⁰
120	7500x10 ⁻⁸	11900x10 ⁻⁸	1.8x10 ⁻¹⁰	2.82x10 ⁻¹⁰
480	24400x10 ⁻⁸	22800x10 ⁻⁸	1.4x10 ⁻¹⁰	1.35x10 ⁻¹⁰
100	31800x10 ⁻⁸	60000x10 ⁻⁸	0.9x10 ⁻¹⁰	1.7x10 ⁻¹⁰
<u>1800°C - 35 a/o Ti:</u>				
10	10000x10 ⁻⁸	11400x10 ⁻⁸	2.85x10 ⁻⁹	3.25x10 ⁻⁹
<u>2000°C - 35 a/o Ti:</u>				
10	68600x10 ⁻⁸	14800x10 ⁻⁸	1.96x10 ⁻⁸	4.2x10 ⁻⁸
<u>Welding Process (1195°C):</u>				
0.1	7x10 ⁻⁹ to 2x10 ⁻¹¹ (Calculated)			

Diffusion during welding based upon the calculated value is negligible. The measured values of 'Dt' for the undiffused couples are not. The 'Dt' values measured from the undiffused couples are as large or larger than values obtained from couples annealed at 1000°C for 120 hours; 1300°C for 0.1, 1.0 and 10 hours; and 1500°C for 0.1 and 1.0 hours. Data from these couples must be considered not significant. For these couples the penetration distance (measured from $C/C_0=0$ to $C/C_0=0.95$) ranged from about 10 to 40 microns and most of these were in the range of 15 to 30 microns. For the present it only will be noted that the electron microprobe as it was used in this study was unable to resolve adequate concentration-penetration curves for diffusion analysis if penetration distances were less than 40 microns. This matter is discussed further in Chapter 4, section 4.2.1.

Examination of the C/C_0 vs. X plots reveals that the straight line portion often includes three-fourths of the data points in the range $0.1 < \frac{C}{C_0} < 0.95$, but that the straight line portion often extends only over a C/C_0 range of 0.2 or 0.3, and sometimes less. This situation is improved for the data of many of the 8.5 a/o alloy couples; but even though the region of evident misfit to a straight line is less for the 8.5 a/o Ti

couples than for 35 a/o Ti couples, the question of where to draw the line is subject to considerable uncertainty. Ideally this would be accomplished by a best least square fit to the data, but if curvature due to concentration does exist, this would be a redundant process. Also, any such analysis should be corrected for accurate 'blank' undiffused data. This is not available. Therefore the Boltzmann-Matano analysis was applied.

3.4 Results of the Boltzmann- Matano Analysis

The analysis of penetration data by the method of Matano was applied to each Cb35a/0Ti vs. Cb couple for anneal times of 10 hours or more and to the data of selected 8.5a/0Ti couples. A complete sample calculation is included in Appendix 3 and all concentration-penetration curves to which the method was applied are presented in Appendix 2. The tabulated results are given in Table 6. These are plotted in Figures 16, 1300°C; 17, 1500°C; 18, 1800°C; and 19, 2000°C. Also, included in the figures are data extracted from reference (20).

Table 6

Diffusion Coefficient, D as a Function of
Composition (C) Computed by the Method of Mantano

<u>1300°C</u>					
<u>35 a/o Ti</u>			<u>8.5 a/o Ti</u>		
<u>120 Hr.</u>			<u>120 Hr.</u>		
C	D		C	D	
<u>(a/o Ti)</u>	<u>(cm²/sec)</u>		<u>(a/o Ti)</u>	<u>(cm²/sec)</u>	
34	7.9×10^{-12}		9.0	3.44×10^{-12}	
30	7.0		8.0	2.15	
22.9	5.1		6.7	11.6	
16	2.0_3		5.0	0.59	
10	2.2_4		4.0	0.42	
4	3.1		3.0	0.28	
			2.0	0.64	

<u>1500°C - 35 a/o Ti</u>						
<u>10 Hr.</u>		-	<u>120 Hr.</u>		<u>1000 Hr.</u>	
C	D		C	D	C	D
<u>(a/o Ti)</u>	<u>(cm²/sec)</u>		<u>(a/o Ti)</u>	<u>(cm²/sec)</u>	<u>(a/o Ti)</u>	<u>(cm²/sec)</u>
34	5.23×10^{-11}		34	16.5×10^{-11}	34	6.44×10^{-11}
30	8.08		30	7.8	30	8.08
23.4	4.29		24.9	4.16	26	9.21
18	2.76		20	2.63	22.0	6.85
14	2.39		15	2.54	16	4.19
10	2.05		10	2.47	10	4.60
5	2.56		5	4.33	4	5.73

Table 6 Continued

Diffusion Coefficient vs. Composition: Boltzmann-Matano Analysis

1500°C - 8.5 a/o Ti

1.0 Hr.			10 Hr.			120 Hr.			1000 Hr.		
C	D		C	D		C	D		C	D	
(a/o Ti)	(cm ² /sec)		(a/o Ti)	(cm ² /sec)		(a/o Ti)	(cm ² /sec)		(a/o Ti)	(cm ² /sec)	
8.5	8.36x10 ⁻¹¹		8.0	6.75x10 ⁻¹¹		8.0	5.93x10 ⁻¹²		10.0	1.94x10 ⁻¹¹	
7.5	4.70		7.0	3.78		7.0	7.5		8.0	2.25	
6.1	3.06		5.56	1.33		6.0	8.79		6.1	1.73	
5.0	2.75		4.0	1.22		4.67	9.3		4.0	1.53	
4.0	2.10		3.0	1.43		4.0	9.3		2.0	2.04	
			2.0	1.84		3.0	10.12				
						2.0	12.32				

Table 6 Continued

1800°C - 35 a/o Ti

10.0 Hr.

<u>C</u> <u>(a/o Ti)</u>	<u>D</u> <u>(cm²/sec)</u>
30	2.49x10 ⁻⁹
28	2.07
26	1.84
24	1.69
21.6	1.44
18	1.24
16	1.23
14	1.10
10	1.17

2000°C - 35 a/o Ti

10.0 Hr.

<u>C</u> <u>(a/o Ti)</u>	<u>D</u> <u>(cm²/sec)</u>
32	6.79x10 ⁻⁸
26	3.45
21.2	2.73
16	2.16
10	2.31
4	3.96

It should be noted that application of this solution to any given concentration range may be spurious at the extremes of that concentration range. This is due to errors inherent in the measurement of area under any asymptotic curve. Keeping this factor in mind, the banded curves indicated probably represent the concentration dependence.

The data of ^{reference} (20) which are included are extracted from data based on measurements of diffusion in Cb vs. Cb50a/oTi and Cb vs. Ti couples and are therefore least accurate approaching 0 a/o Ti, but are more reliable beyond 20 a/o Ti. On the other hand, the 8.5 a/o Ti couples of this study should be highly accurate in the low concentration range. At 1500°, Figure 17, the obvious convergence for the three different anneal times included in the region of 2 to 4 a/o Ti gives strong credibility to the value of D indicated. The diffusion coefficient computed by the Grube solution for the same couples is in excellent agreement.

The apparent upward displacement of the 1000 hour - 35 a/o couple at 1500°C, Figure 17, is considered due to contamination, not to some inherent time dependency. This is discussed later.

From Figures 16, 17, 18, and 19, averaged values of D may be extracted as a function of composition. These results at 0, 10, 20, and 30 a/o Ti are presented in Table 7, and are plotted as Arrhenius-type plots in Figures 20, 21, 22, and 23.

Table 7

Diffusion Coefficients as a Function of Composition:Extracted from the D vs. C plots of the Boltzmann-Matano Data at 1300°, 1500°, 1800°, and 2000°C

Temp. (°C)	2000	1800	1500	1300
Temp. (°K)	2273	2073	1773	1573
$\frac{1}{T} \left(\frac{10^4}{\text{°K}} \right)$	<u>4.40</u>	<u>4.82</u>	<u>5.64</u>	<u>6.36</u>
<u>Composition</u>	<u>D (cm²/sec)</u>			
0 a/o Ti	1.6x10 ⁻⁸	1.0x10 ⁻⁹	1.5x10 ⁻¹¹	0.3x10 ⁻¹²
10 a/o Ti	2.0x10 ⁻⁸	1.2x10 ⁻⁹	2.2x10 ⁻¹¹	1.5x10 ⁻¹²
20 a/o Ti	2.7x10 ⁻⁸	1.25x10 ⁻⁹	3.0x10 ⁻¹¹	3.8x10 ⁻¹²
30 a/o Ti	4.5x10 ⁻⁸	2.5x10 ⁻⁹	5.0x10 ⁻¹¹	6.5x10 ⁻¹²

The confidence limits shown in these curves are taken from the data bands of the D vs. composition curves, Figures 16, 17, 18, and 19. Without indicating confidence limits, these curves are superimposed on Figure 24.

Two phenomena are evident: (i) the concentration dependence of D increases as temperature decreases and (ii) the Arrhenius plot exhibits curvature.

3.5 Activation Energy and Frequency Factor

If diffusion data follow the usual Arrhenius behavior, the temperature dependence of D may be described by

$$D = D_0 e^{-Q/RT} \quad \text{where} \quad [11]$$

R = universal gas constant

T = absolute temperature

Q = activation energy

D₀ = Frequency Factor ≠ f(T).

Taking logs,

$$\ln D = \ln D_0 - \frac{Q}{RT} \quad [12]$$

and differentiating,

$$\frac{2.3 \, d \log D}{d\left(\frac{1}{T}\right)} = - \frac{Q}{R} \quad [13]$$

If [11] holds, log D vs. $\frac{1}{T}$ will give a straight line, the slope of which equals -Q/R and the intercept at $\left(\frac{1}{T}\right) = 0$ gives D₀.

Values of Q and D₀ extracted from Figures 20, 21, 22, and 23 along with data from Steedly (19) and self-diffusion data for Cb⁹⁵ in Cb from Peart, Graham and Tomlin (21) and from Resnick, Castleman and Seigle (22) are given in Table 8.

Table 8
Activation Energies and Frequency Factors

<u>Composition</u> (a/o Ti)	<u>Q</u> (k cal/g atom)	<u>Do</u> (cm ² /sec)
Present work, 1300° to 2000°C:		
0	110	500
Present work, 1300° and 1500°C only:		
10	76	1.8×10^{-1}
20	57	2.8×10^{-3}
30	57	1.8×10^{-3}
Steadly <u>et al</u> (19) 1000° to 1588°C:		
20	63	2.6×10^{-3}
30	60	2.9×10^{-3}
40	66	3.1×10^{-3}
Self-diffusion Cb ⁹⁵ in Cb:		
Resnick <u>et al</u> (22)	95	1.3
Graham <u>et al</u> (21)	105	12.4

CHAPTER 4

DISCUSSION

4.1 Marker Experiments

The marker shift and extensive void formation at 1800° and 2000°C prove that in this temperature range a vacancy mechanism causes a net outward flux of titanium and a corresponding inward flux of vacancies. Failure to resolve a marker shift at the lower temperatures may be attributed to too narrow a diffusion zone. The appearance of voids in the alloy adjacent to the markers in some of the 1500°C couples demonstrates the existence of a net vacancy flux at the lower temperature.

These observations positively resolve this portion of the problem as stated in the introduction.

4.2 Limits on the Penetration Data

Confidence in the concentration-penetration data at both extremes of the time span included in ^{the} 1300° and 1500°C anneals must be limited.

4.2.1 Short Time Limit; the Microprobe Data

The failure of the microprobe data to resolve adequately the concentration-penetration curves for the shorter time anneals

might be due to the orientation of the specimens in the probe. As shown in Figure 9, the weld interface is nearly perpendicular to the direction of X-ray measurement. This is in opposition to recommended practice (23). It could be expected that the best results would be obtained if the emergent X-rays only passed through material of the same composition as that being measured, i.e., if the weld interface were parallel to the emergent X-rays.

Secondly, irregularities in the flatness of a surface being examined by the microprobe (23) are known to cause spurious effects in X-ray intensity. In a diffusion couple composed of materials of grossly different polishing behavior, a contour such as that exaggerated in Figure 25 might develop. It must be emphasized that in the polishing procedure which was used, every effort was made to minimize any effect like that hypothesized in Figure 25; however, if the spectrometer directions were parallel to the weld (perpendicular to the paper in Figure 25) the situation would be improved.

There is some evidence which may be taken as a measure of the degree of improvement that is possible. Seebold and Birks (24) have indicated that in their experience resolution of the order of 10 microns is possible for diffusion penetration zones. In fact it was this figure upon which the short time anneals in this series of experiments was based. However, more recent results from extensive data on several binary alloy systems which have been analyzed quantitatively for diffusion

parameters indicate that penetration distances greater than 25 microns are required (25).

4.2.2 Long Time Limit; Contamination

The vulnerability of the refractory metals and especially alloys of them to contamination is clearly documented in Appendix 4. The 8.5 a/o couple at 1300°C-1000 hours contained the oxide contamination described in Appendix 4. A second kind of contamination took place during the 1500°C-1000 hours anneals.

Examination of the polished 35 a/o Ti couple after 1000 hours at 1500°C revealed massive hydride-type precipitates, Figure 26(a,b). The size of the Widmanstätten plates imply extensive growth of only a few nuclei. Kinetically, this is the kind of behavior one might expect if the supply of a reactant were the rate controlling factor and if the rate of supply of this reactant were very low. The supply of hydrogen to the furnace by the migration and cracking of diffusion pump oil could satisfy such a requirement. The use of a liquid nitrogen cold trap would have minimized this kind of effect. Table 9 shows that although some contamination may also take place in shorter times at 1500°C, the effects are much less than at 1000 hours.

Table 9

Hardness vs. Anneal Time at 1500°C

	<u>Hardness, VPH, at Center of Alloy*</u>			
	<u>1 Hr</u>	<u>10 Hr</u>	<u>120 Hr</u>	<u>1000 Hr</u>
8.5 a/o Ti	128	132	138	221
35 a/o Ti	166	179	202	498

* The hardness in the alloy 0.020-inch from the marker is the same as above and the hardness in the columbium remained low even after 1000 hours (VPH = 75).

The absence of contamination in the 1800° and 2000°C couples may be evaluated similarly, for although the specific reaction rate (for contamination) would be much greater at the higher temperatures, the relatively short anneal time (10 hr) simply limits the amount of the contaminant.

With the above in mind, the greatest confidence may be placed on results from couples at the moderate (1, 10 and 120 hr) anneal times. Shorter times give penetration distances too short for adequate resolution by the probe, and the very long anneal times (1000 hr) may produce significant contamination, even in the high vacuum environment.

4.3 Time Dependence of D

The interdiffusion coefficient, D, determined by the Boltzmann-Matano analysis of the diffusion data at 1500°C for times of 10, 120 and 1000 hours for Cb/Cb 8.5a/oTi couples and

for times of 10 and 120 hours for Cb/Cb 35a6Ti couples, shows no dependence on the time of diffusion, Figure 17. The slight increase in D for the 1000 hour data of the Cb/Cb 35a6Ti couple is attributed to the contamination discussed above.

It is not surprising that no time dependence of D is found, for as was pointed out in the introduction, the only examples of a time dependence of D in binary metal alloy diffusion previously reported (5, 9) have been observed in very steep concentration gradients in systems of appreciably different atomic volume. In the present work neither of these conditions exists. Lattice parameter differences between columbium and titanium at the diffusion temperatures are less than 0.1 percent and in the limited composition range examined here, and indeed for the complete system, must be considered negligible. Lattice strains across the diffusion zone due to atomic volume differences thus must be negligible.

4.4 Concentration Dependence of D

The increase in the concentration dependence of D with decreasing temperature is in accord with Steedly's results which extend across the complete alloy system. These are:

T (°C)	D (cm ² /sec)		Δ log D
	100% Ti	100% Cb	
1588	1 x 10 ⁻⁷	2 x 10 ⁻¹¹	3.8
1500	5.8 x 10 ⁻⁸	3.7 x 10 ⁻¹²	4
1300	1.0 x 10 ⁻⁸	5 x 10 ⁻¹²	4.5
1000	1 x 10 ⁻⁹	1 x 10 ⁻¹⁴	5

Much has been published concerning the concentration dependence of D (26), but little if anything has been written concerning the rate of change of this concentration dependence with temperature. However, a somewhat cursory review of the D (c) data prepared by Seitz and Heuman (26) indicates that the rate of change of D with concentration generally decreases with increasing temperature.

4.5 Curvature of the Arrhenius Plot

Curvature of the so-called Arrhenius-type plot for diffusion data, $\log D$ vs. $\frac{1}{T}$, has been observed for Mo⁵⁵, Nb⁹⁵, Cr⁵¹, Mn⁵⁴, Fe⁵⁵, Co⁶⁶ and Ni⁶³ tracers in β titanium and b.c.c. alloys of titanium by Gibbs, Graham and Tomlin (27) over a temperature range of 900° to 1650°C, and for Zr⁹⁵ and Cb⁹⁵ in b.c.c. zirconium by Federer and Lundy (28) over temperatures of 900° to 1750°C. Steedly (26) observed that for interdiffusion in Cb-Mo couples no curvature was evident between 1800° and 2163°C, but that a value of D at 1300°C was too high by two orders of

magnitude, thus requiring curvature.

Both Gibbs et al and Federer and Lundy attribute earlier failure to observe curvature as due to too small a temperature range. In the present work, Figure 24, as well as in the data of Steedly, this too is evident.

If a linear relationship is assumed and applied to only the 1300° and 1500°C points at 20 and 30 a/o in Figure 24, the composition range in which the present work most accurately overlaps Steedly's data, Table 8, it is seen that the 'apparent' Q and D_0 values (at 20 and 30 a/o Ti) are in quite good agreement. Steedly's data show no curvature because of the more limited temperature range.

Federer and Lundy choose to describe their data by an equation of the form

$$D = D_0(T) \exp \frac{-Q(T)}{RT} . \quad [12]$$

Gibbs et al prefer a summation such that

$$D = D_{o_1} \exp \frac{-Q_1}{RT} + D_{o_2} \exp \frac{-Q_2}{RT} . \quad [13]$$

The use of [12] implies a single mechanism of diffusion with kinetic parameters D_0 and Q , which vary with temperature while the latter [13] implies two competing processes -- one operative at higher temperature and one at low temperature. This latter concept has been successfully applied to the enhancement of diffusion by high diffusivity paths such as grain boundaries (29), but the high homologous temperatures and the large grain size in the present work make these mechanisms unlikely here.

The concept of Federer and Lundy is preferred, for as they point out, "Neither absolute rate theory nor thermodynamics demand a constant activation energy - in fact, for diffusion data the usual Arrhenius-type expression is true only when so proved by the data". That this is true is unquestionable, however, reluctance to accept it is due to long familiarity with 'well behaved' f.c.c. systems and there may be reluctance to change.

CHAPTER 5

SUMMARY AND CONCLUSIONS

Interdiffusion has been studied in the columbium-titanium b.c.c. alloy system in the temperature range 1000° to 2000°C and at times ranging from 0.1 to 1000 hours. The electron microprobe has been used for measurement of the diffusion-penetration curves and the data have been treated by both the Grube and Boltzmann-Matano solutions to the diffusion equation.

At 1800° and 2000°C thoria markers were observed to shift toward the alloy section of Cb/Cb 35 a/o Ti diffusion couples. This shift in marker position was accompanied by the formation of porosity in the alloy. Porosity, but no evident marker shift, was also observed after long anneals at 1500°C.

Reliable data at 1500°C for couples of Cb/Cb 8.5 a/o Ti and Cb/Cb 35 a/o Ti for times of 10, 120 and 1000 hours and 10 and 120 hours, respectively, reveal no dependence of the interdiffusion coefficient, D , with time.

The results -- in terms of D , D_0 and Q -- are in agreement with other work on the Cb-Ti system over the common composition and temperature spans, 20-30 a/o Ti, <1500°C. However, when the 1800° and 2000°C data and the more accurate low concentration data of the present work are included, the Arrhenius-type plot of $\log D$ vs. $\frac{1}{T}$

develops curvature with increasing composition. At 0 a/o Ti a nearly perfect straight line is obtained giving $Q = 110$ k cal /g-atom and $D_0 = 500 \text{ cm}^2/\text{sec}$. At the higher temperature range the concentration dependence of D which leads to the curvature decreases.

The following conclusions are made:

1. The vacancy mechanism is operative in diffusion in the b.c.c. Cb-Ti alloy system -- certainly over the temperature range 1500° to 2000°C .
2. The results do not indicate a dependence of D on the time of diffusion for the range of composition, 0 to 35 a/o Ti, and time, 10 to 1000 hours, for which reliable data are available.
3. The concentration dependence of D increases with decreasing temperature and this is reflected in curvature of the $\log D$ vs. $\frac{1}{T}$ plot as concentration increases from 0 to 30 a/o Ti.

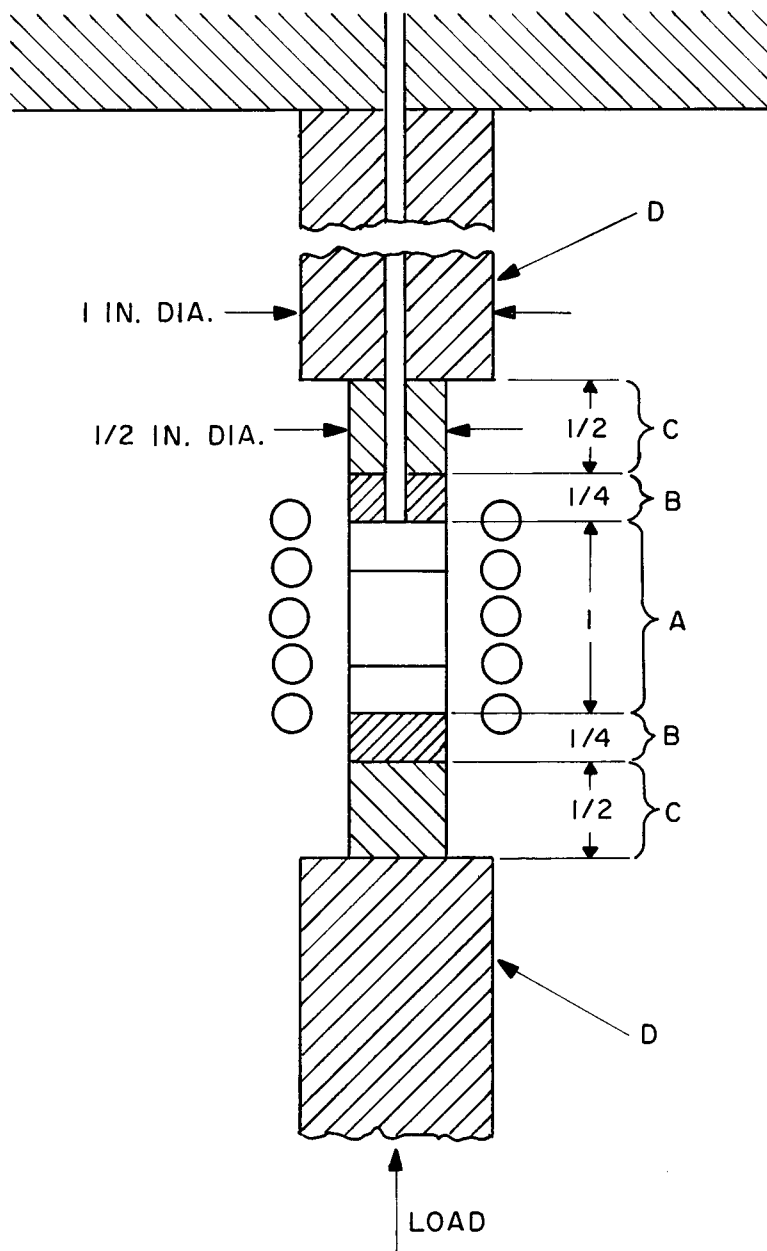


Figure 1 - Assembly for pressure welding diffusion couples.

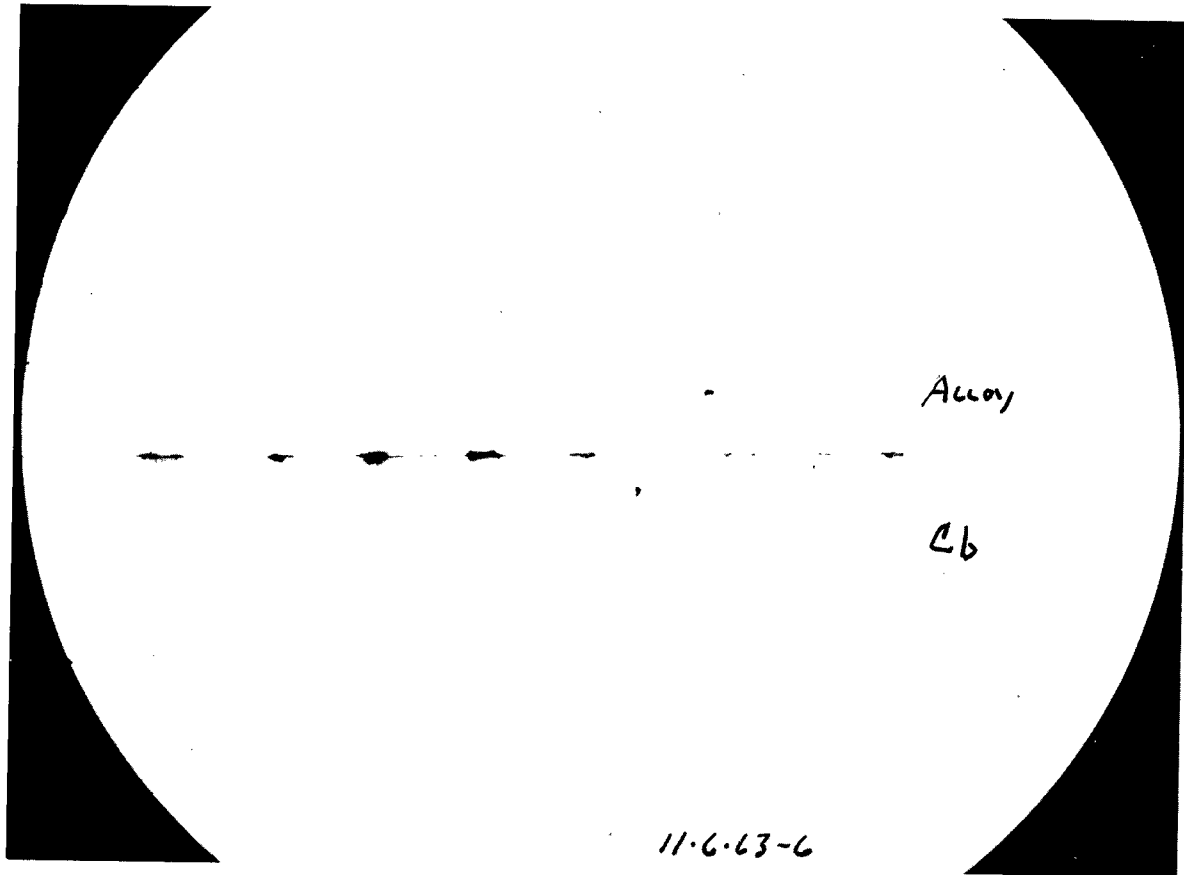


Figure 2- Photomicrograph of a diffusion couple as welded showing thoria marker material at the weld interface. Light etch in 9:1:1, Lactic Acid:HF:HNO₃. X50.

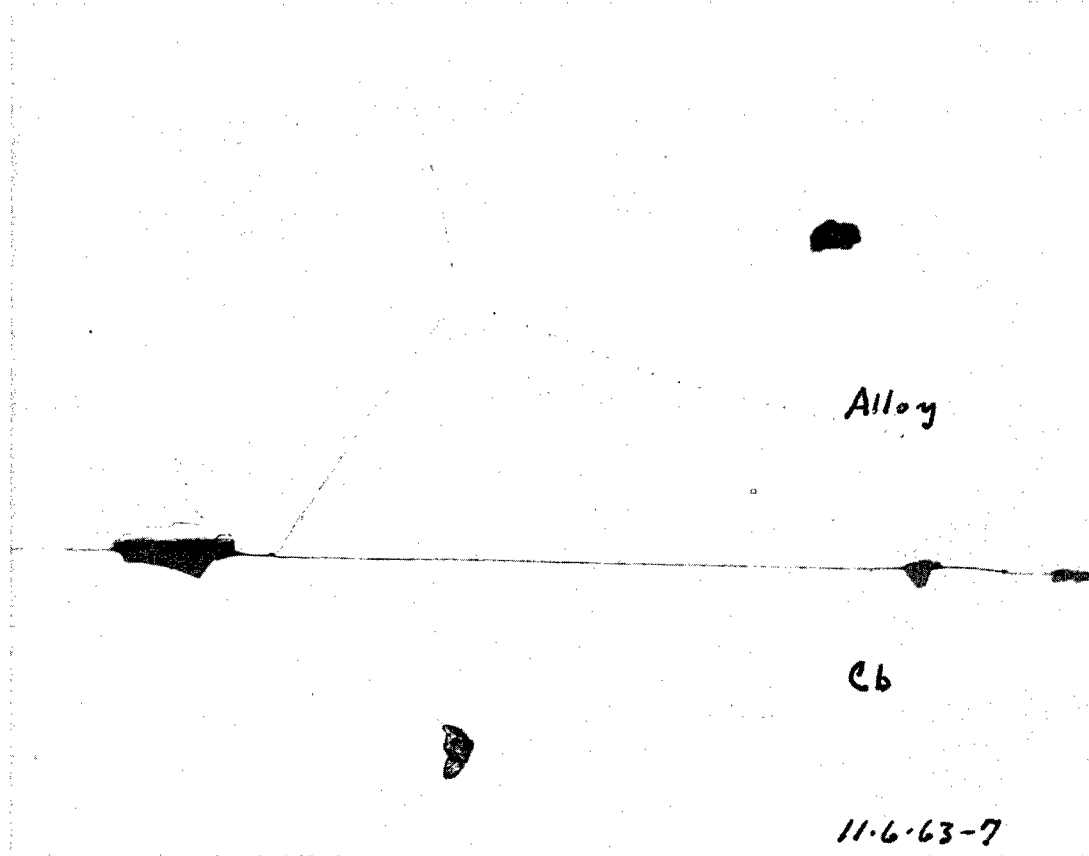


Figure 3 - Photomicrograph of a diffusion couple as welded showing thoria markers at the weld interface. Note evidence of recrystallization in the alloy adjacent to the markers. Light etch. Same as Figure 2. X250.

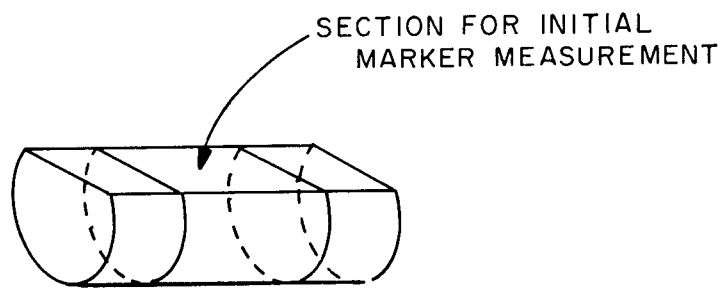


Figure 4 - Sketch of welded diffusion couple sectioned for initial marker measurement.

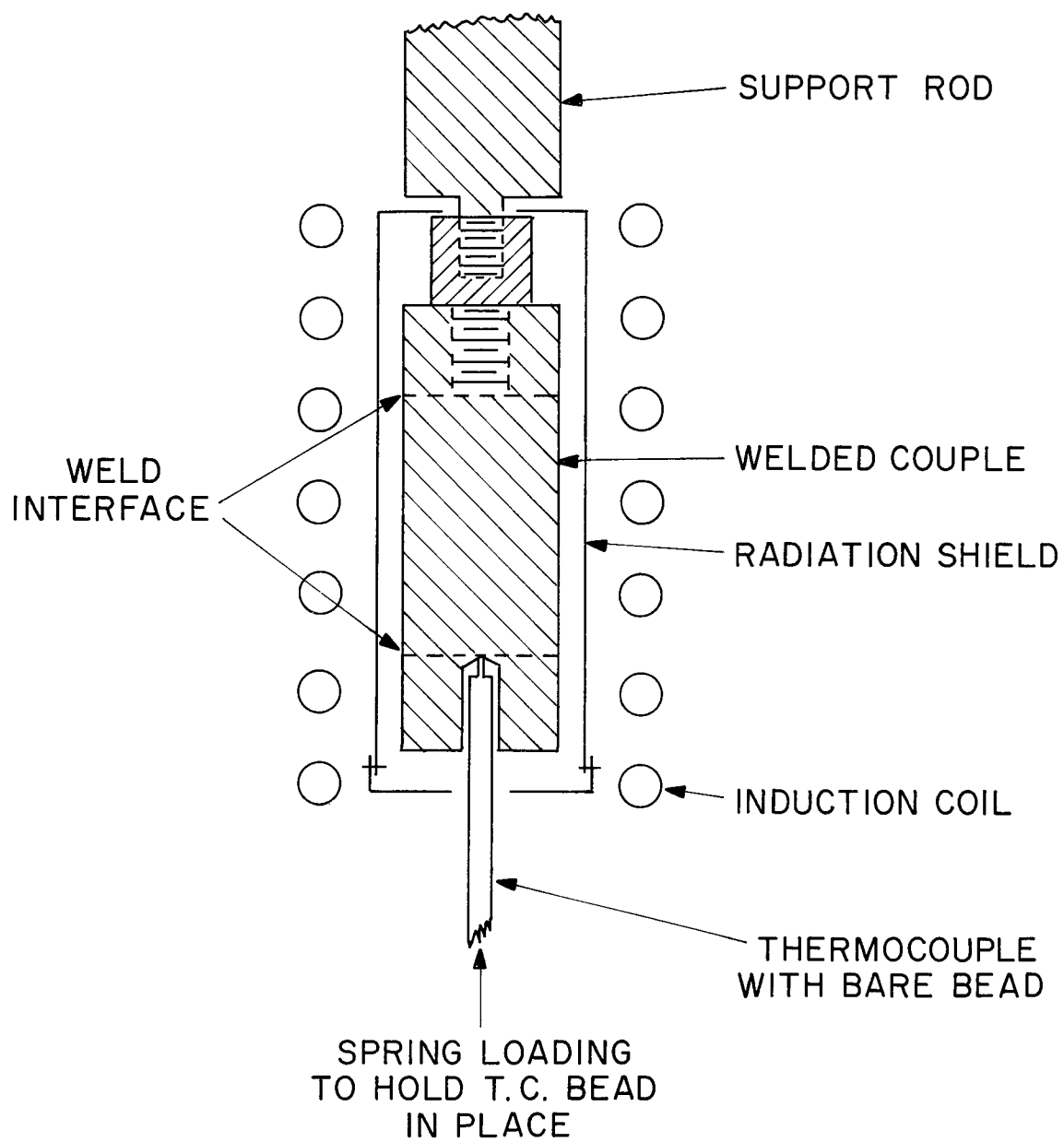


Figure 5 - Arrangement for induction heating of 0.1 hour diffusion anneals.

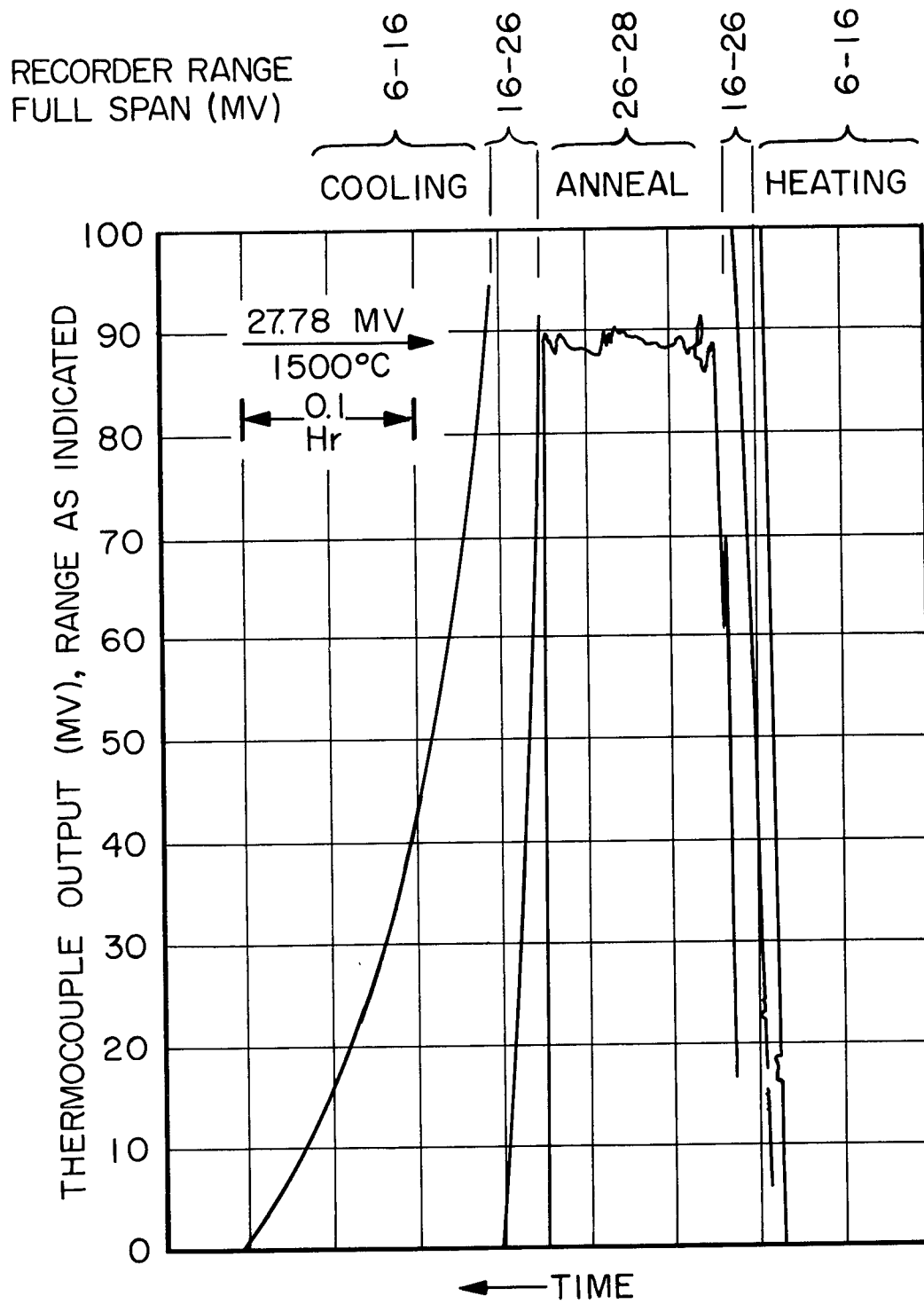


Figure 6 - Temperature measurement record for 0.1 hour anneal at 1500°C by induction heating. Couple #59, Cb-Cb 35 a/o Ti. Thermocouple: W3Re vs. W25Re; 0.018 mv/°C at 1500°C. The recorder span and zero were changed during the annealing process as indicated.



Figure 7 - Photo showing a mounted and polished pair of diffusion couples ready for insertion into the electron microprobe. Silver paint has been applied to achieve a grounding circuit between samples, standards and fixture ring. Fluorescing powder is also present. Couples #37 and #38. About 5X.

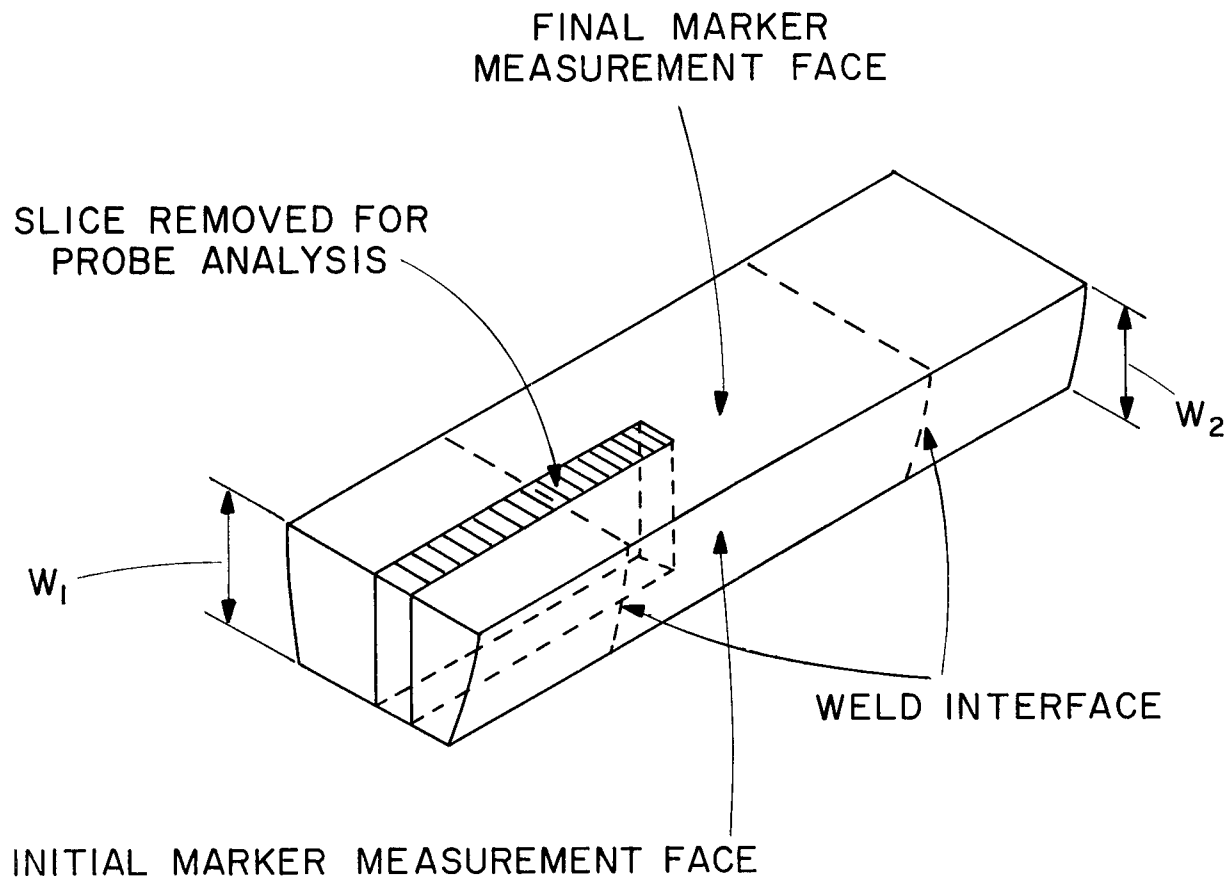


Figure 8 - Sketch showing the sectioning of a diffusion couple for microprobe analysis.

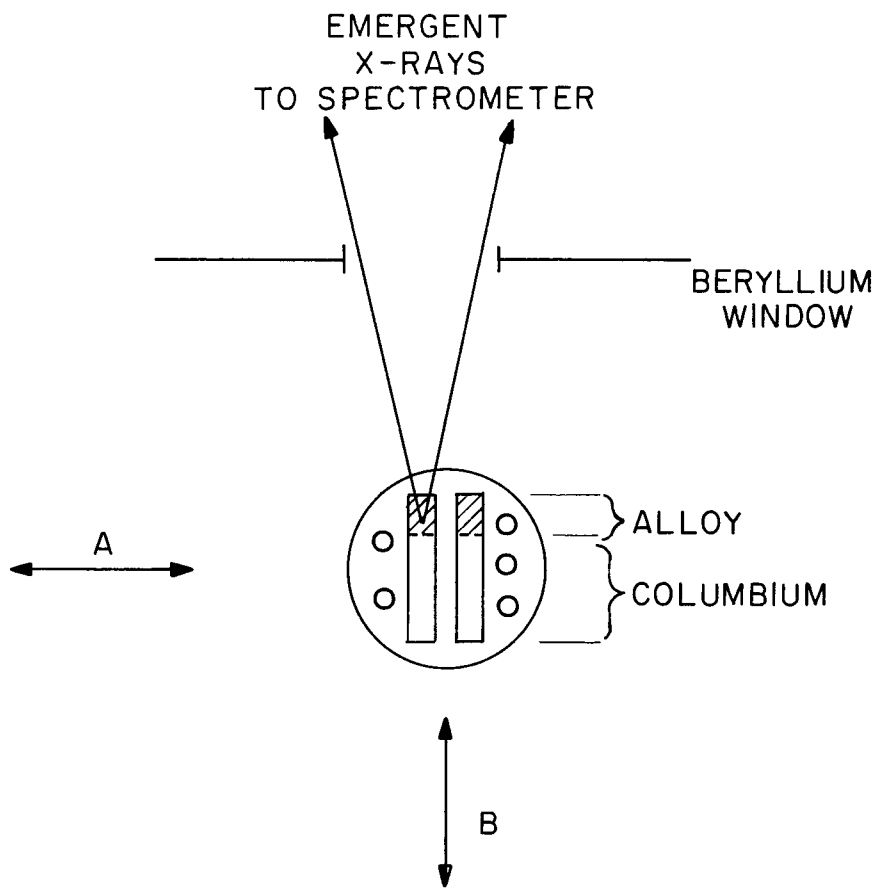


Figure 9 - Arrangement of specimen in microprobe.



Figure 10 - Photomicrograph of voids in the diffusion zone of a Cb-Cb 35 a/o Ti couple after diffusion at 2000°C for 10 hours. Couple #47. X200.

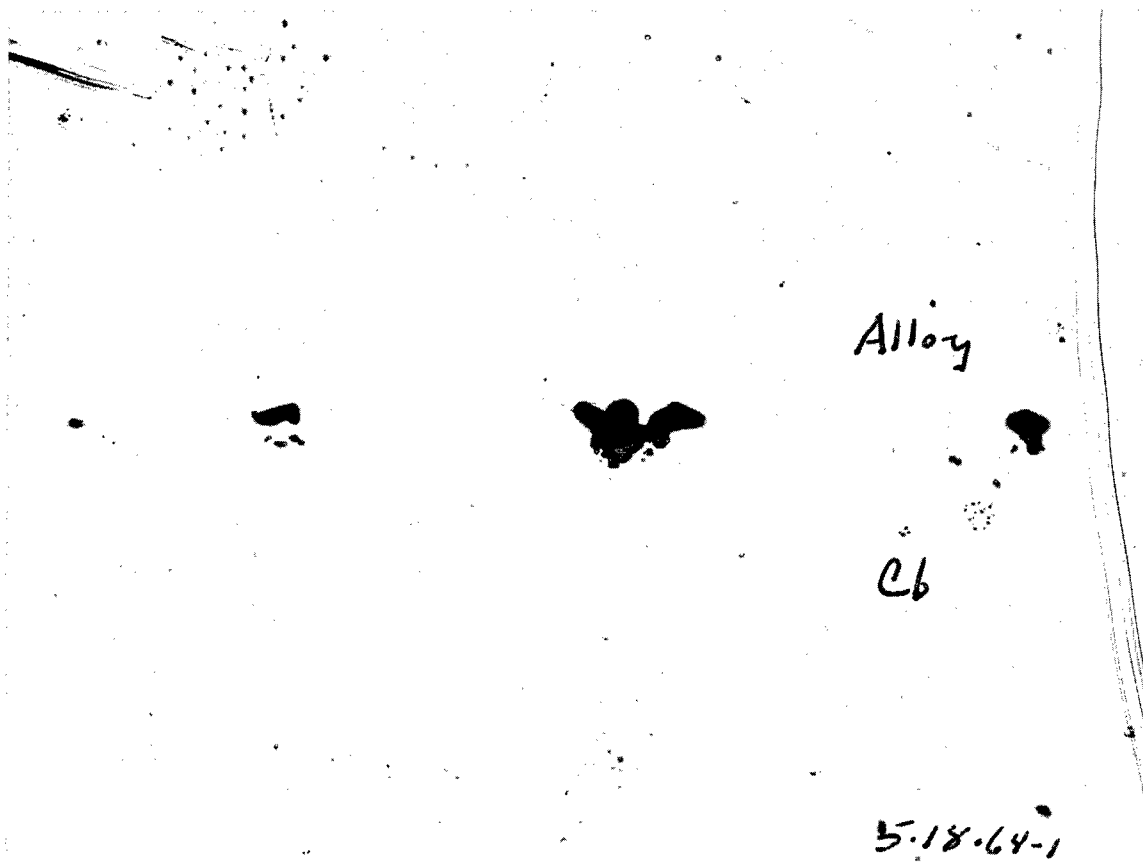


Figure 11 - Photomicrograph showing voids adjacent to marker material. Cb-Cb 35 a/o Ti couple diffused at 1500°C for 1000 hours. Voids are on the alloy side of the marker. Couple #48. X200.

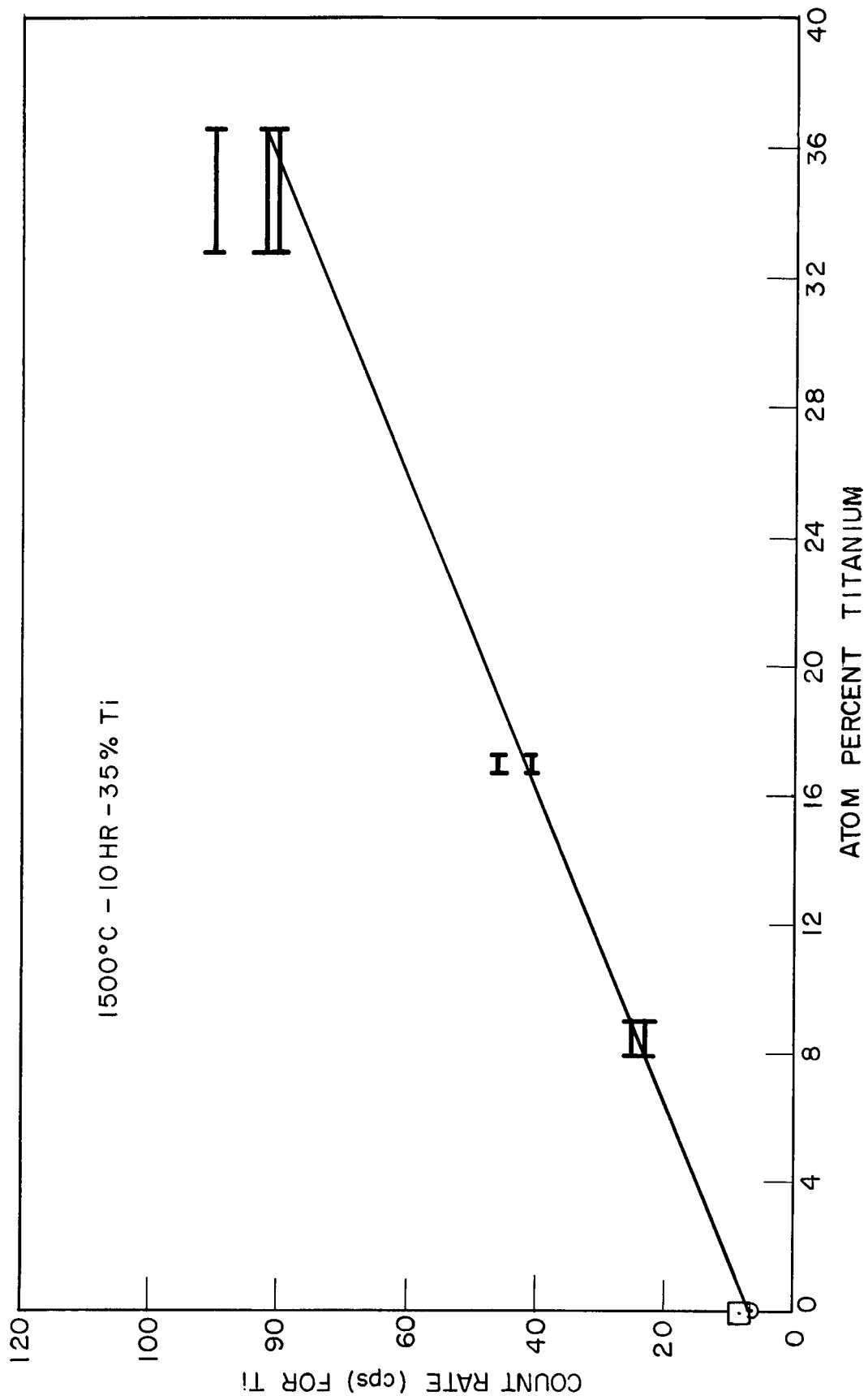


Figure 12 - Calibration curve: Count rate versus atom percent titanium. Couple #33; Cb-Cb 35 a/o Ti, 1500°C, 10 hr.

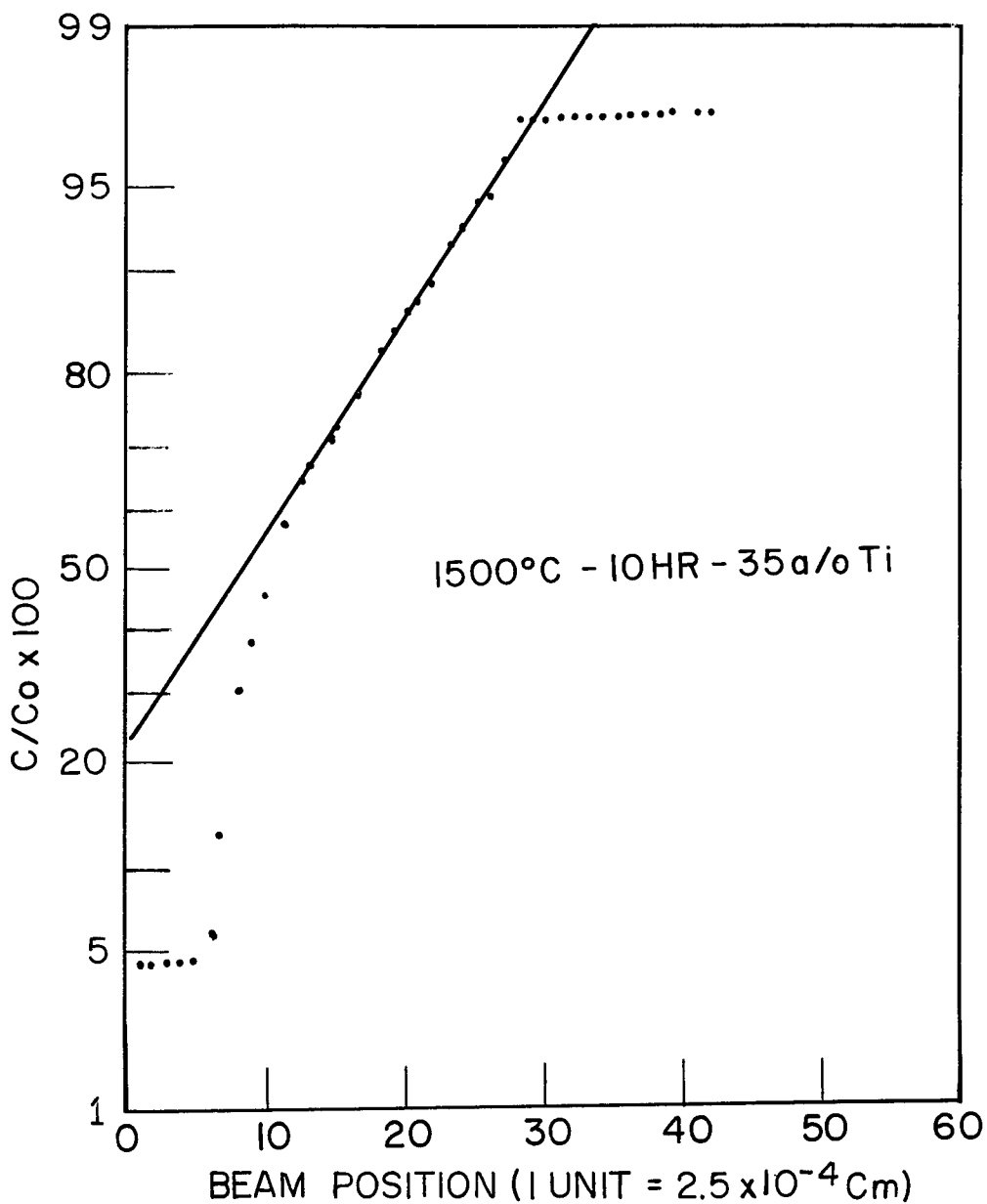


Figure 13(a) - Example of probability plot of relative concentration, C/C_0 , versus penetration distance. Couple #33, Cb-Cb 35 a/o Ti, 1500°C, 10 hr.

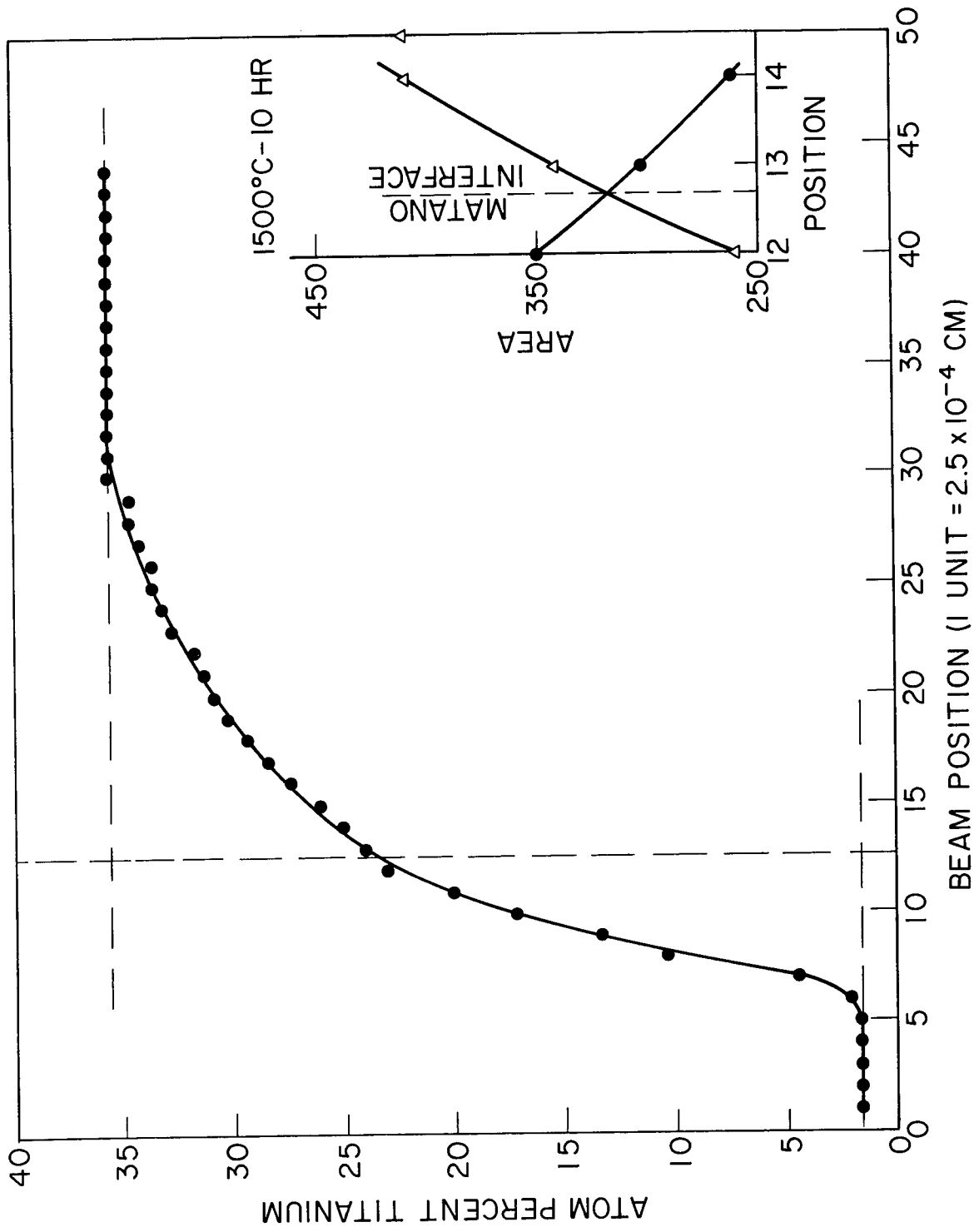


Figure 13(b) - Example of linear concentration (atom percent titanium) versus penetration distance (probe units). Couple #33, Cb-Cb 35 a/o Ti, 1500°C, 10 hr.

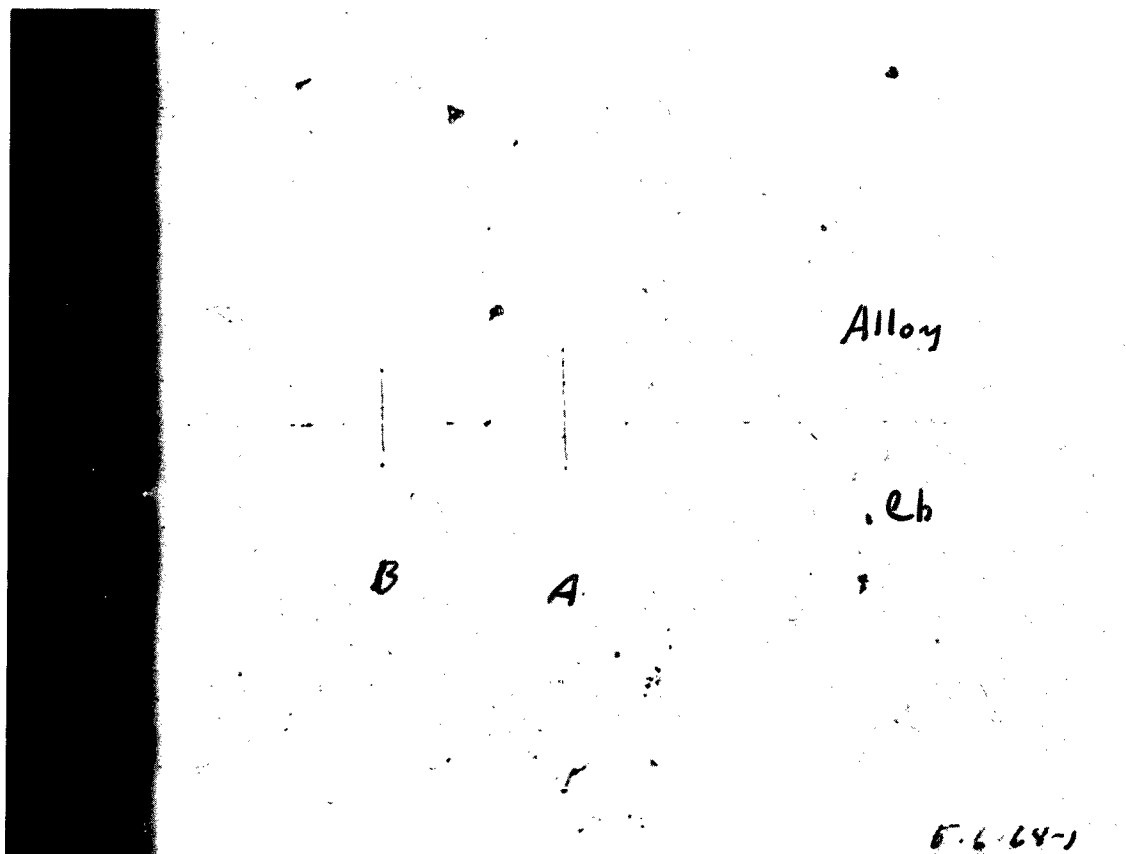


Figure 14(a) - Photomicrograph of contamination traces which indicate the region scanned by the electron microprobe. Couple #33 (Cb-Cb 35 a/o Ti, 1500°C, 10 hours). Thoria markers are clearly visible. X100.



Figure 14(b) - Same as in Figure 14(a), trace 'A'. X500.

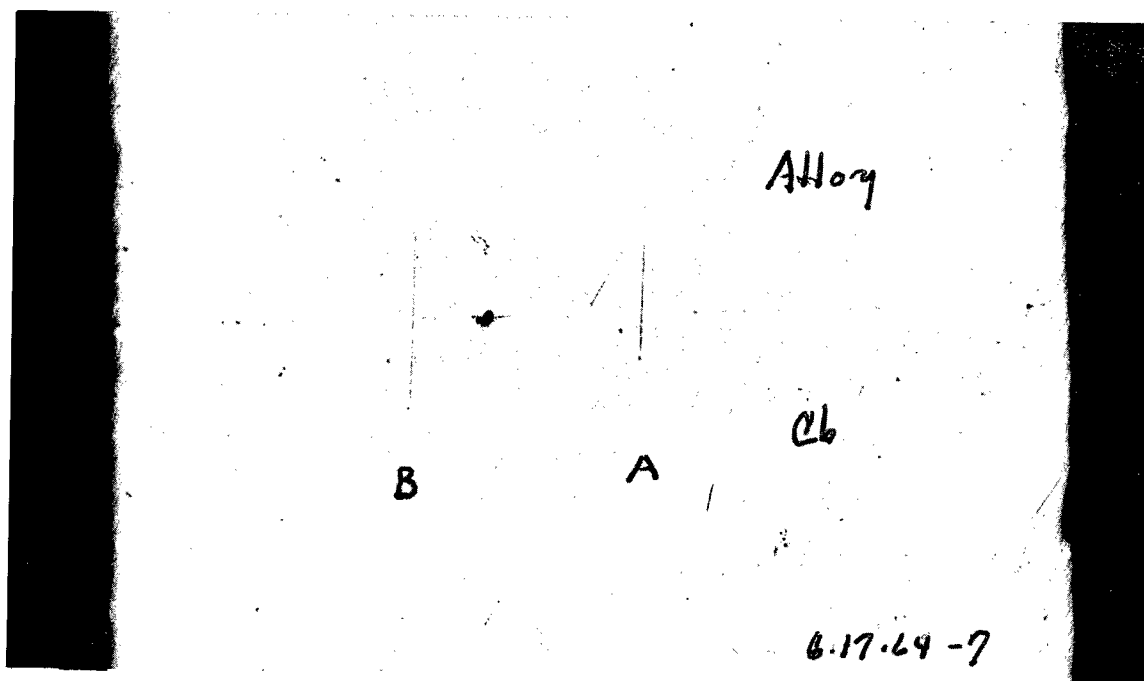


Figure 15(a) - Photomicrograph of microprobe contamination traces on diffusion couple #38 (Cb-Cb 8.5 a/o Ti, 1500°C, 120 hours). X100.

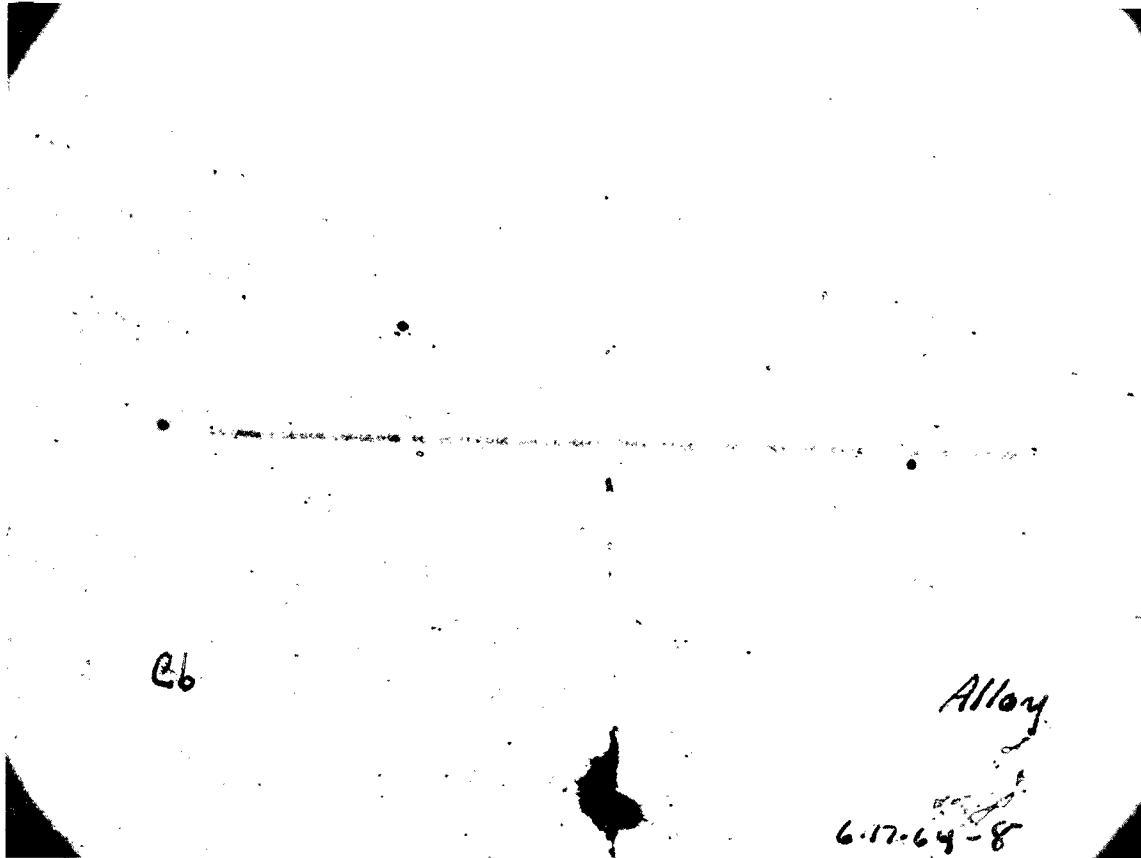


Figure 15(b) - Same as in Figure 15(a), trace 'B'. X500.

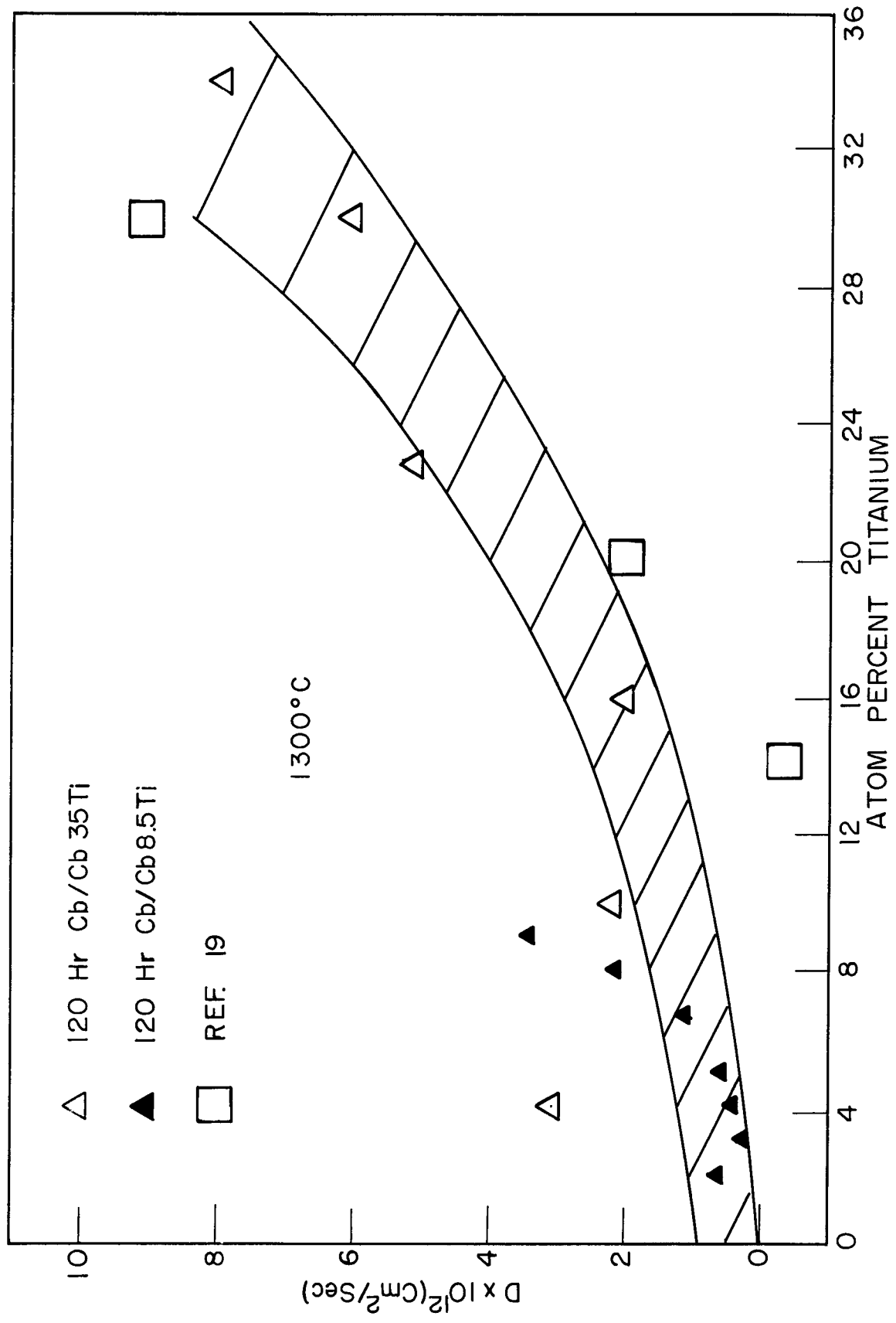


Figure 16 - Interdiffusion coefficient, D, versus composition (atom percent titanium) at 1300°C. Matano analysis.

0771166970MG

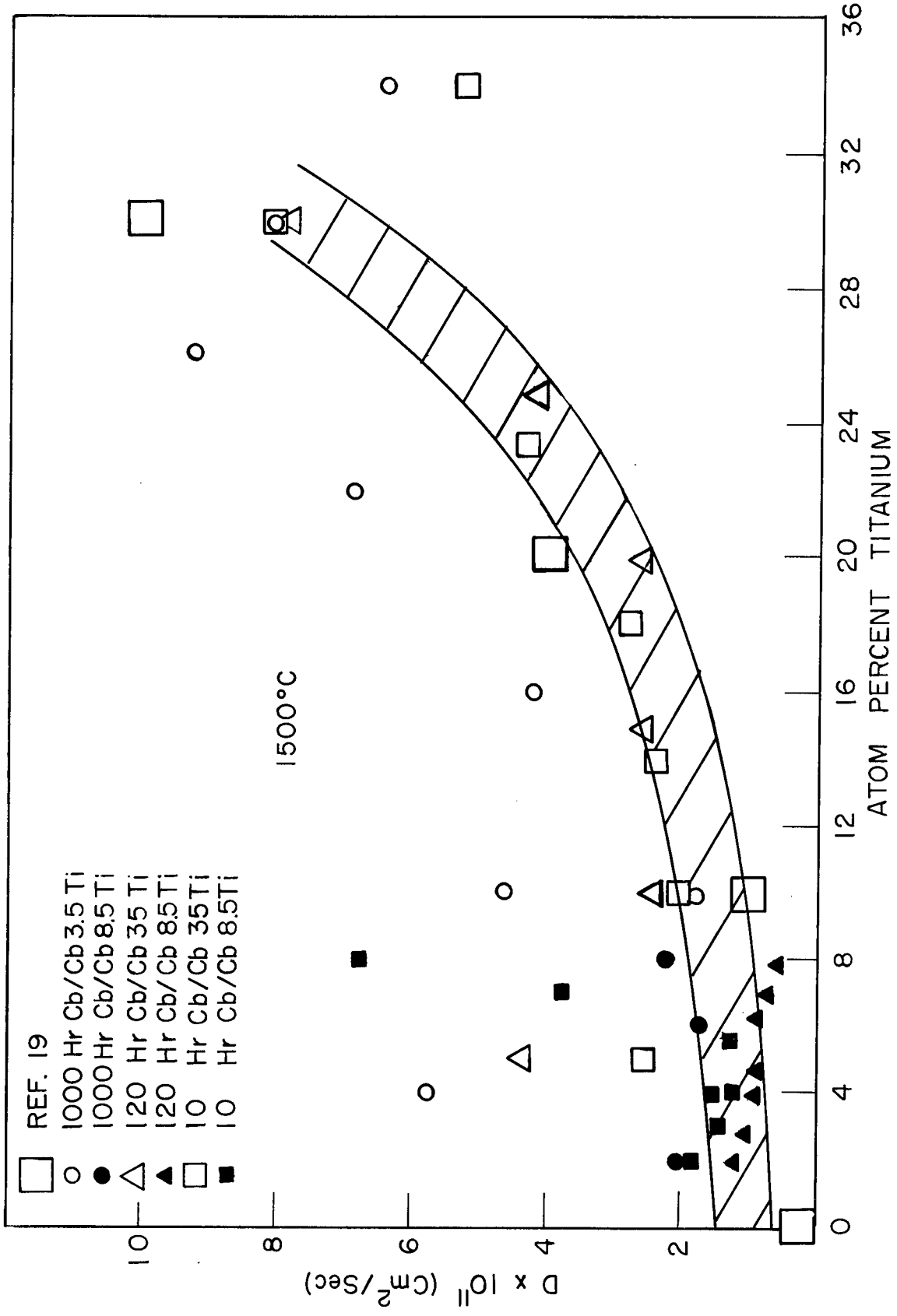


Figure 17 - Interdiffusion coefficient, D, versus composition (atom percent titanium) at 1500°C. Matano analysis.

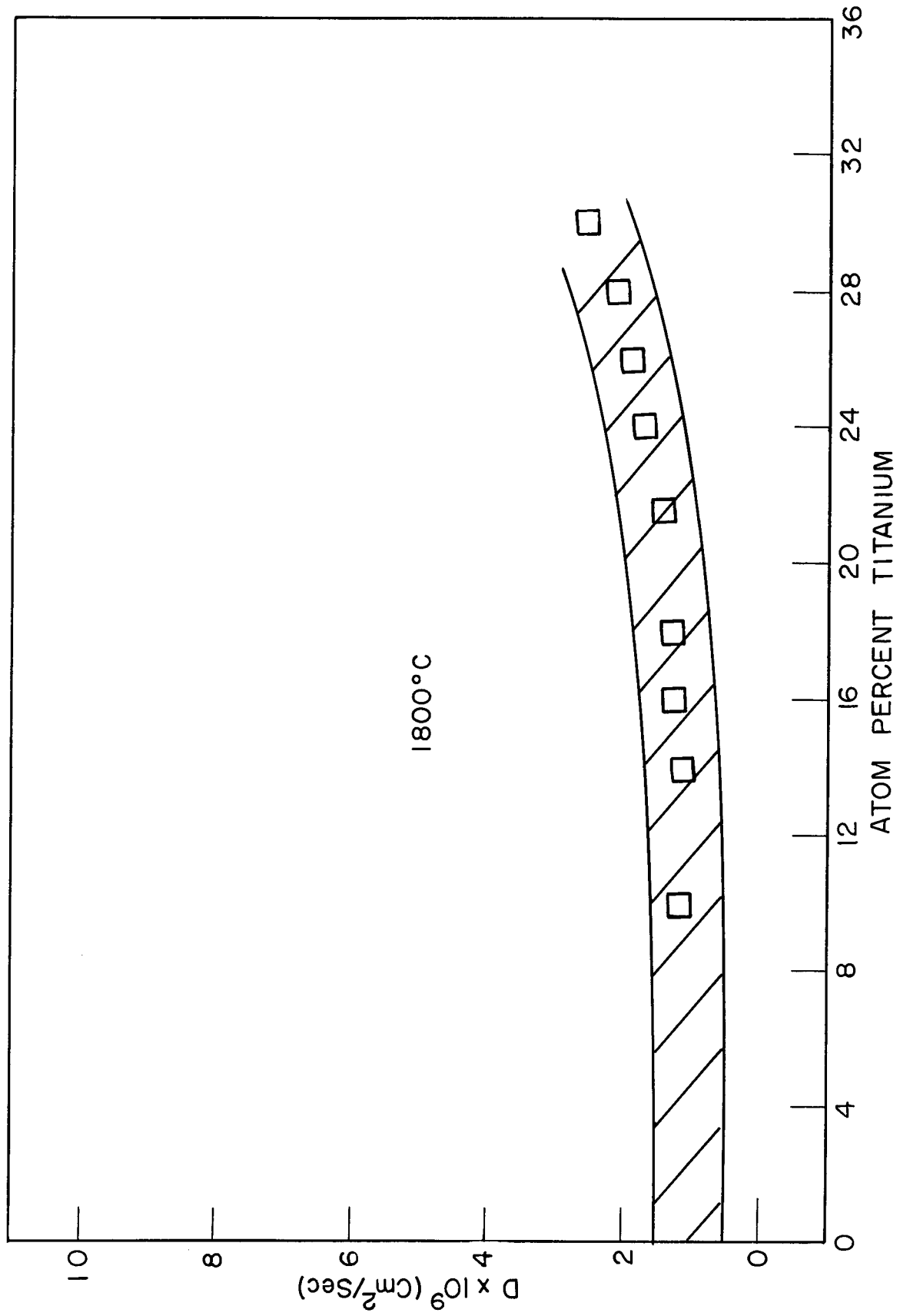


Figure 18 - Interdiffusion coefficient, D, versus composition (atom percent titanium) at 1800°C. Matano analysis.

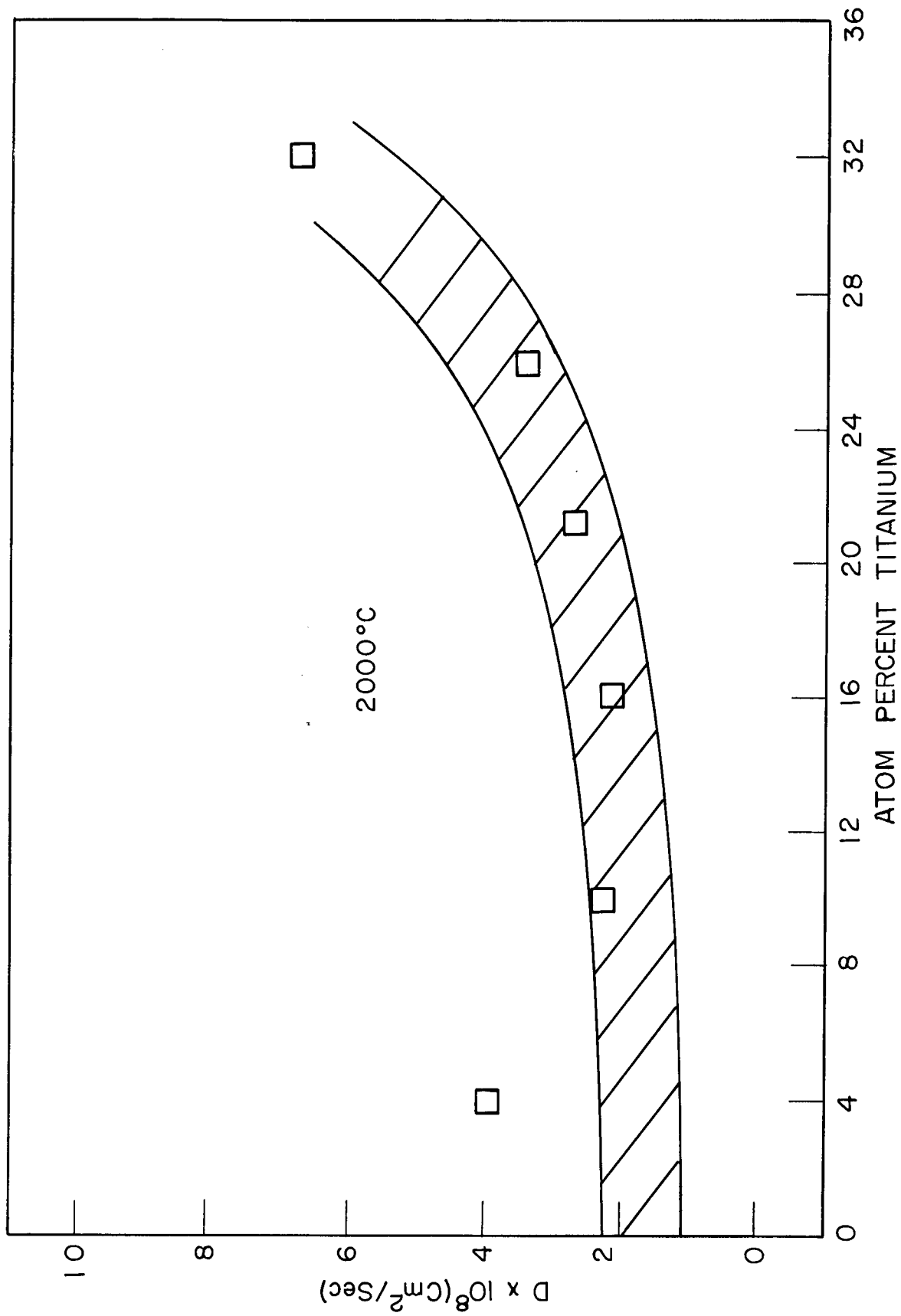


Figure 19 - Interdiffusion coefficient, D , versus composition (atom percent titanium) at 2000°C. Matano analysis.

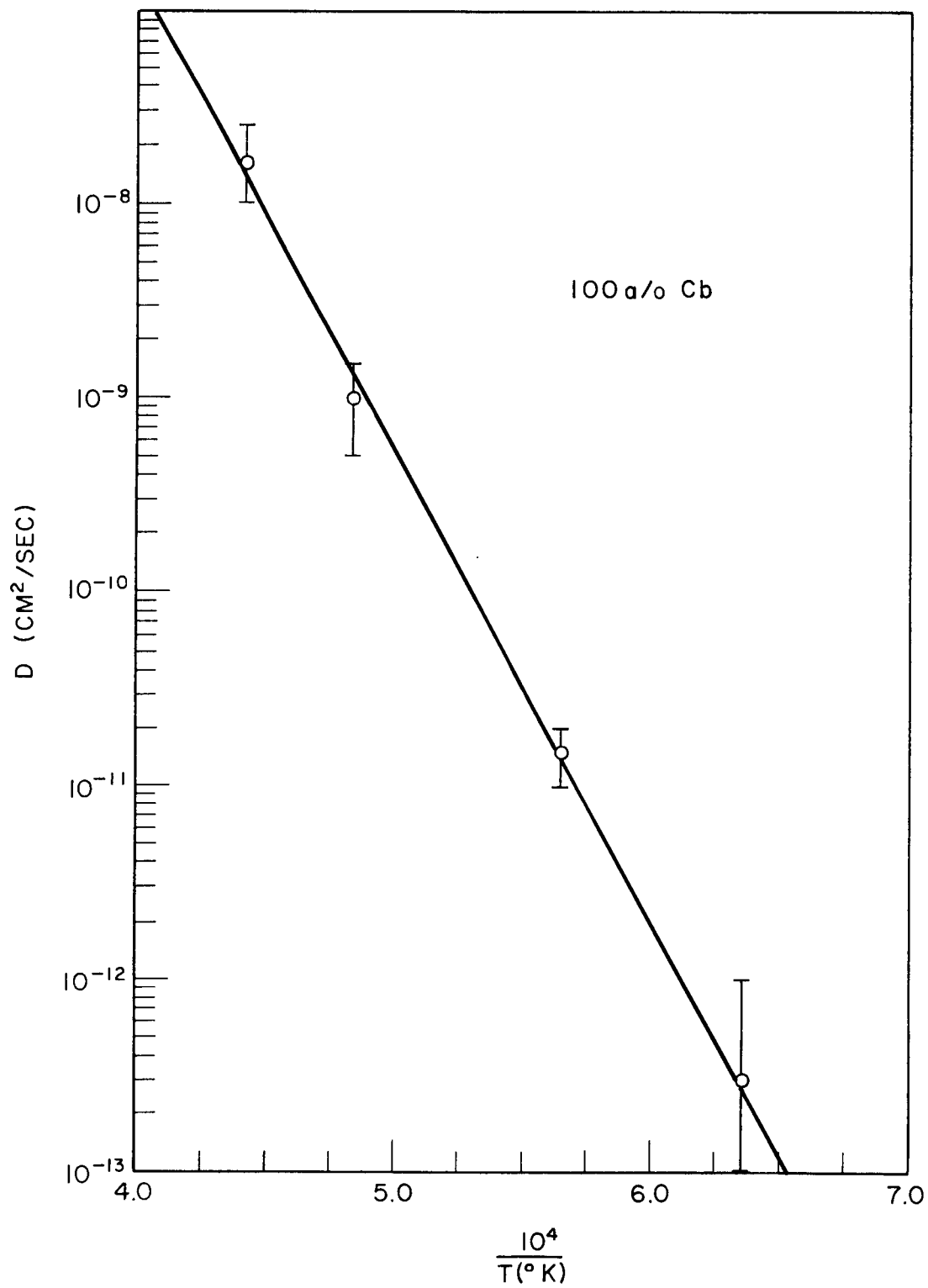


Figure 20 - Arrhenius plot of $\log D$ versus $\frac{1}{T}$ at 0 a/o Ti.
Data extracted from Figures 16-19.

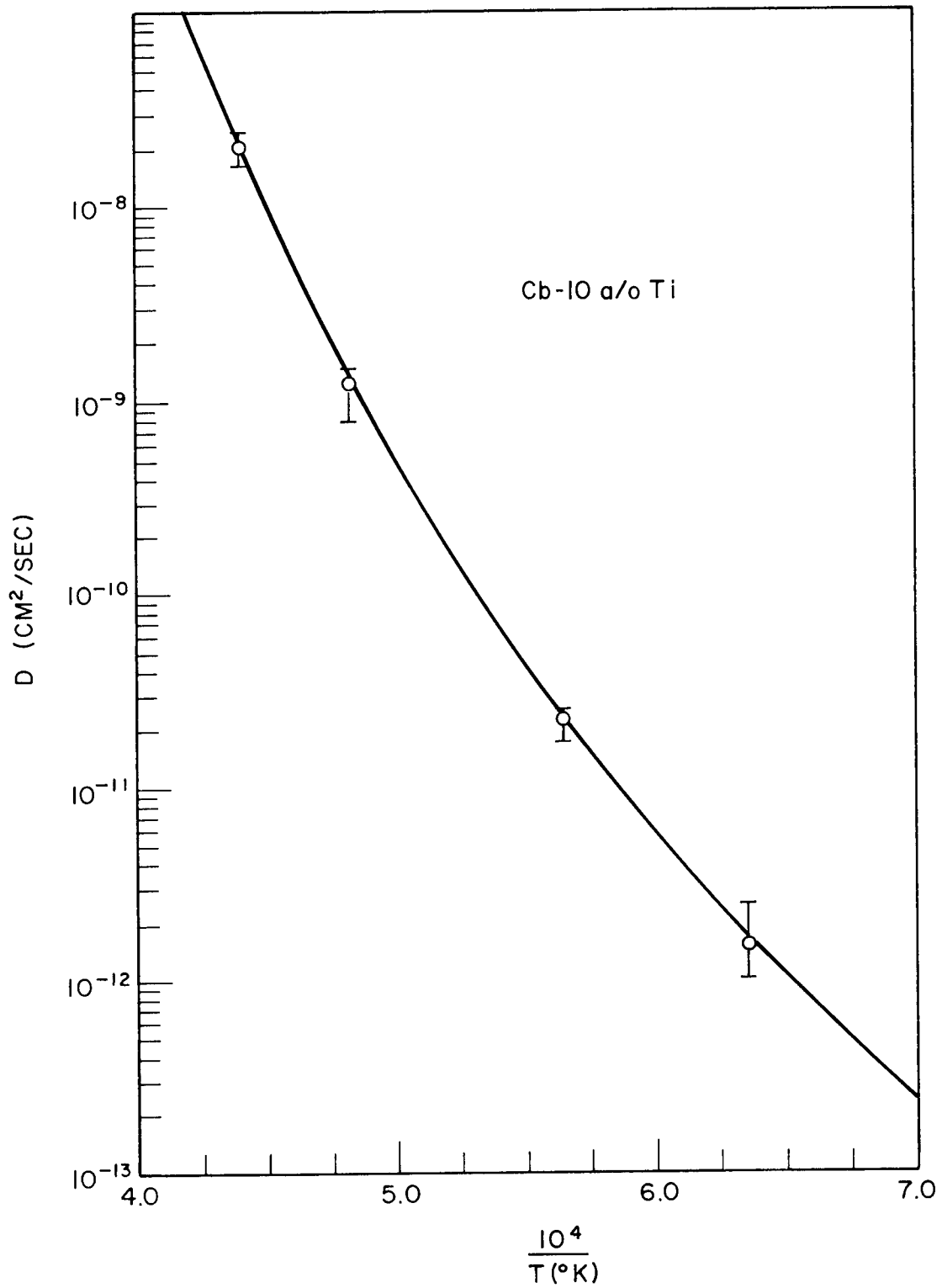


Figure 21 - Arrhenius plot of $\log D$ versus $\frac{1}{T}$ at Cb 10 a/o Ti.
Data extracted from Figures 16-19.

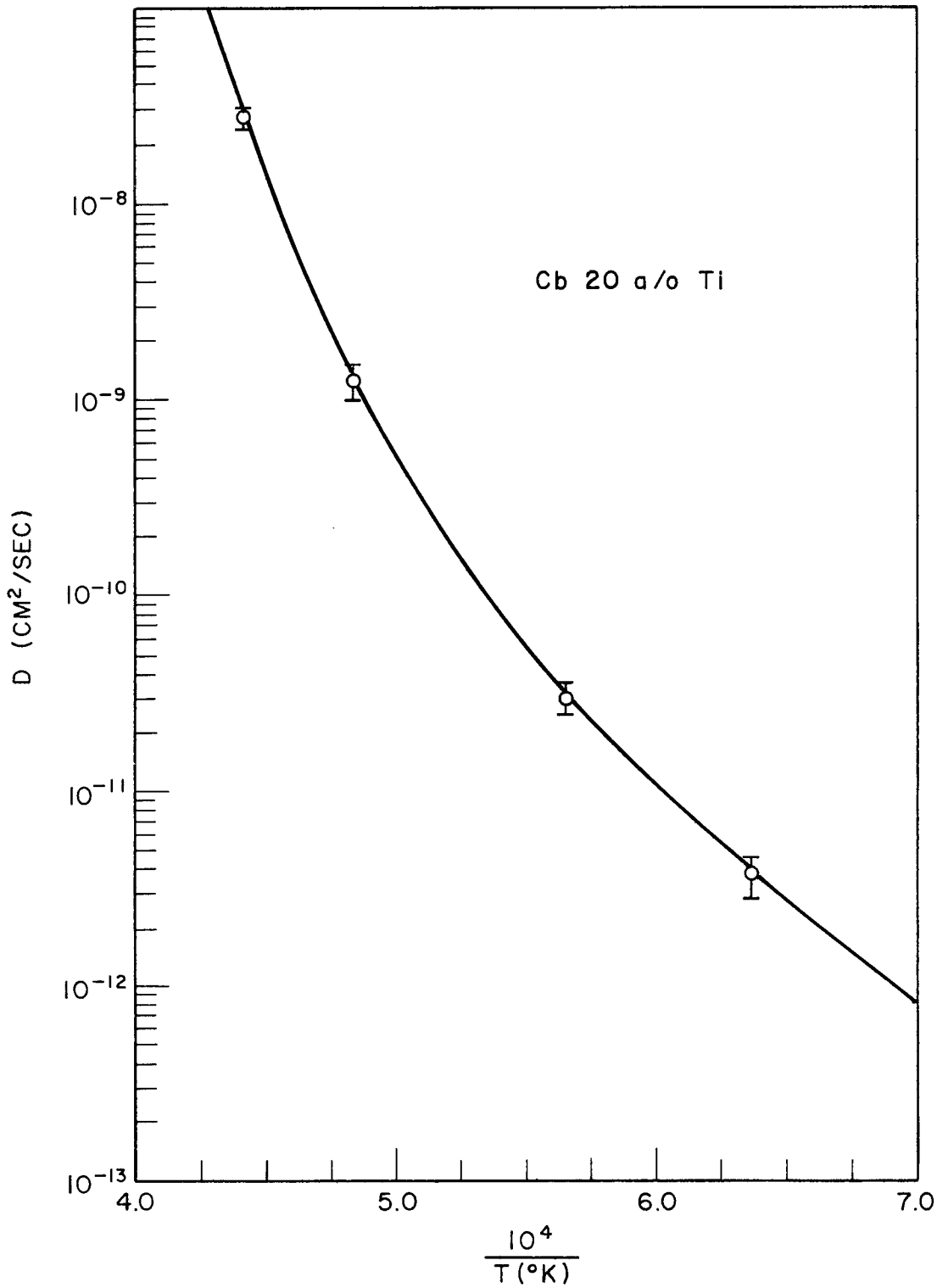


Figure 22 - Arrhenius plot of log D versus $\frac{1}{T}$ at Cb 20 a/o Ti. Data extracted from Figures 16-19.

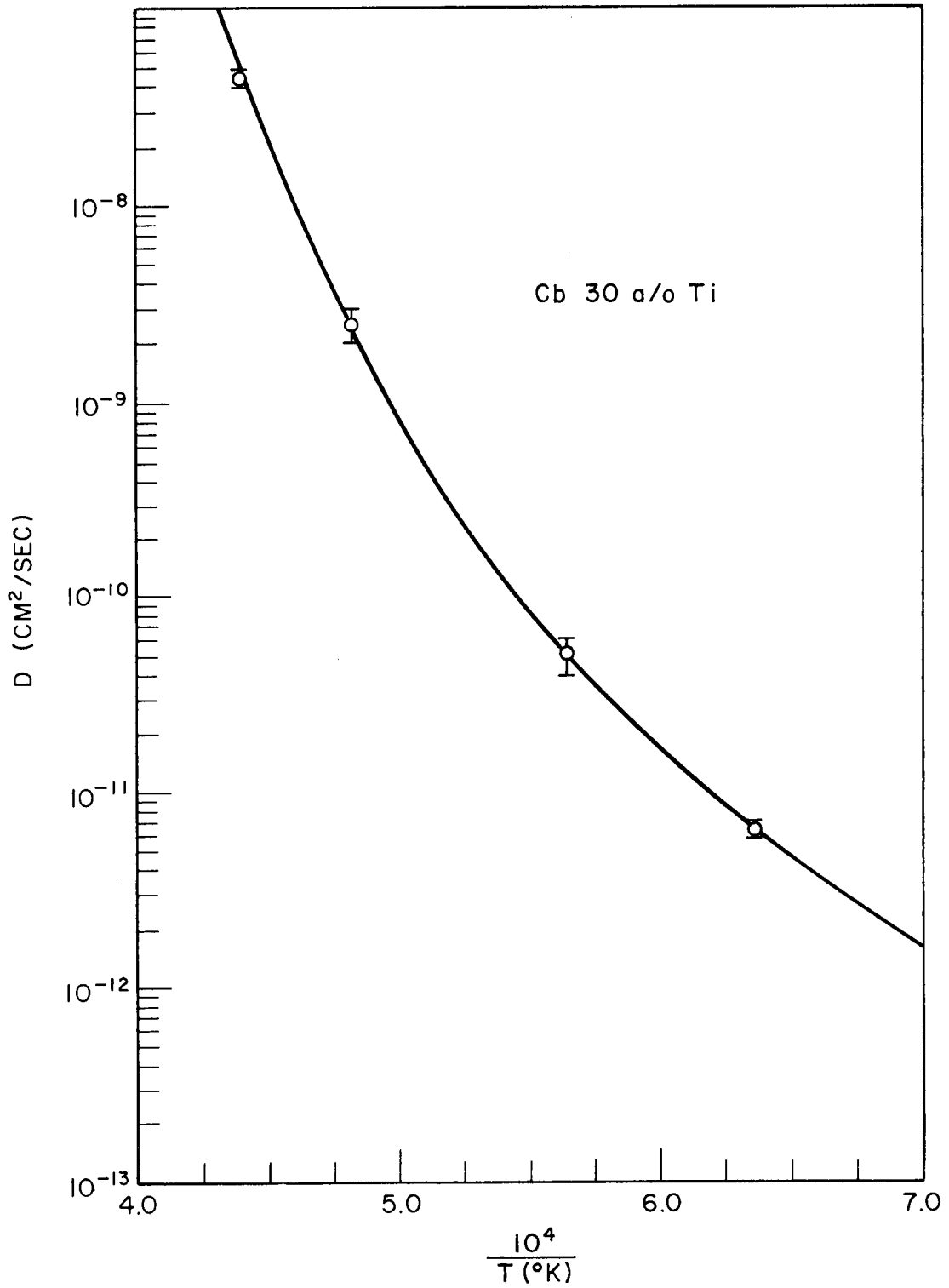


Figure 23 - Arrhenius plot of log D versus $\frac{1}{T}$ at Cb 30 a/o Ti.
 Data extracted from Figures 16-19.

Log D vs $\frac{1}{T}$ AT 0, 10, 20, AND 30 a/o Ti

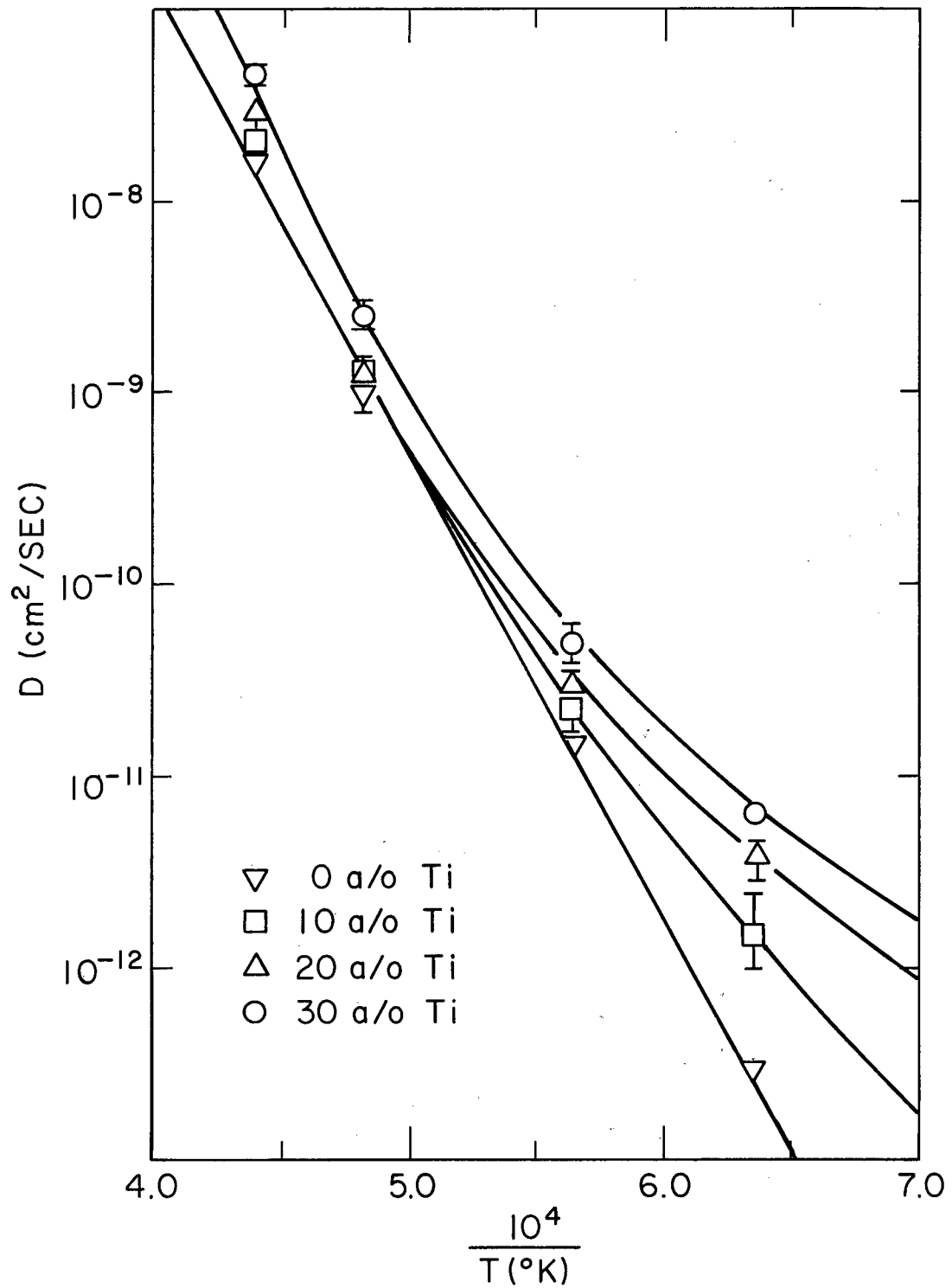


Figure 24 - Arrhenius plot of log D versus $\frac{1}{T}$ at 0, 10, 20 and 30 a/o Ti. (Superimpositions of Figures 20-23.)

UNCLASSIFIED

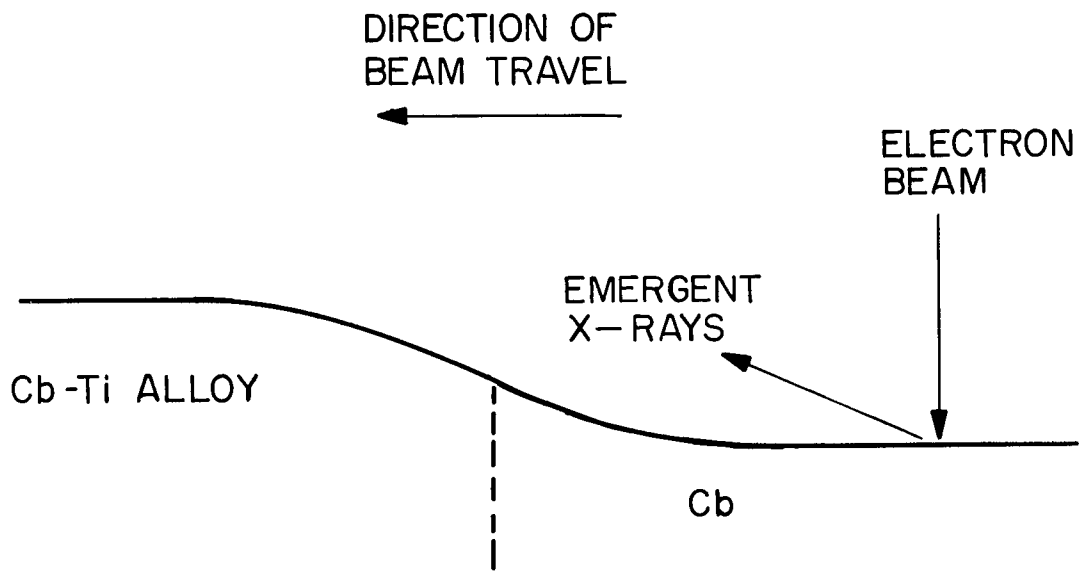


Figure 25 - Hypothetical section through diffusion couple perpendicular to weld interface.

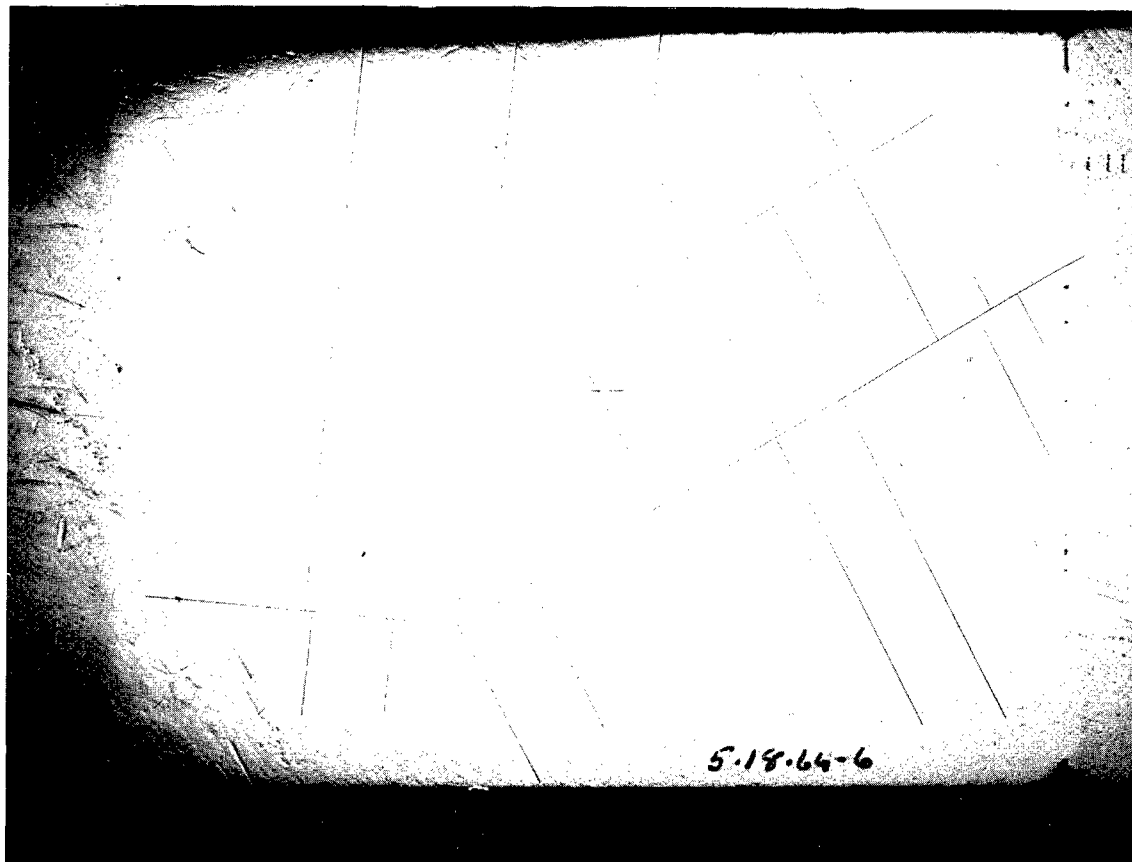


Figure 26(a) - Photomicrograph of couple #48, (Cb-Cb 35 a/o Ti, 1500°C, 1000 hours), showing a hydride-type of Widmanstätten precipitate. The crystallographic 'kink' in the center alloy section delineates a grain boundary -- the alloy consists of only two grains. Unetched. X20.

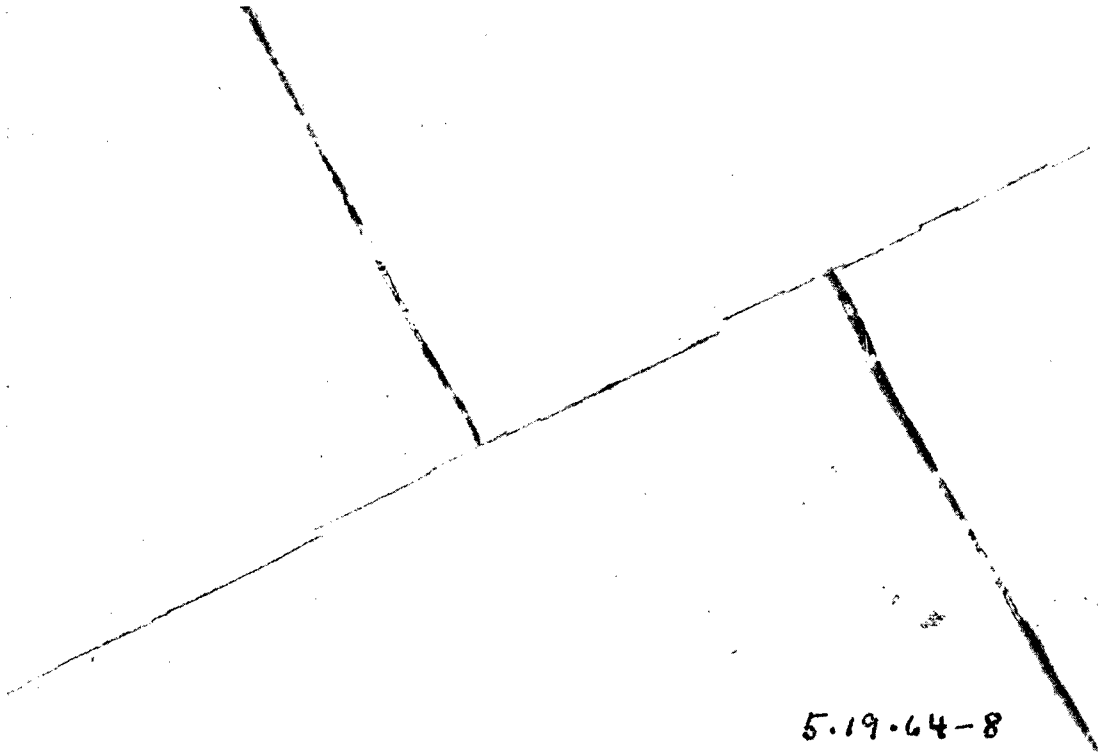


Figure 26(b) - Same as in Figure 26(a). Lightly etched, X100.

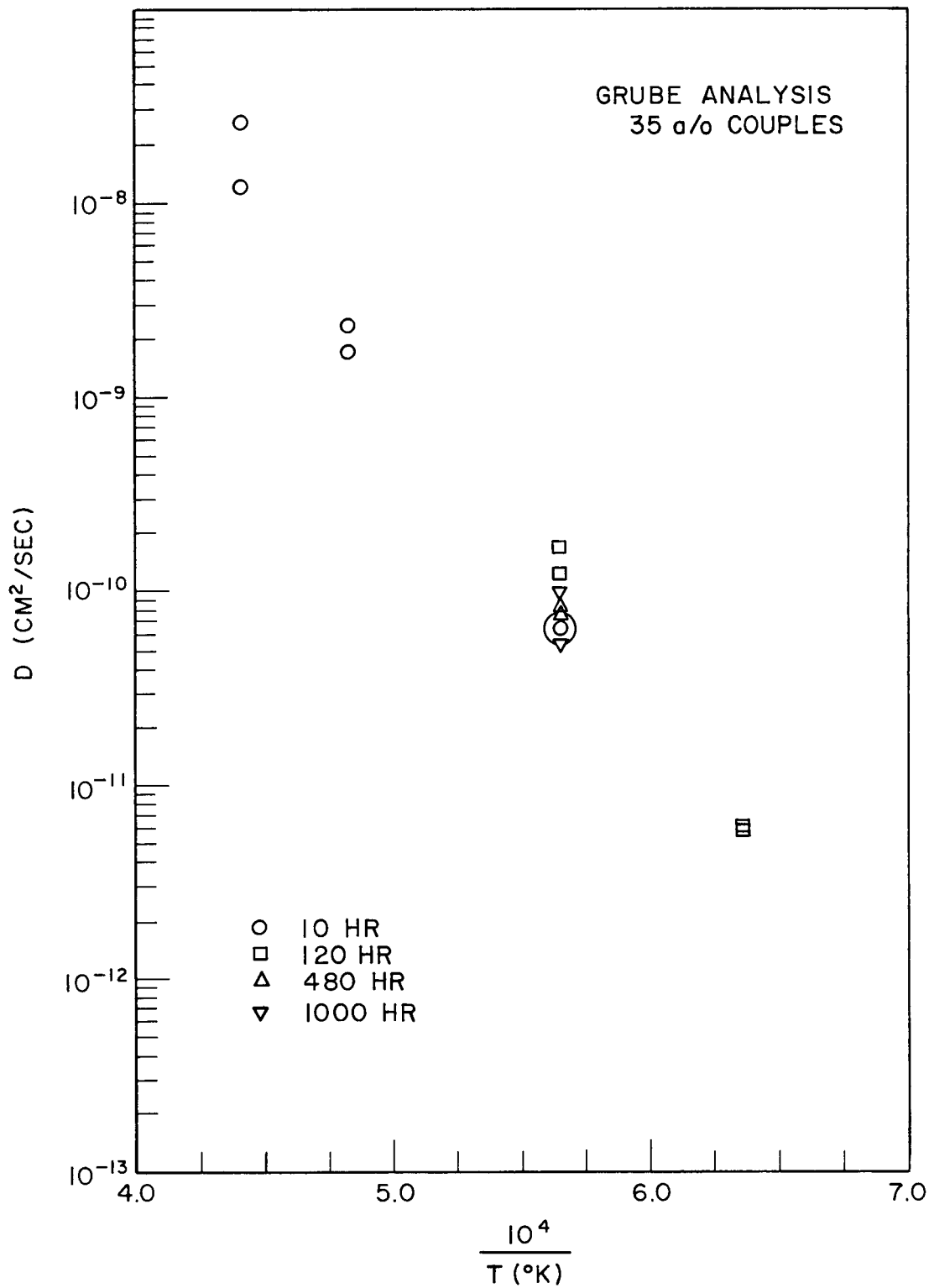


Figure 27(a) - Arrhenius plot of log D versus $\frac{1}{T}$ for Grube analysis of 35 a/o Ti couples.

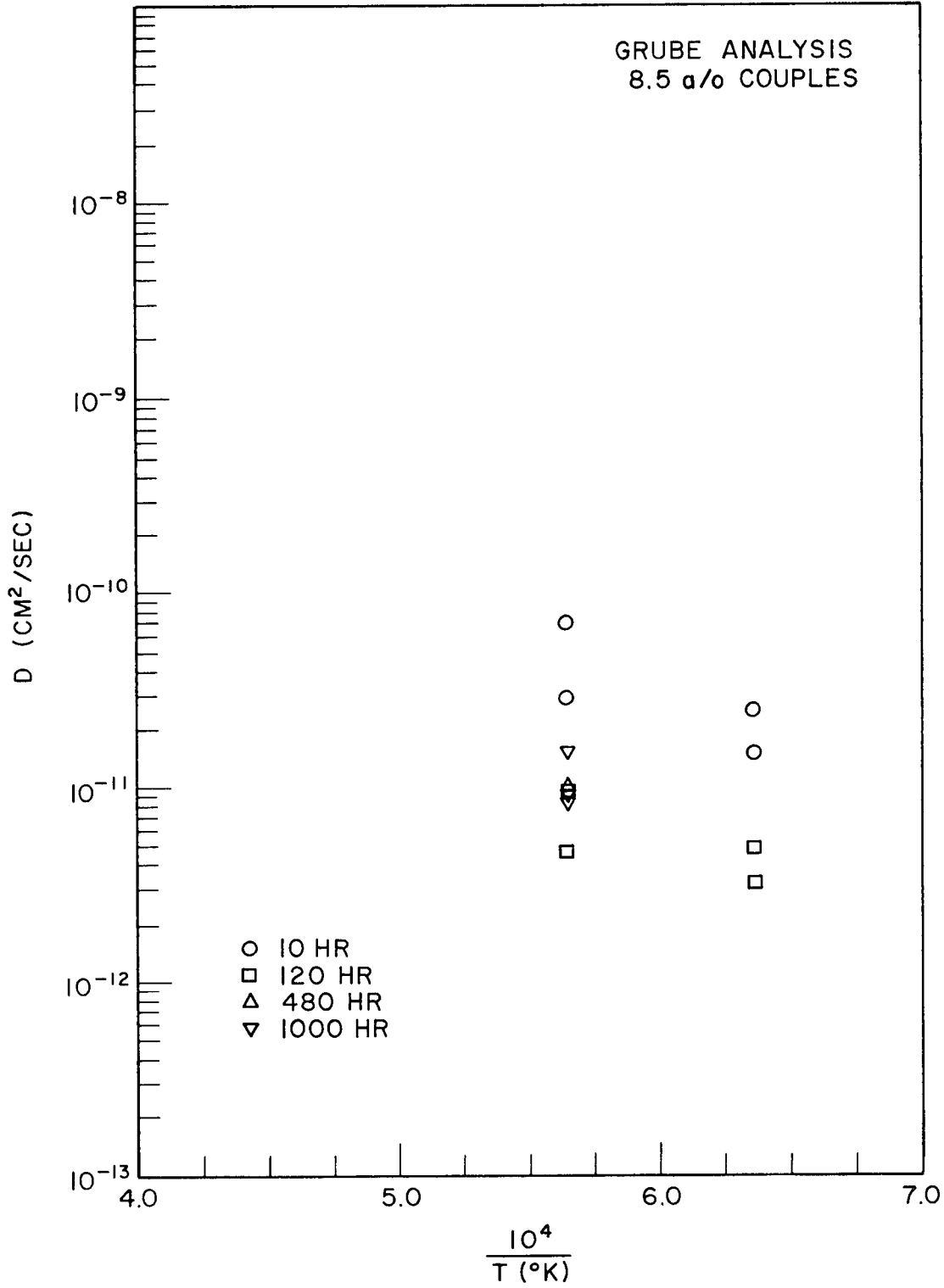


Figure 27(b) - Arrhenius plot of log D versus $\frac{1}{T}$ for Grube analysis of 8.5 a/o couples.

APPENDIX 1

DEVELOPMENT OF THE DIFFUSION
EQUATIONS AND THE REQUIRED SOLUTIONS*A.1-1 Formal Mathematical Development of Fick's Laws

The theory of diffusion in isotropic materials due to the random motion of molecules within that material is based upon the assumption that the rate of transfer of a diffusing substance through unit area of a reference plane within the material is proportional to the concentration measured normal to that plane. Thus,

$$F = - D \frac{\partial C}{\partial x} \quad [A.1-1]$$

where F is the rate of transfer per unit area of reference plane.

C is the concentration of diffusing substance.

x is the co-ordinate normal to the reference plane.

and D is the diffusion coefficient.

If F is in g/cm²-sec, C in g/cm³ and x in cm, D will have the usual units of cm²/sec. This is known as Fick's first law. In vector notation this becomes, for three dimensions,

* The present development of the equations and the solutions as utilized in this study follow Crank (2) and Andelin (30).

$$\vec{F} = - D \nabla C = - D (\vec{i} \frac{\partial C}{\partial x} + \vec{j} \frac{\partial C}{\partial y} + \vec{k} \frac{\partial C}{\partial z}) \quad [A.1-2]$$

where \vec{F} represents the flux at each point in the system.

Fick's second law, the differential equation describing the rate of accumulation in a unit volume, i.e., the rate of change of concentration with time may be obtained by considering a unit volume $dx dy dz$.

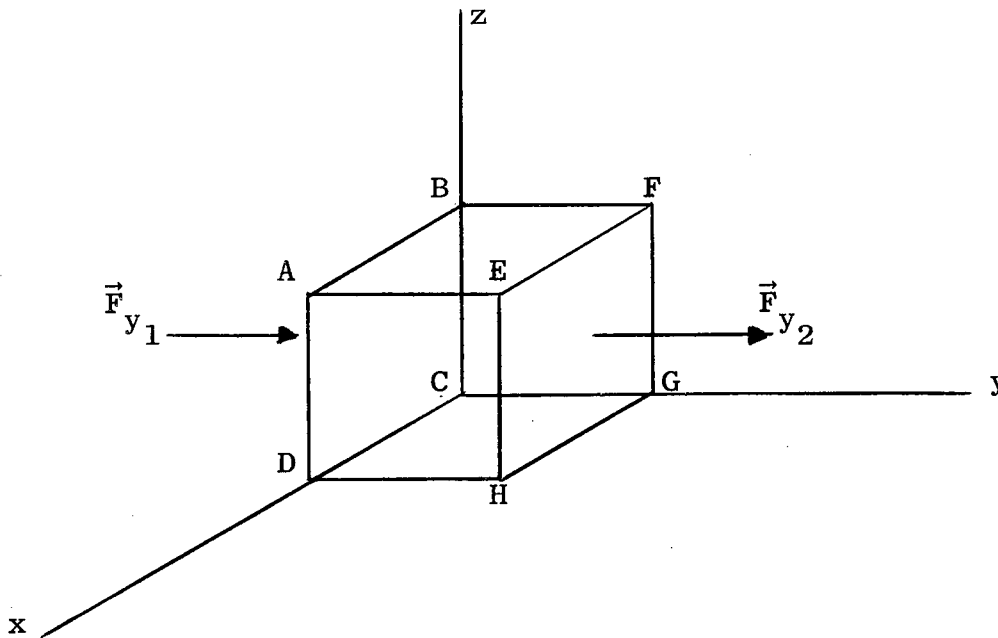


Fig. A.1-1

The material balance for this element of volume will be the sum of the inward and outward flux. The rate at which material enters through face A B C D is

$$\vec{j} \cdot [\vec{F}(x, y, z)] dx dz,$$

and from face E F G H is

$$\vec{j} \cdot [\vec{F}(x, y, z) + \frac{\partial \vec{F}}{\partial y} dy] dx dz$$

The net loss between these two faces is

$$\vec{j} \cdot \frac{\partial \vec{F}}{\partial y} dx dy dz.$$

Similarly, for the other two pairs of faces, the net flux will be

$$\vec{i} \cdot \frac{\partial \vec{F}}{\partial x} dx dy dz \text{ and } \vec{k} \cdot \frac{\partial \vec{F}}{\partial z} dx dy dz.$$

The total rate at which material is diffusing from the volume unit is

$$\left[\vec{i} \cdot \frac{\partial \vec{F}}{\partial x} + \vec{j} \cdot \frac{\partial \vec{F}}{\partial y} + \vec{k} \cdot \frac{\partial \vec{F}}{\partial z} \right] dx dy dz \quad [\text{A.1-3}]$$

$$= \nabla \cdot \vec{F} dV$$

This is also given by

$$- \frac{\partial C}{\partial t} dV. \quad [\text{A.1-4}]$$

Combining Eq. [A.1-3] and Eq. [A.1-4] we have

$$- \frac{\partial C}{\partial t} = \nabla \cdot \vec{F}.$$

Substituting Eq. [A.1-2] for \vec{F} we have Fick's second law in its general form,

$$- \frac{\partial C}{\partial t} = \nabla \cdot \vec{F} = - \nabla \cdot (D \nabla C). \quad [\text{A.1-5}]$$

For one dimension this becomes

$$\frac{\partial C}{\partial t} = \frac{\partial}{\partial x} \left(D \frac{\partial C}{\partial x} \right), \quad [\text{A.1-6}]$$

and if D is constant,

$$\frac{\partial C}{\partial t} = D \frac{\partial^2 C}{\partial x^2}. \quad [\text{A.1-7}]$$

A.1-2 Solution when D is constant:

The solution to the diffusion equation for constant D,

$$\frac{\partial C}{\partial t} = D \frac{\partial^2 C}{\partial x^2}, \quad [\text{A.1-7}]$$

is $C = \frac{A}{t^{1/2}} e^{-x^2/4Dt}$

where A is a constant.

This may be checked by differentiation. Crank (2) shows that for a plane source of quantity M deposited at $x = 0$,

$$A = \frac{M}{2\sqrt{\pi D}}$$

or
$$C = \frac{M}{2\sqrt{\pi D t}} e^{-x^2/4Dt} \quad [A.1-8]$$

The conditions of the present experimental investigation are given by the boundary conditions describing diffusion from one homogeneous infinite cylinder into another. These conditions are

$$\begin{aligned} t = 0, x < 0, C &= 0 \\ t = 0, x > 0, C &= C_0 \\ \text{all } t, x = \pm \infty, \frac{\partial C}{\partial x} &= 0 \end{aligned} \quad [A.1-9]$$

The solution for these conditions may be obtained by considering an infinite number of line sources and by superposing the corresponding elementary solutions, Eq.[A.1-8].

In Figure A.1-2 consider the quantity of Material, M , in the

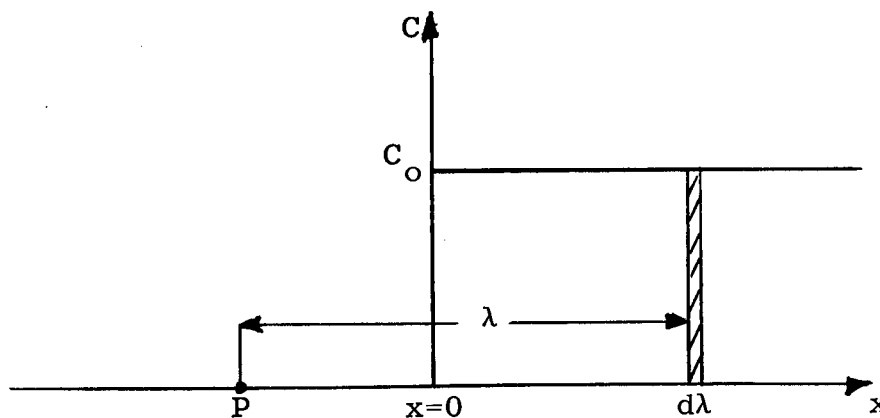


Fig. A.1-2

element $C_o d\lambda$ to be a line source. The concentration at some point, P, at a time, t, is then given by Eq.[A.1-8] to be

$$C_p = \frac{C_o d\lambda}{2 \sqrt{\pi Dt}} e^{-\lambda^2/4 Dt}$$

The summation of the complete initial distribution is

$$C(x, t) = \frac{C_o}{2 \sqrt{\pi Dt}} \int_x^\infty e^{-\lambda^2/4 Dt} d\lambda. \quad [A.1-10]$$

Substituting $\eta = \frac{\lambda}{2 \sqrt{Dt}}$, we have the solution

$$C(x, t) = \frac{C_o}{\sqrt{\pi}} \int_{\frac{x}{2\sqrt{Dt}}}^\infty e^{-\eta^2} d\eta. \quad [A.1-11]$$

A standard mathematical function, the error function, is defined by

$$\text{erf}(z) = \frac{2}{\sqrt{\pi}} \int_0^z e^{-\eta^2} d\eta.$$

The properties of the error function are such that

$$\int_z^\infty e^{-\eta^2} d\eta = \int_0^\infty e^{-\eta^2} d\eta - \int_0^z e^{-\eta^2} d\eta = 1 - \text{erf}(z) = \text{erfc}(z)$$

Comparing terms with Eq.[A.1-11], the required solution to Eq.[A.1-7] for the infinite boundary conditions, Eq.[A.1-9], may be written

$$C(x, t) = \frac{C_o}{2} \left[1 - \text{erf} \left(\frac{x}{2 \sqrt{Dt}} \right) \right]$$

or

$$C(x, t) = \frac{C_o}{2} \text{erfc} \left(\frac{x}{2 \sqrt{Dt}} \right)$$

} [A.1-12]

From the properties of the error function (2) it follows that all $t > 0$, at $x = 0$,

$$C = \frac{C_0}{2}. \quad [A.1-13]$$

This last relationship defines the origin from which x is reckoned for applications to Eq.[A.1-12].

The relationships Eq.[A.1-12] and Eq.[A.1-13] are known as the Grube Solution to the diffusion equation after G. Grube (14) who first applied them to diffusion in solid metals.

A.1-3 Boltzmann-Matano Solution

If the diffusion coefficient is a single valued function of concentration, the diffusion equation is

$$\frac{\partial C}{\partial t} = \frac{\partial}{\partial x} \left(D \frac{\partial C}{\partial x} \right). \quad [A.1-6]$$

Boltzmann (31) showed that for the infinite boundary conditions Eq.[A.1-9] the transformation

$$\lambda = \frac{x}{2\sqrt{t}} \quad [A.1-14]$$

may be applied to yield the ordinary differential equation

$$- 2\lambda \frac{dC}{d\lambda} = \frac{d}{d\lambda} \left(D \frac{dC}{d\lambda} \right). \quad [A.1-15]$$

Integration with respect to λ yields

$$- 2 \int_{C_0}^C \lambda dC = \left[D \frac{dC}{d\lambda} \right]_{C_0}^{C_1}. \quad [A.1-16]$$

The boundary condition that $\left. \frac{dC}{dx} \right|_{x=+\infty} = 0$ gives $\left. \frac{dC}{d\lambda} \right|_{C_0} = 0$ so that

$$- 2 \int_{C_0}^C \lambda dC = D \left. \frac{dC}{d\lambda} \right|_{C_1}.$$

Rearranging and introducing x and t for λ yields

$$D_{C_1} = - \frac{1}{2t} \frac{dx}{dC} \Big|_{C_1} \cdot \int_{C_0}^{C_1} x dC . \quad [A.1-17]$$

When the condition that $\frac{dC}{dx} \Big|_{x=-\infty} = 0$ is also applied to Eq. [A.1-16],

then

$$\int_0^{C_0} \lambda dC = \int_0^{C_0} x dC = 0 . \quad [A.1-18]$$

The significance of this final relationship in the evaluation of D is evident from Fig. A.1-3.

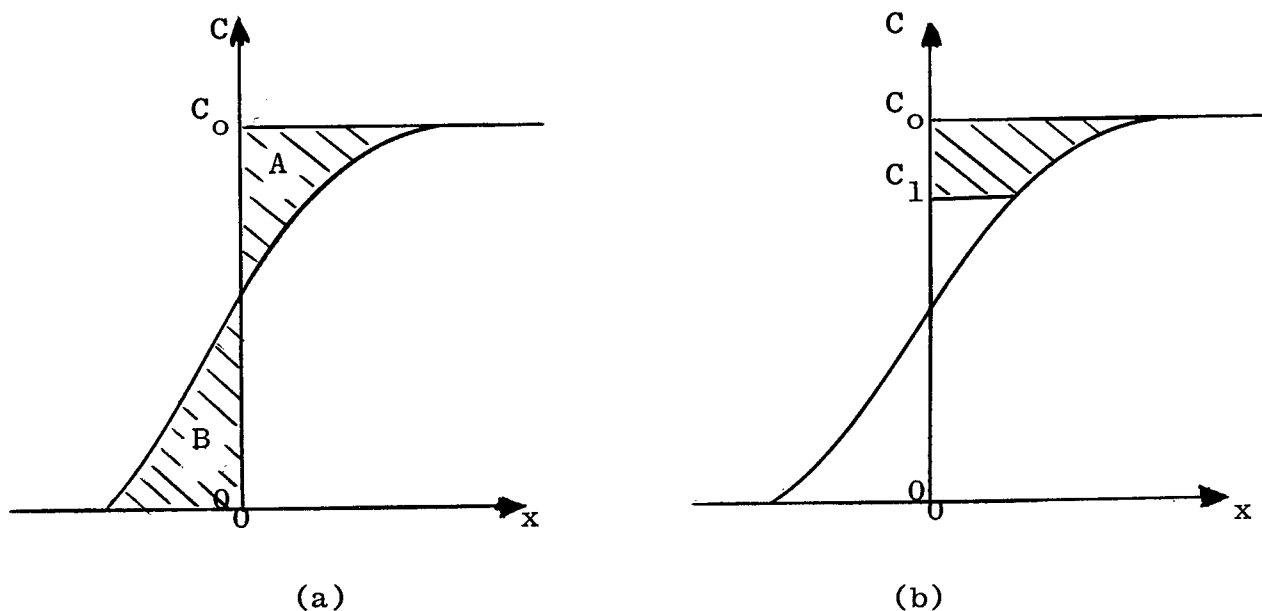


Fig. A.1-3

Equation [A.1-18] requires that in (a) the areas indicated 'A' and 'B' be equal. From (b) the area and slope terms of Eq. [A.1-17] may be evaluated graphically at various values of C_1 to yield D vs. C . This latter is known as the Matano method

and the origin defined by Eq. [A.1-18] and Fig. A.1-3(a) is known as the Matano interface after Chugino Matano (6) who first applied the Boltzmann transformation and solution to the evaluation of diffusion coefficients as a function of composition.

APPENDIX 2

EXPERIMENTAL DATA

The complete experimental data converted from count rate to normalized concentration, C/Co, are given in Section A.2-1 of this appendix. These normalized concentration data are plotted on probability paper as C/Co x 100 (probability axis) vs distance (linear axis) in microprobe measuring units where one unit equals 2.5×10^{-4} centimeters. Results based upon data contained in these probability plots and the Grube solution are found in Table 5, p. 36.

The second section of this appendix, A.2-2, contains linear plots of those concentration-penetration curves to which the Boltzmann-Matano analysis was applied. The data are plotted as concentration (atom percent titanium) vs distance (probe units). Also included on each figure is the plot from which the Matano interface was determined. Results computed from these figures are given in Table 6, p. 40.

A.2-1 Normalized Concentration (C/Co) vs Penetration Distance (Probe Units)

<u>Figure</u>	<u>Conditions</u>
A.2-1	Undiffused 8.5% Ti
-2	" 35% Ti
-3	1300°C 0.1 hr 8.5% Ti Scan 1

<u>Figure</u>	<u>Conditions</u>			
A.2-4	1300°C	0.1 hr	8.5% Ti	Scan 2
-5	"	1.0 hr	"	Scan 1
-6	"	"	"	Scan 2
-7	"	10 hr	"	Scan 1
-8	"	"	"	Scan 2
-9	"	120 hr	"	Scan 1
-10	"	"	"	Scan 2
-11	"	"	35% Ti	Scan 1
-12	"	"	"	Scan 2
-13	1500°C	0.1 hr	8.5% Ti	Scan 1
-14	"	"	"	Scan 2
-15	"	1.0 hr	"	Scan 1
-16	"	"	"	Scan 2
-17	"	10 hr	"	Scan 1
-18	"	"	"	Scan 2
-19	"	120 hr	"	Scan 1
-20	"	"	"	Scan 2
-21	"	480 hr	"	Scan 1
-22	"	"	"	Scan 2
-23	"	1000 hr	"	Scan 1
-24	"	"	"	Scan 2
-25	"	0.1 hr	35% Ti	Scan 1
-26	"	"	"	Scan 2
-27	"	1.0 hr	"	Scan 1
-30	"	10 hr	"	Scan 2
-31	"	120 hr	"	Scan 1
-32	"	"	"	Scan 2

<u>Figure</u>	<u>Conditions</u>			
A.2-33	1500°C	480 hr	35% Ti	Scan 1
-34	"	"	"	Scan 2
-35	"	1000 hr	"	Scan 1
-36	"	"	"	Scan 2
-37	1800°C	10 hr	"	Scan 1
-38	"	"	"	Scan 2
-39	2000°C	"	"	Scan 1
-40	"	"	"	Scan 2

A.2-2 Concentration (atom percent titanium)
vs Penetration Distance (probe units)

<u>Figure</u>	<u>Conditions</u>		
A.2-41	1300°C	120 hr	35% Ti
-42	"	"	8.5% Ti
-44	1500°C	"	35% Ti
-45	"	1000 hr	"
-46	"	1.0 hr	8.5% Ti
-47	"	10 hr	"
-48	"	120 hr	"
-49	"	1000 hr	"
-50	1800°C	10 hr	35% Ti
-51	2000°C	"	"

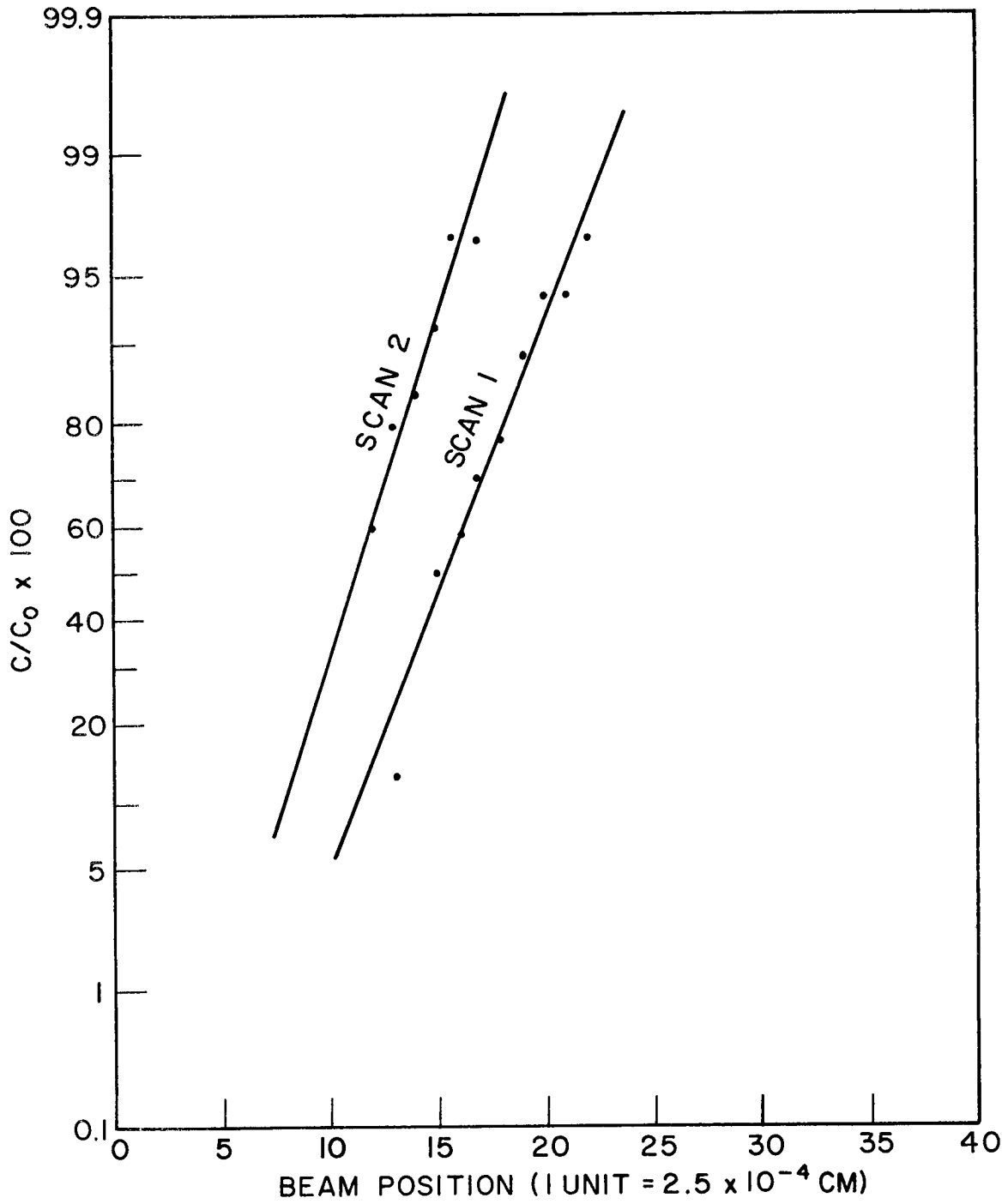


Figure A.2-1 - Probability plot of relative concentration, C/C_0 , versus penetration distance; undiffused, Cb/Cb 8.5 a/o Ti.

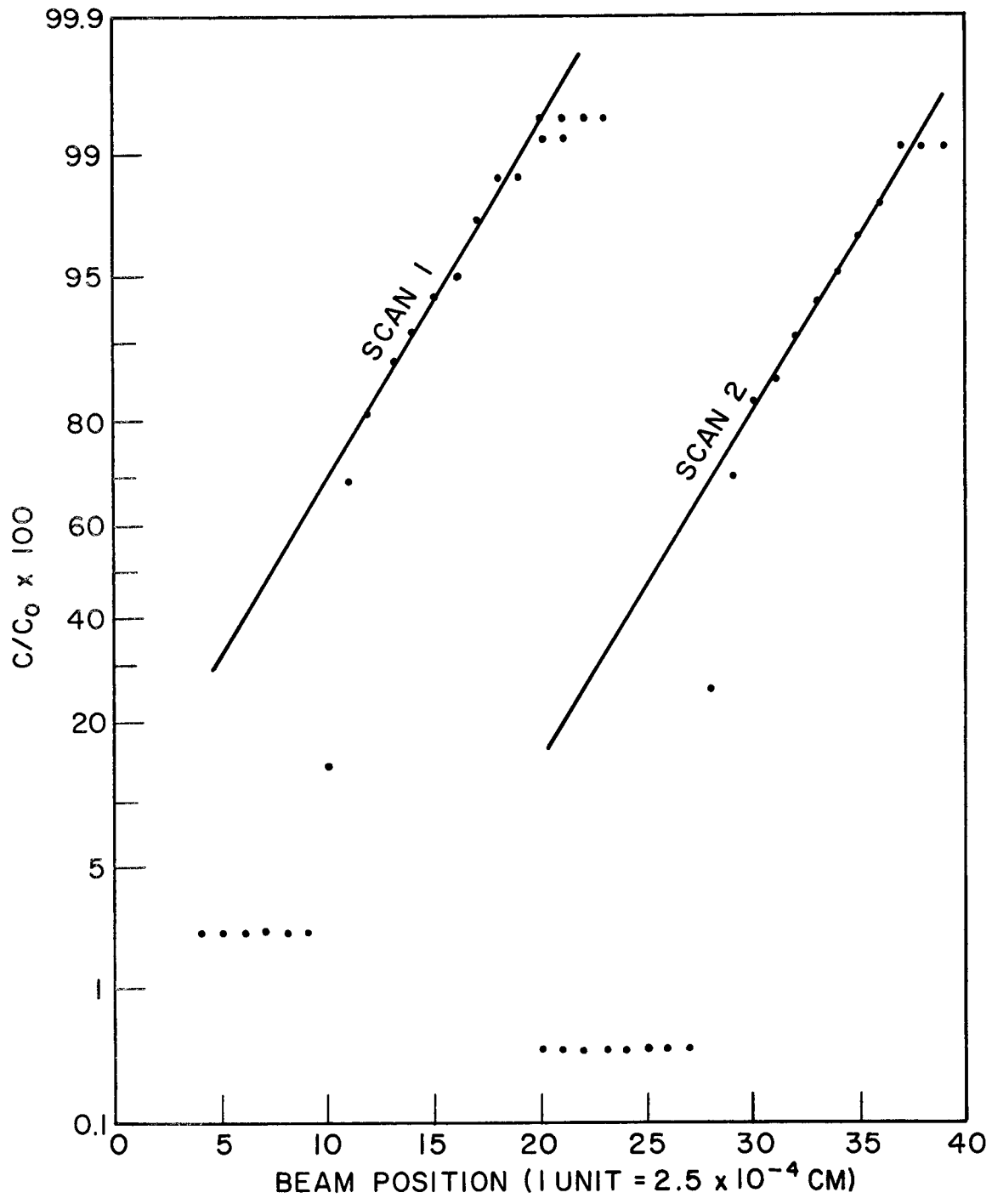


Figure A.2-2 - Probability plot of relative concentration, C/C_0 , versus penetration distance; undiffused, Cb/Cb 35 a/o Ti.

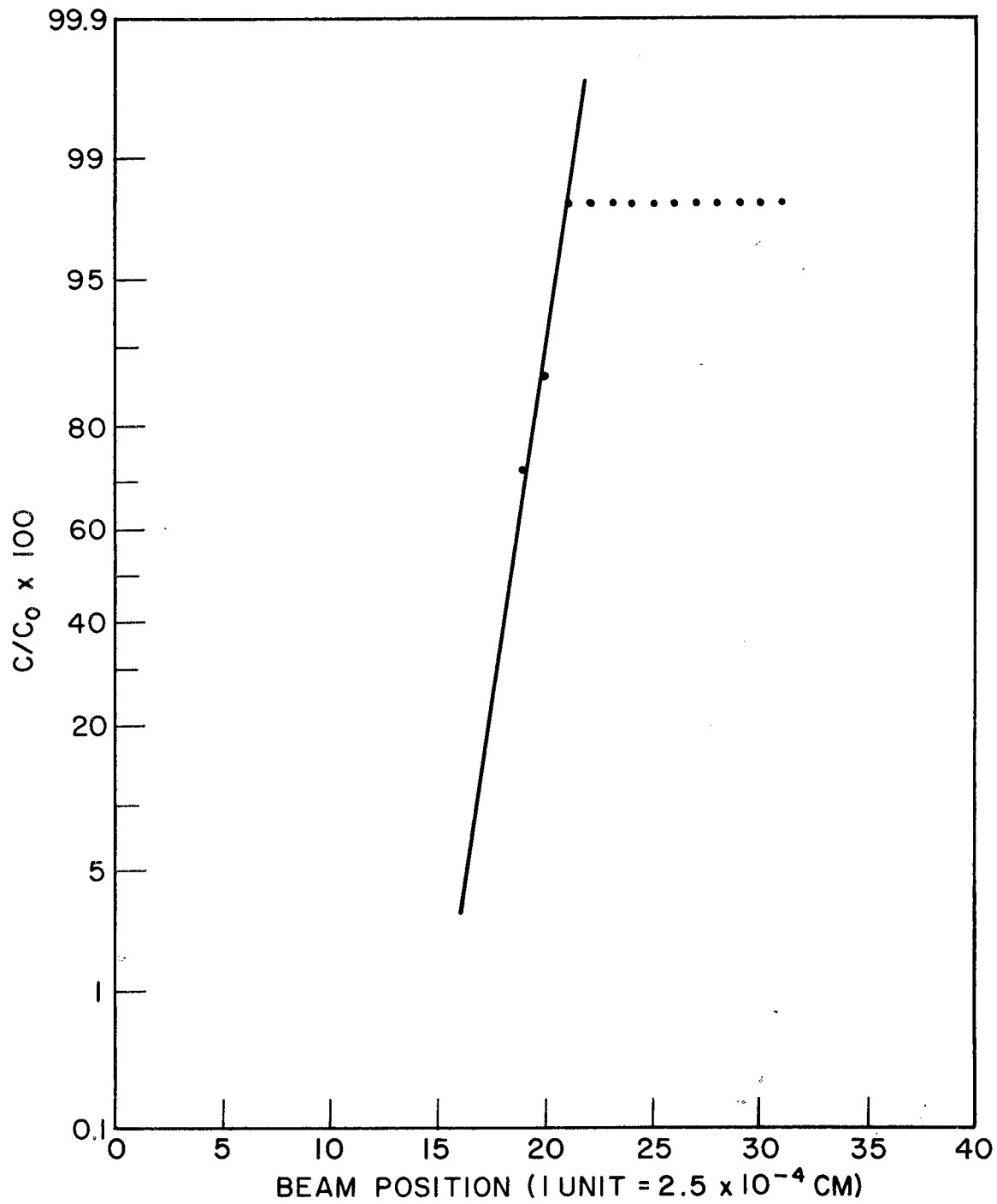


Figure A.2-3 - Probability plot of relative concentration, C/C_0 , versus penetration distance; 1300°C, 0.1 hr, 8.5% Ti, Scan 1.

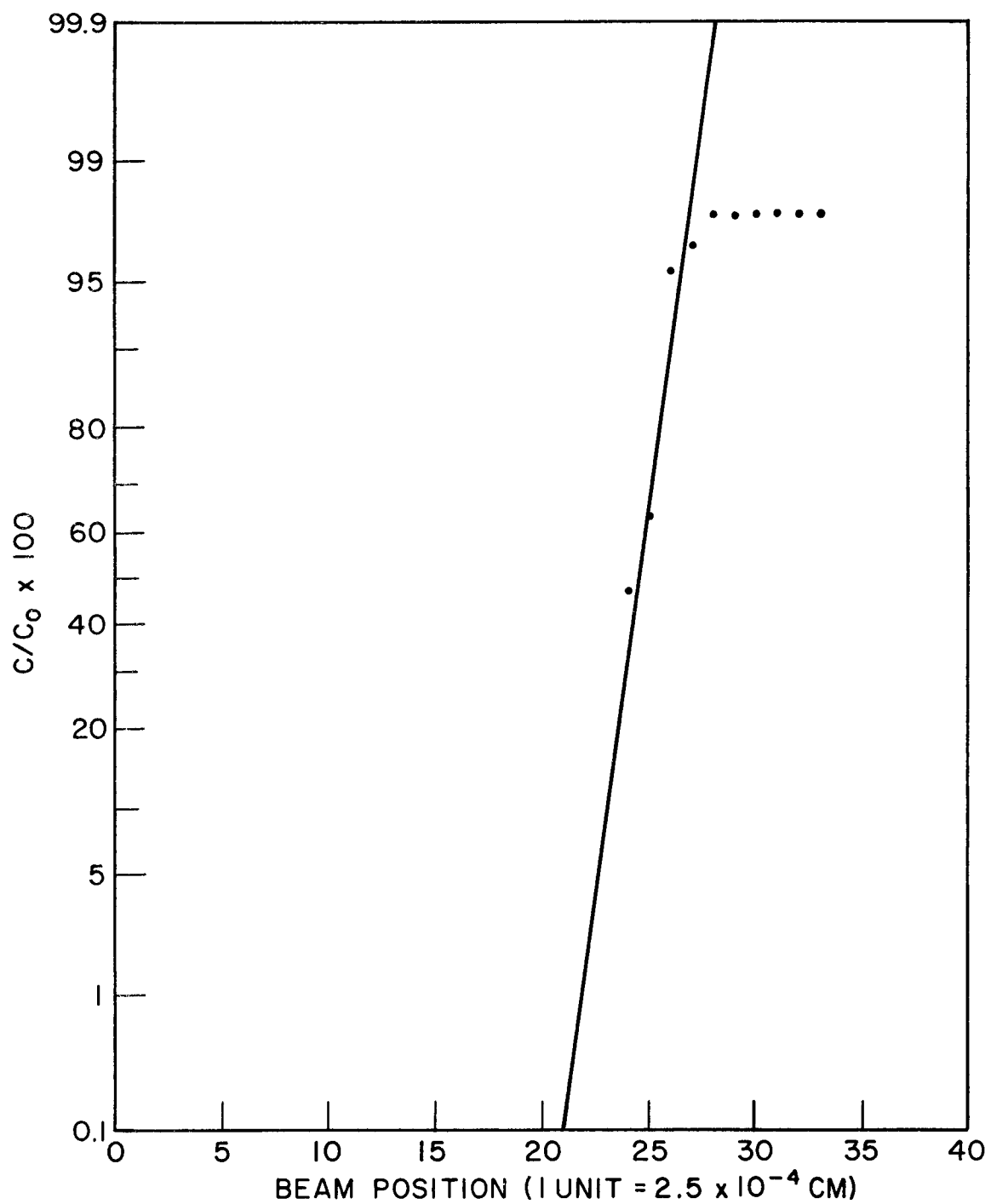


Figure A.2-4 - Probability plot of relative concentration, C/C_0 , versus penetration distance; 1300°C, 0.1 hr, 8.5% Ti, Scan 2.

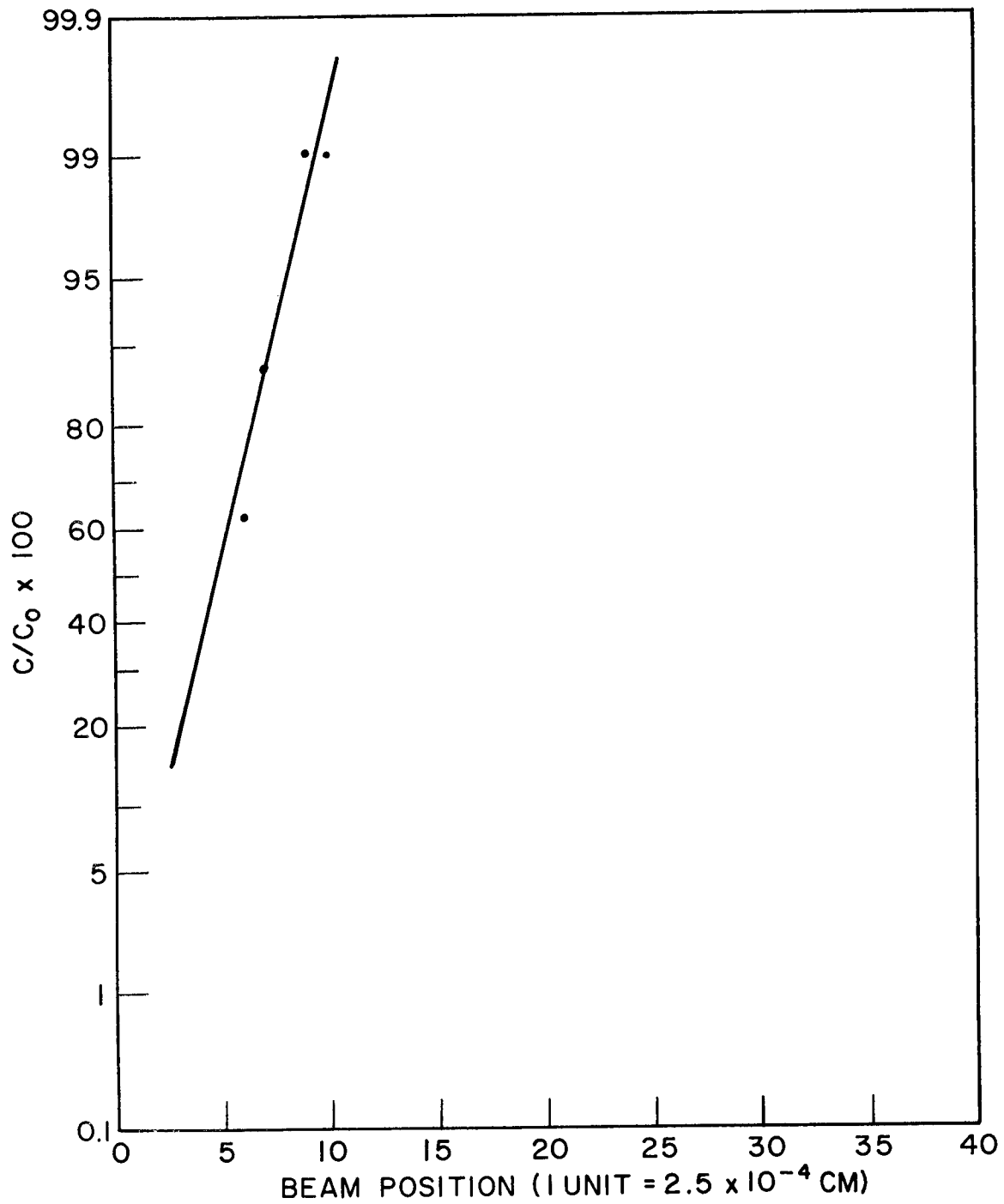


Figure A.2-5 - Probability plot of relative concentration, C/C_0 , versus penetration distance; 1300°C, 1.0 hr, 8.5% Ti, Scan 1.

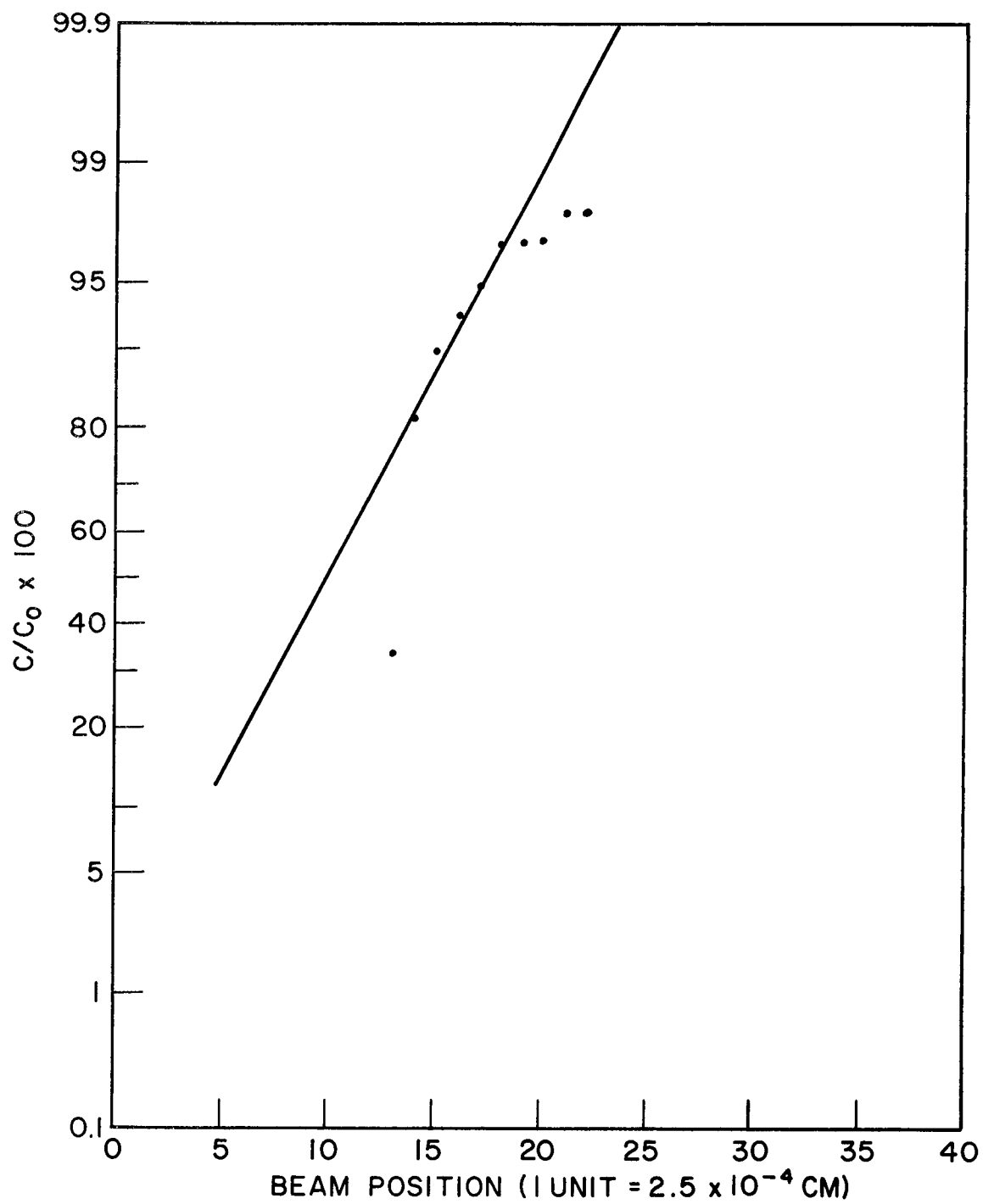


Figure A.2-6 - Probability plot of relative concentration, C/C_0 , versus penetration distance; 1300°C, 1.0 hr, 8.5% Ti, Scan 2.

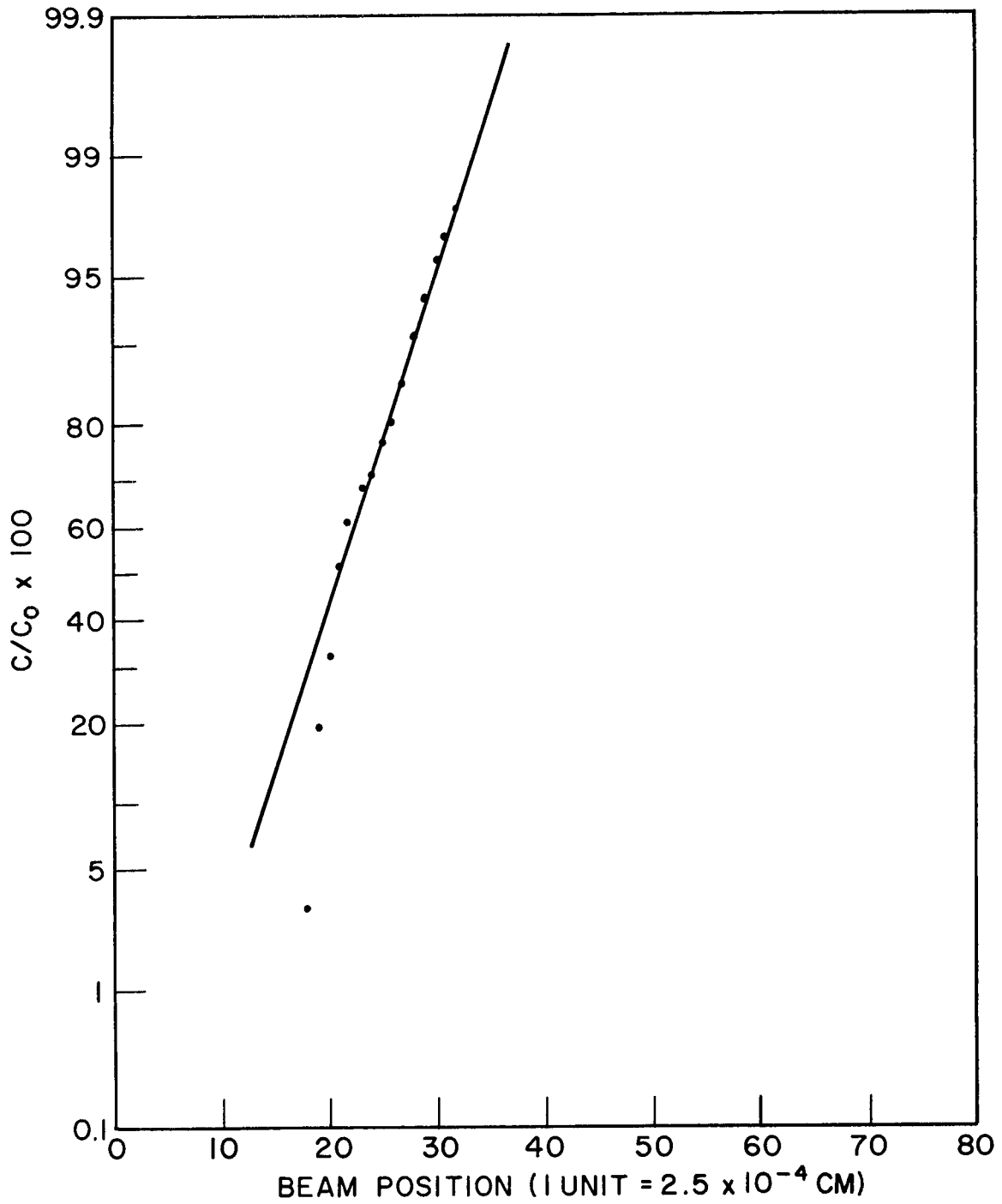


Figure A.2-7 - Probability plot of relative concentration, C/C_0 , versus penetration distance; 1300°C, 10 hr, 8.5% Ti, Scan 1.

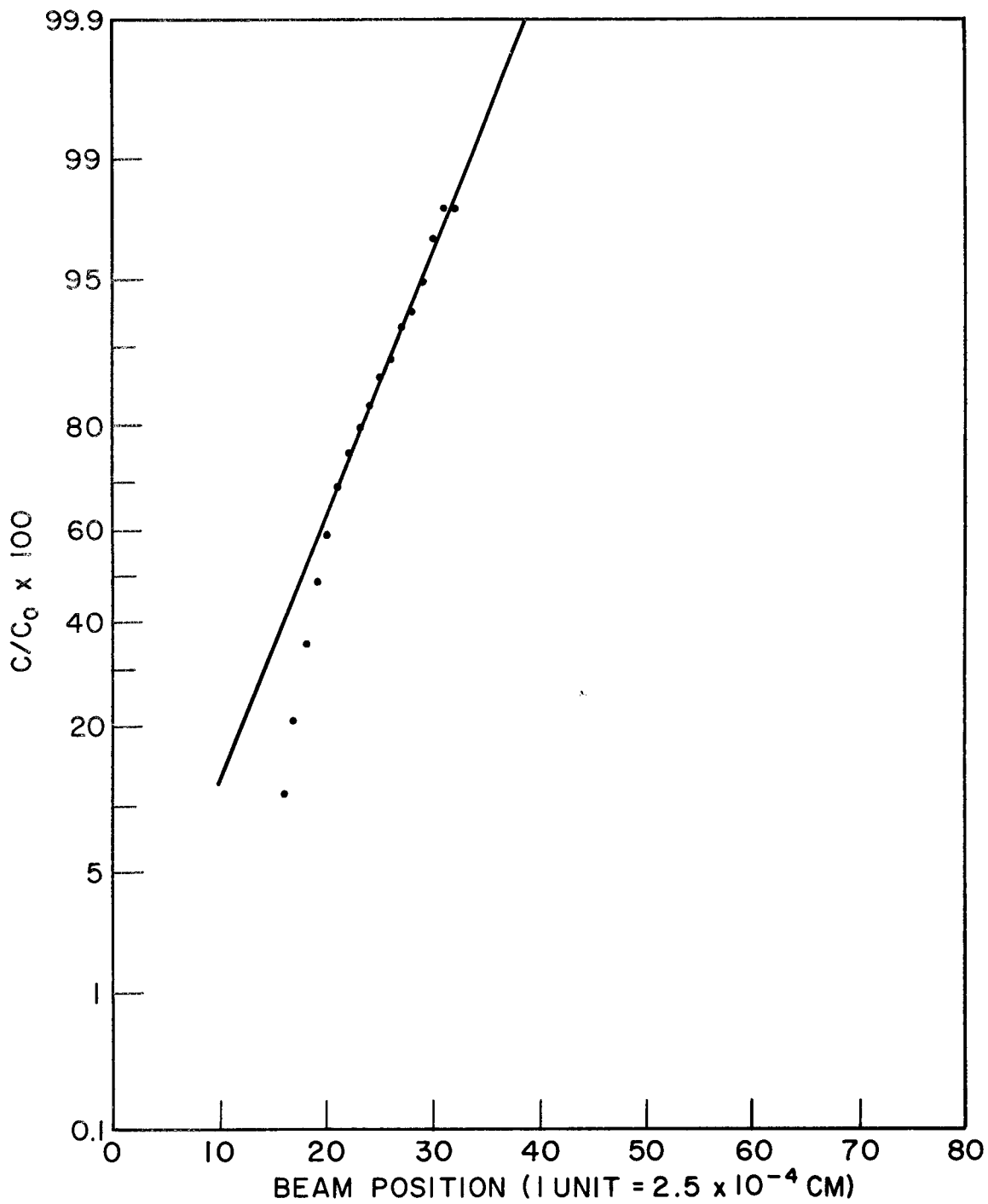


Figure A.2-8 - Probability plot of relative concentration, C/C_0 , versus penetration distance; 1300°C, 10 hr, 8.5% Ti, Scan 2.

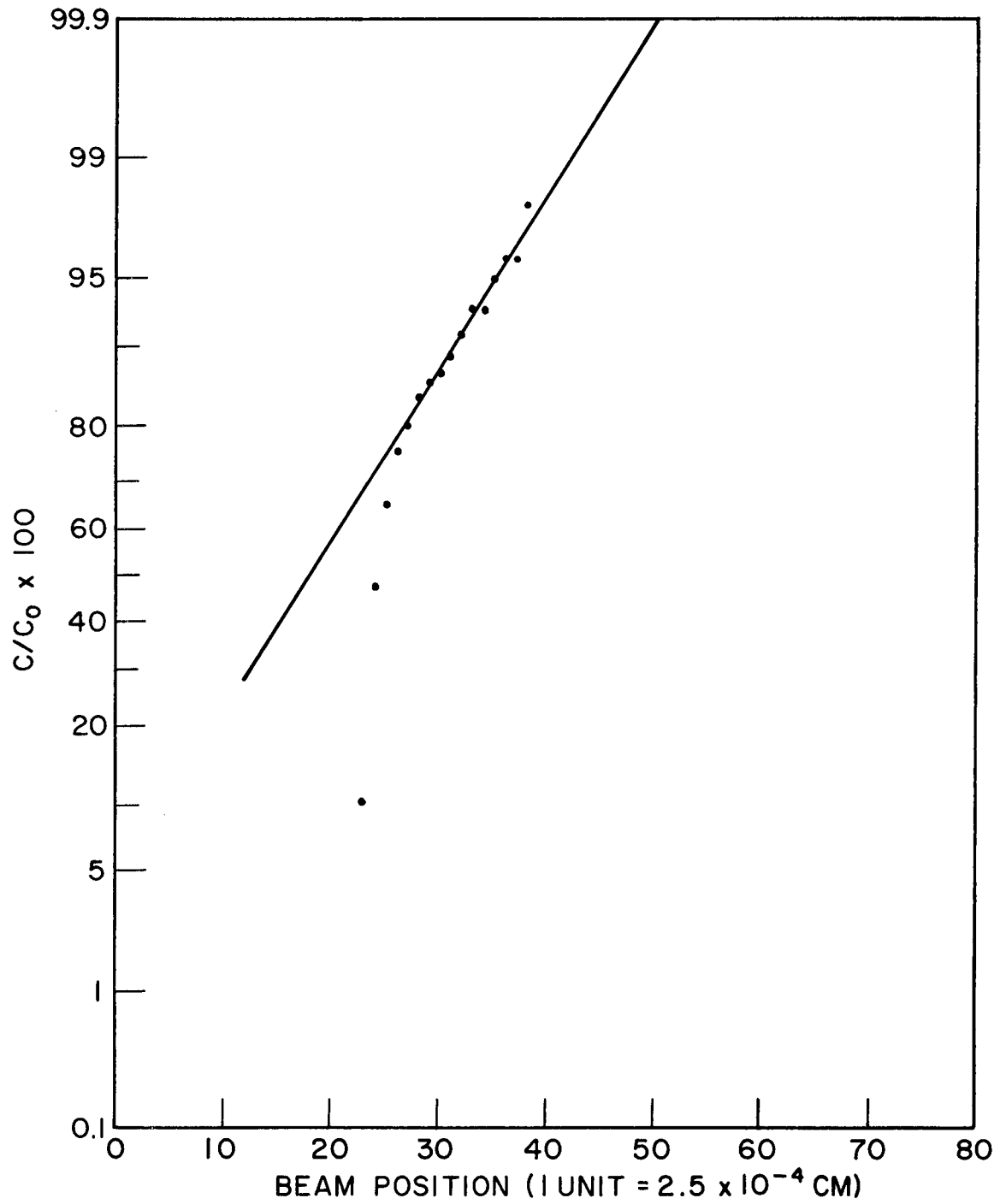


Figure A.2-9 - Probability plot of relative concentration, C/C_0 , versus penetration distance; 1300°C, 120 hr, 8.5% Ti, Scan 1.

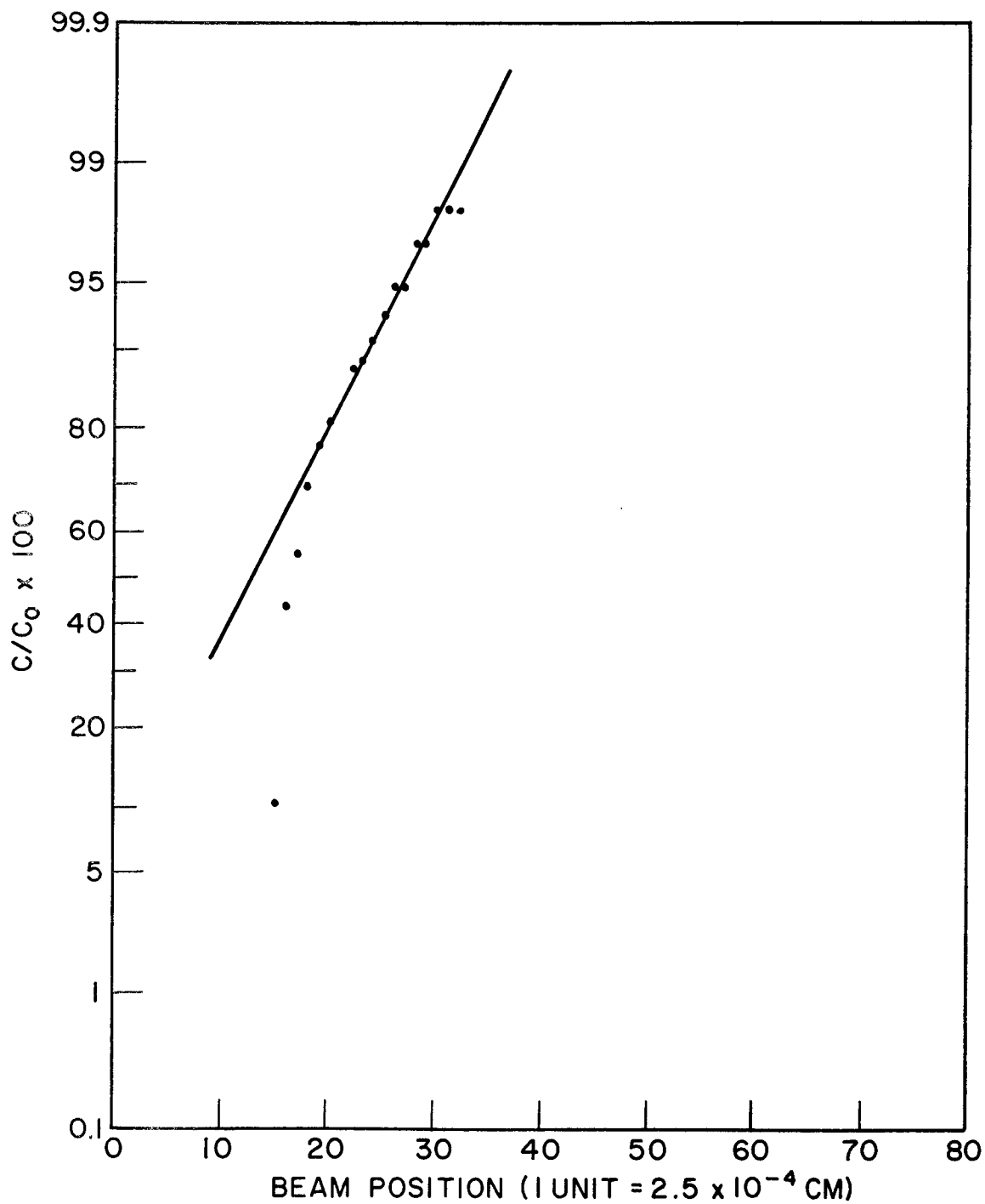


Figure A.2-10 - Probability plot of relative concentration, C/C_0 , versus penetration distance; 1300°C, 120 hr, 8.5% Ti, Scan 2.

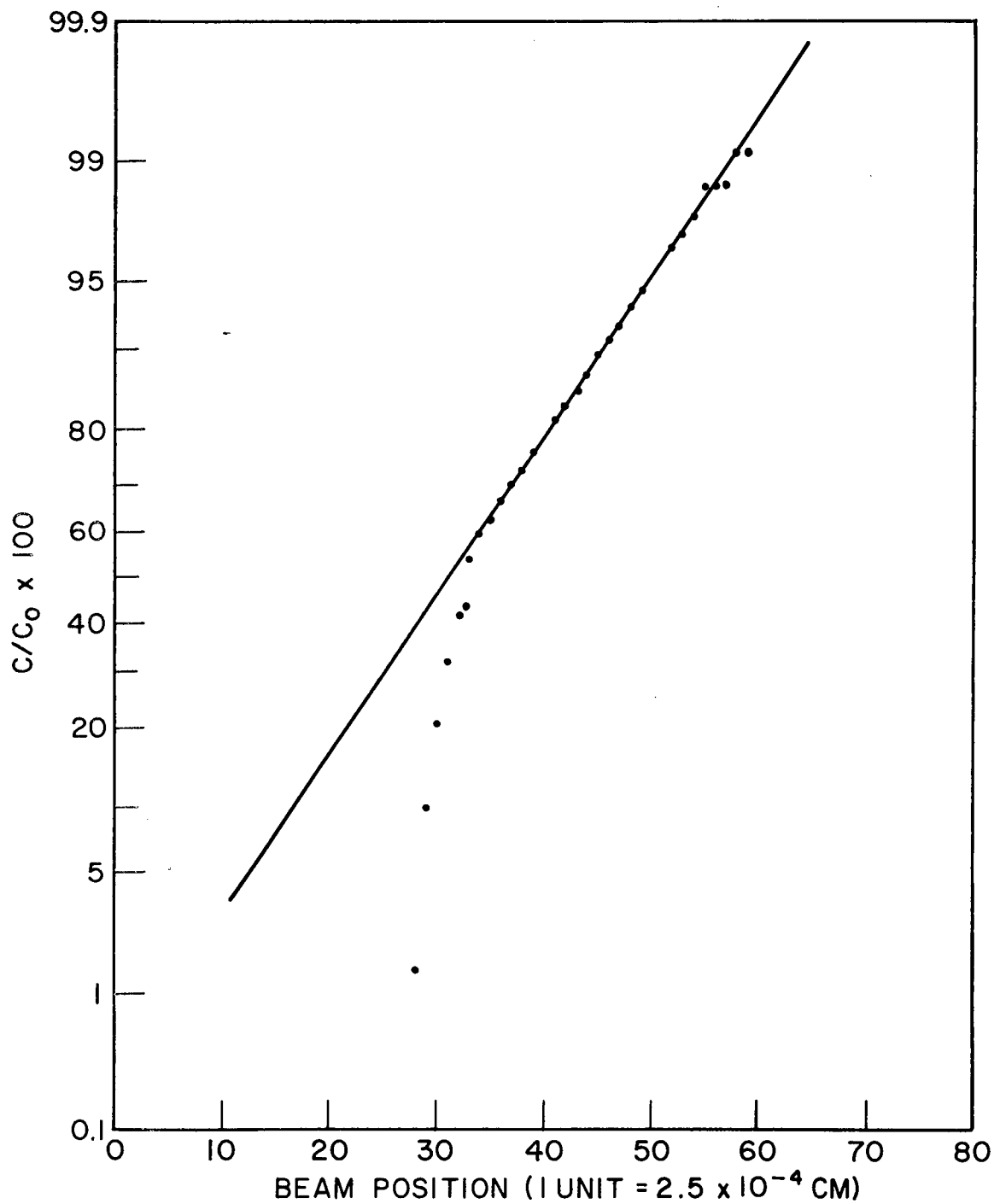


Figure A.2-11 - Probability plot of relative concentration, C/C_0 , versus penetration distance; 1300°C, 120 hr, 35% Ti, Scan 1.

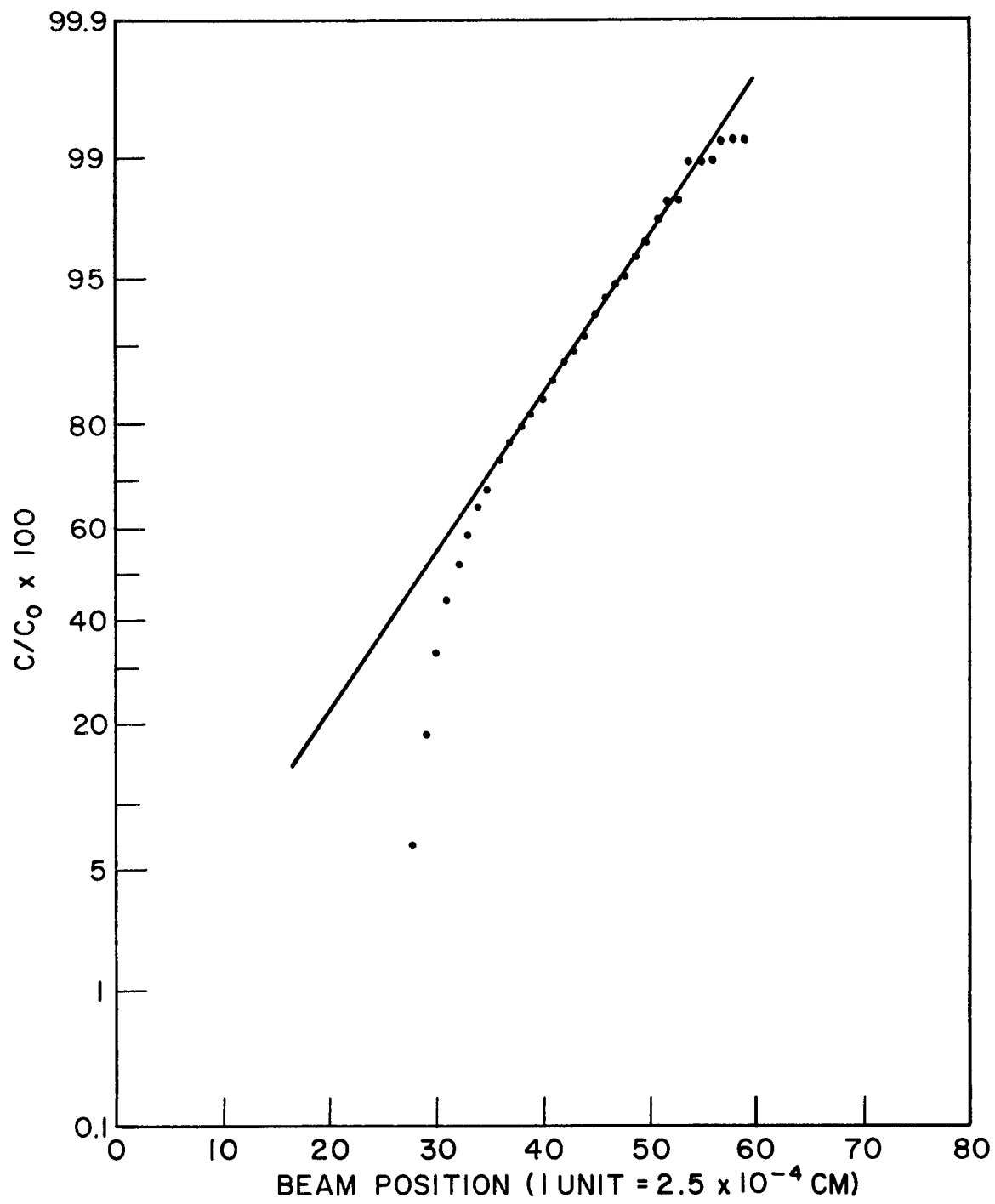


Figure A.2-12 - Probability plot of relative concentration, C/C_0 , versus penetration distance; 1300°C, 120 hr, 35% Ti, Scan 2.

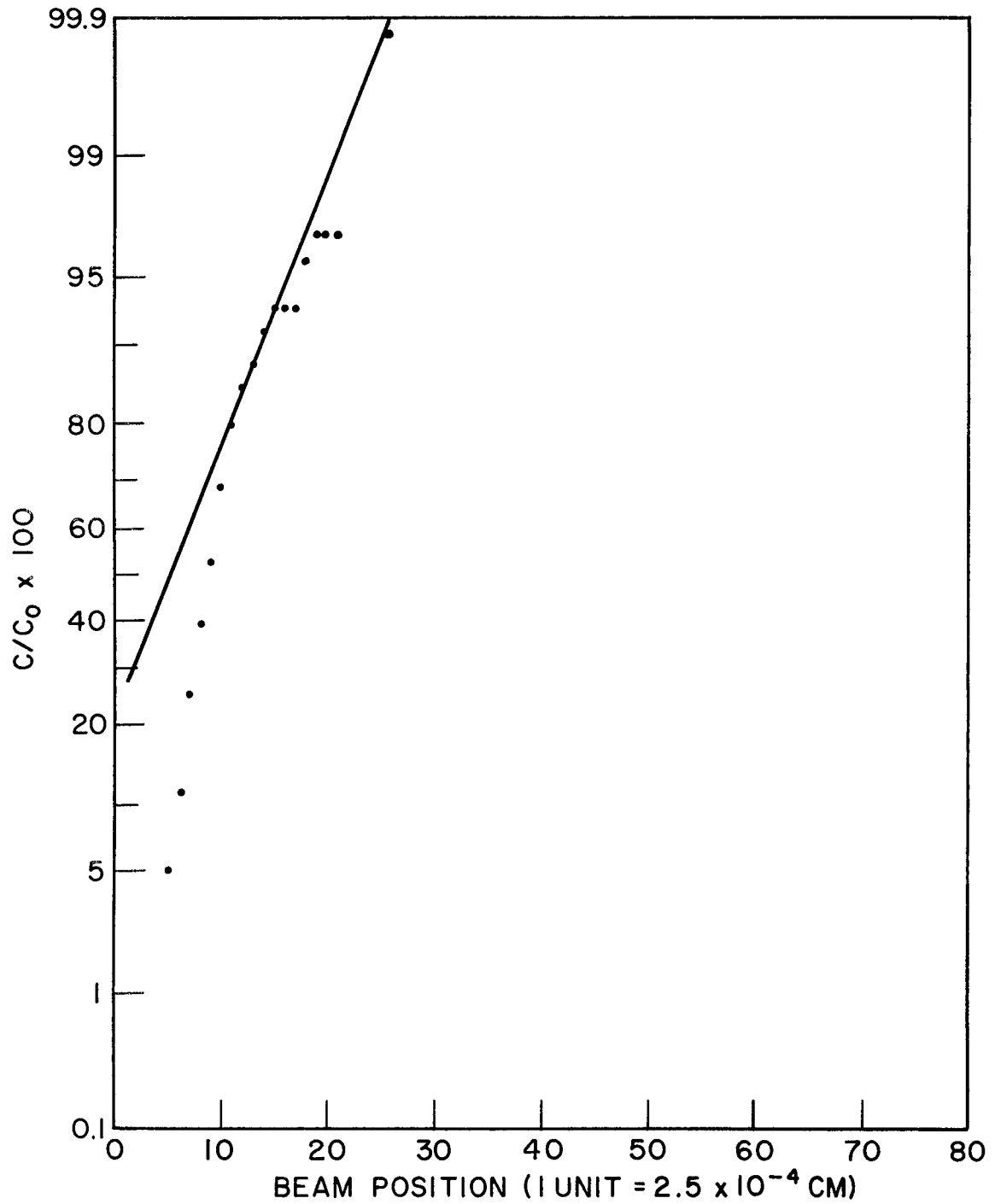


Figure A.2-14 - Probability plot of relative concentration, C/C_0 , versus penetration distance; 1500°C, 0.1 hr, 8.5% Ti, Scan 2.

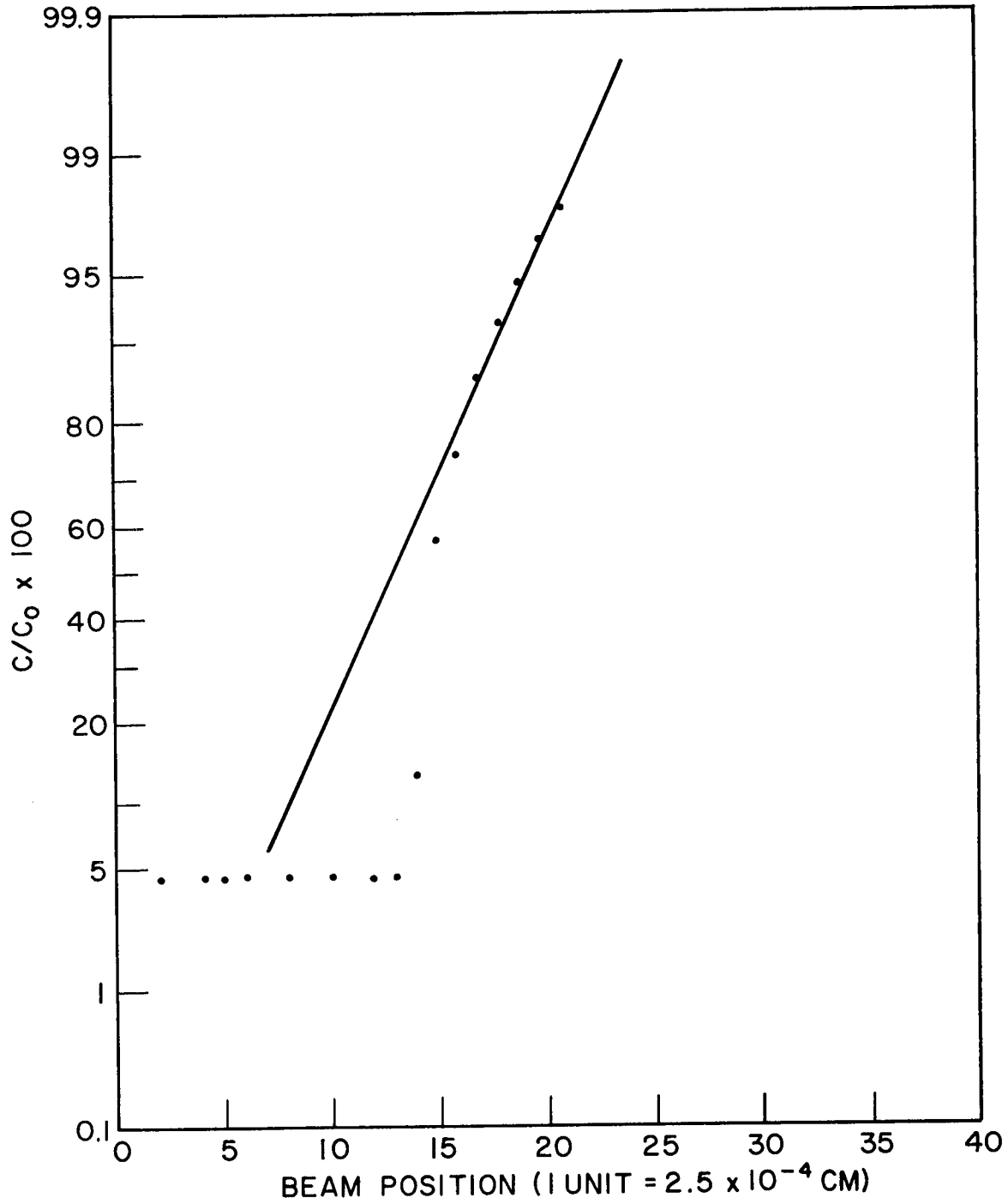


Figure A.2-15 - Probability plot of relative concentration, C/C_0 , versus penetration distance; 1500°C, 1.0 hr, 8.5% Ti, Scan 1.

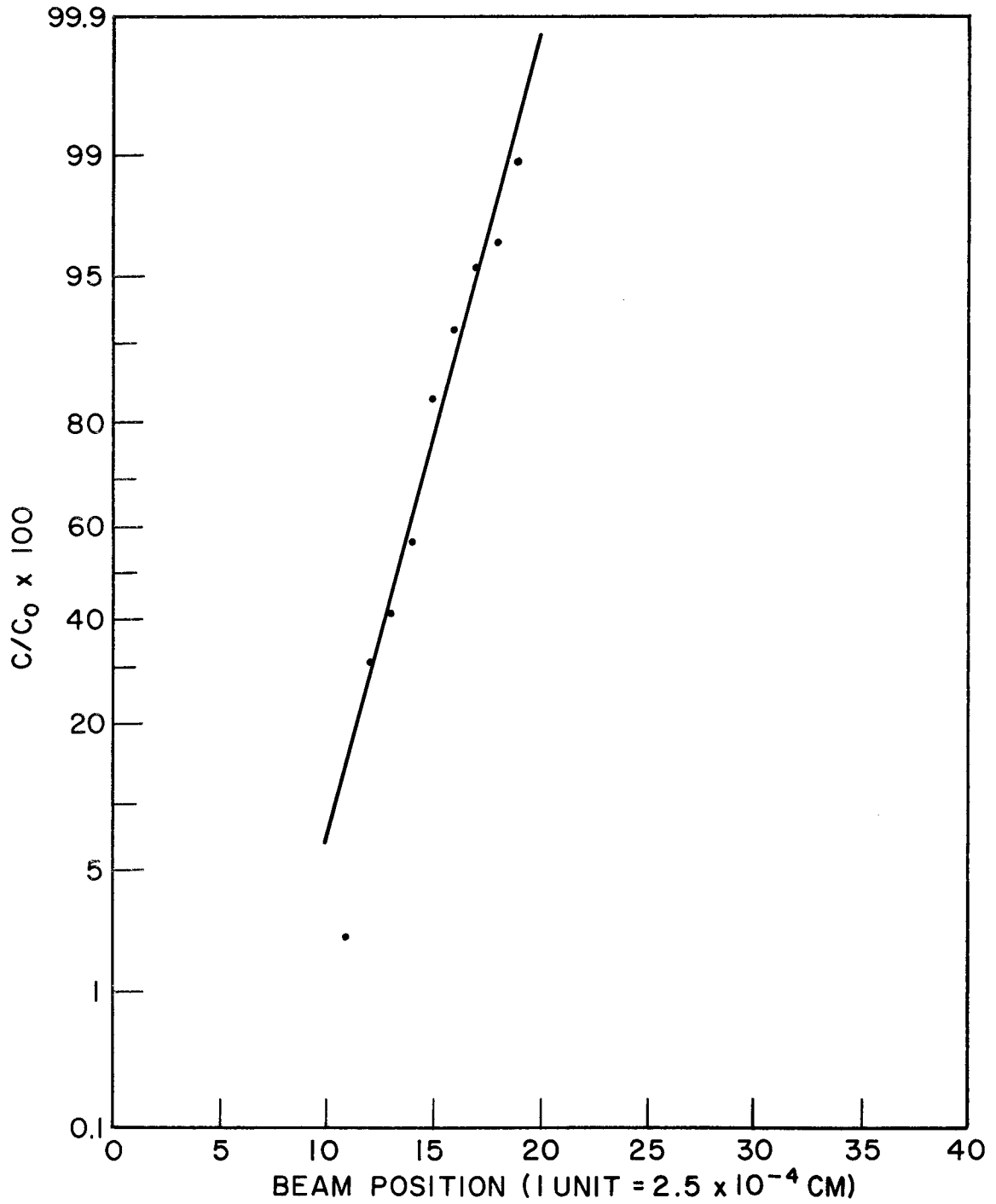


Figure A.2-16 - Probability plot of relative concentration, C/C_0 , versus penetration distance; 1500°C, 1.0 hr, 8.5% Ti, Scan 2.

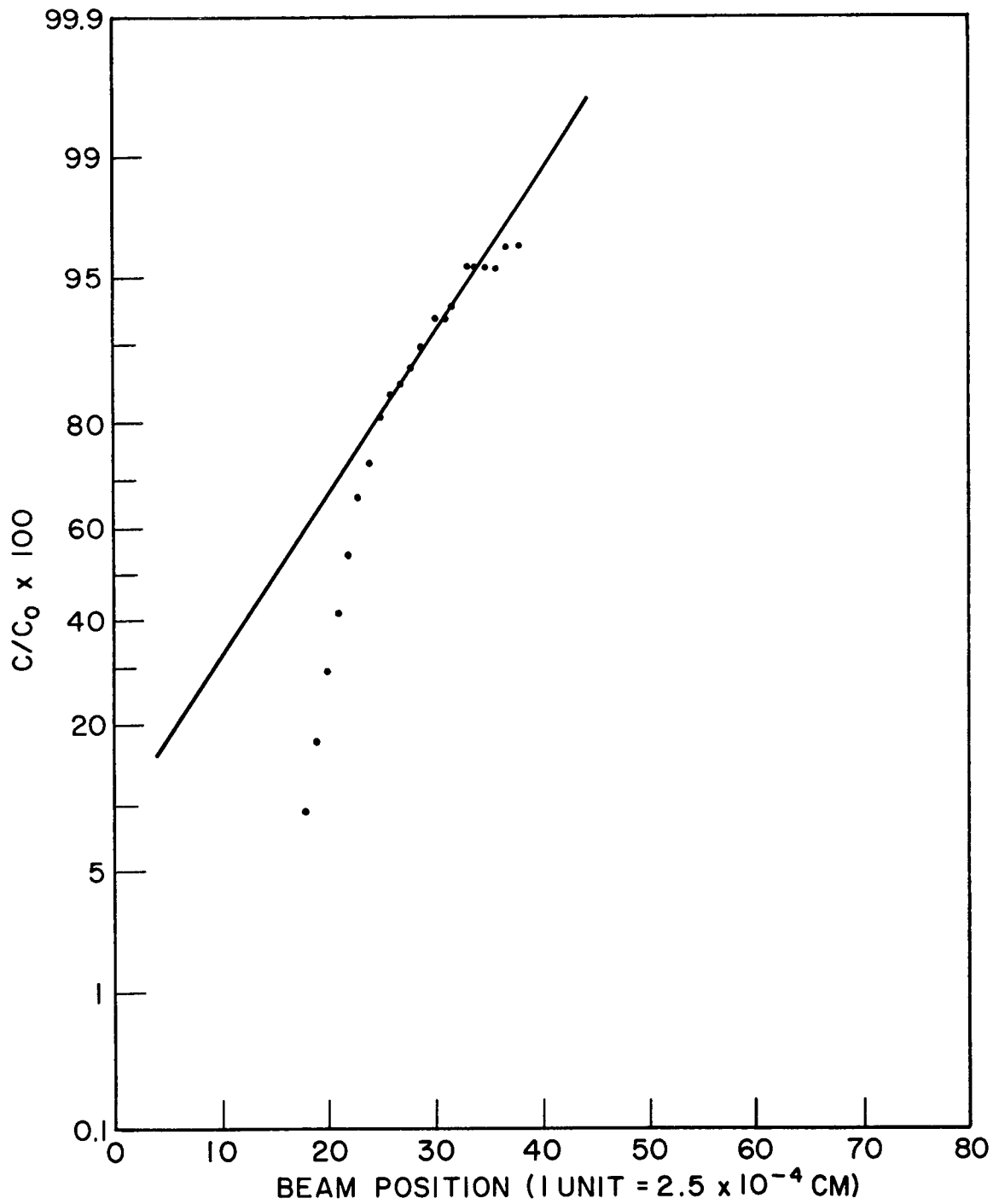


Figure A.2-18 - Probability plot of relative concentration, C/C_0 , versus penetration distance; 1500°C, 10 hr, 8.5% Ti, Scan 2.

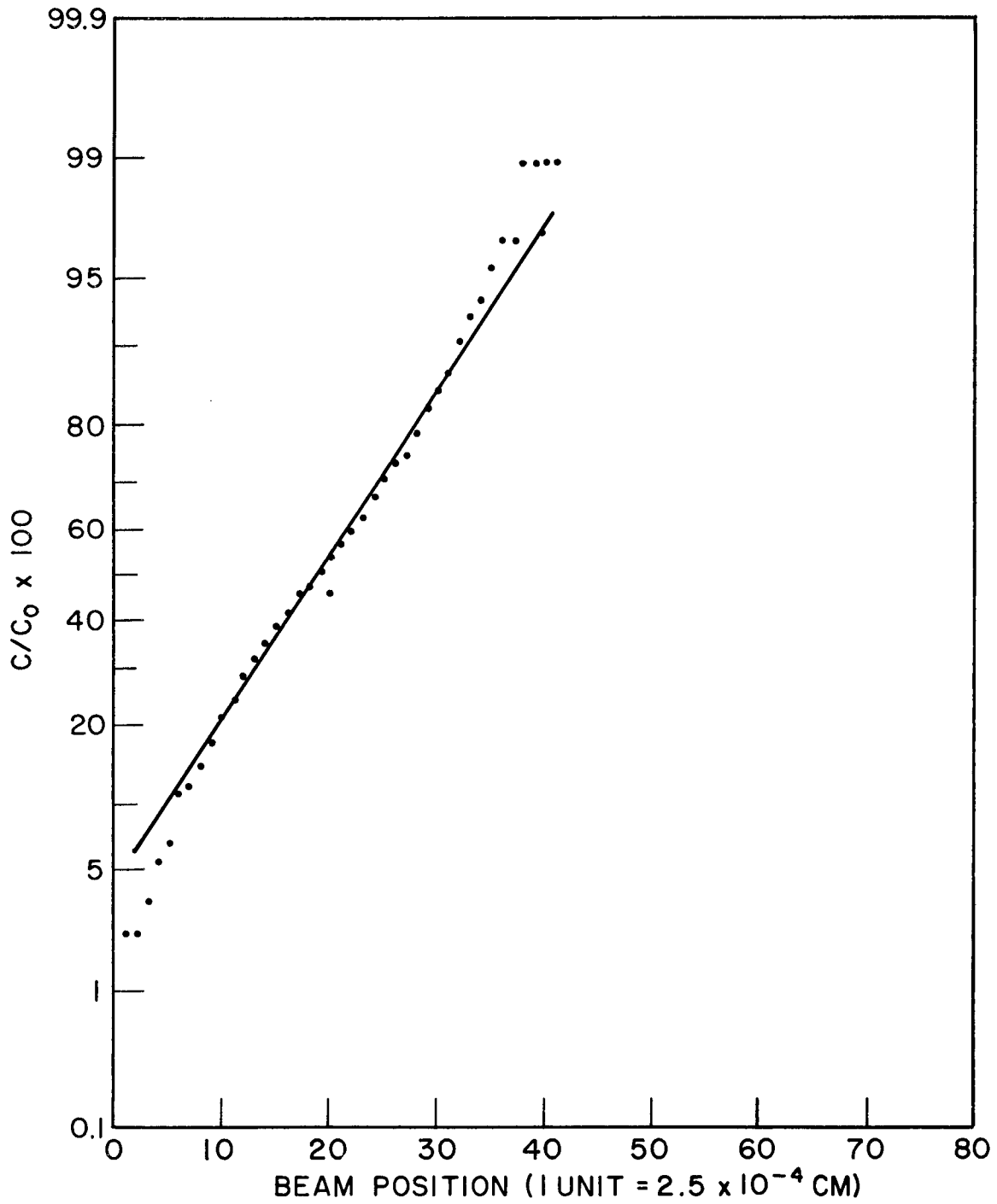


Figure A.2-19 - Probability plot of relative concentration, C/C_0 , versus penetration distance; 1500°C, 120 hr, 8.5% Ti, Scan 1.

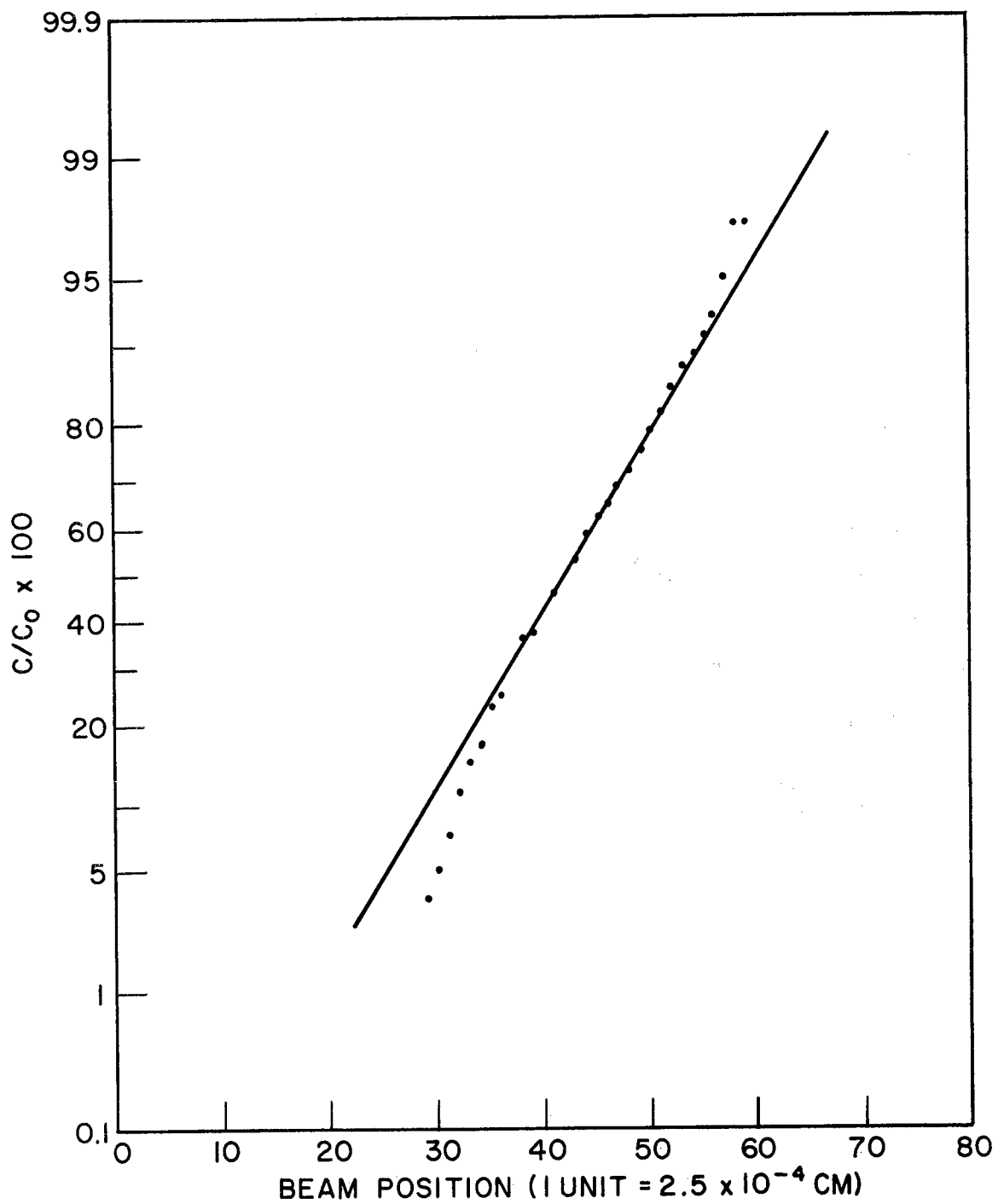


Figure A.2-20 - Probability plot of relative concentration, C/C_0 , versus penetration distance; 1500°C, 120 hr, 8.5% Ti, Scan 2.

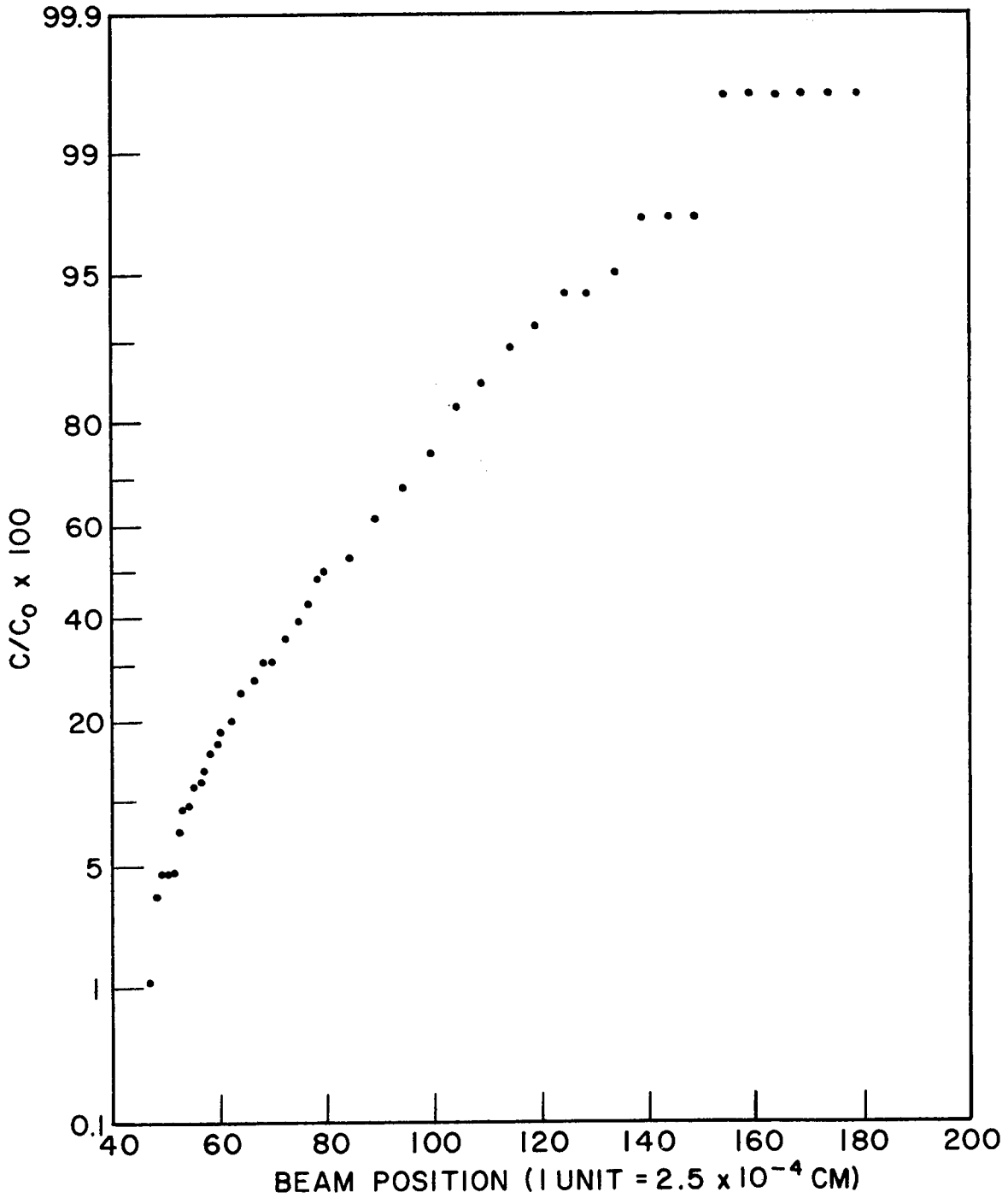


Figure A.2-21 - Probability plot of relative concentration, C/C_0 , versus penetration distance; 1500°C, 480 hr, 8.5% Ti, Scan 1.

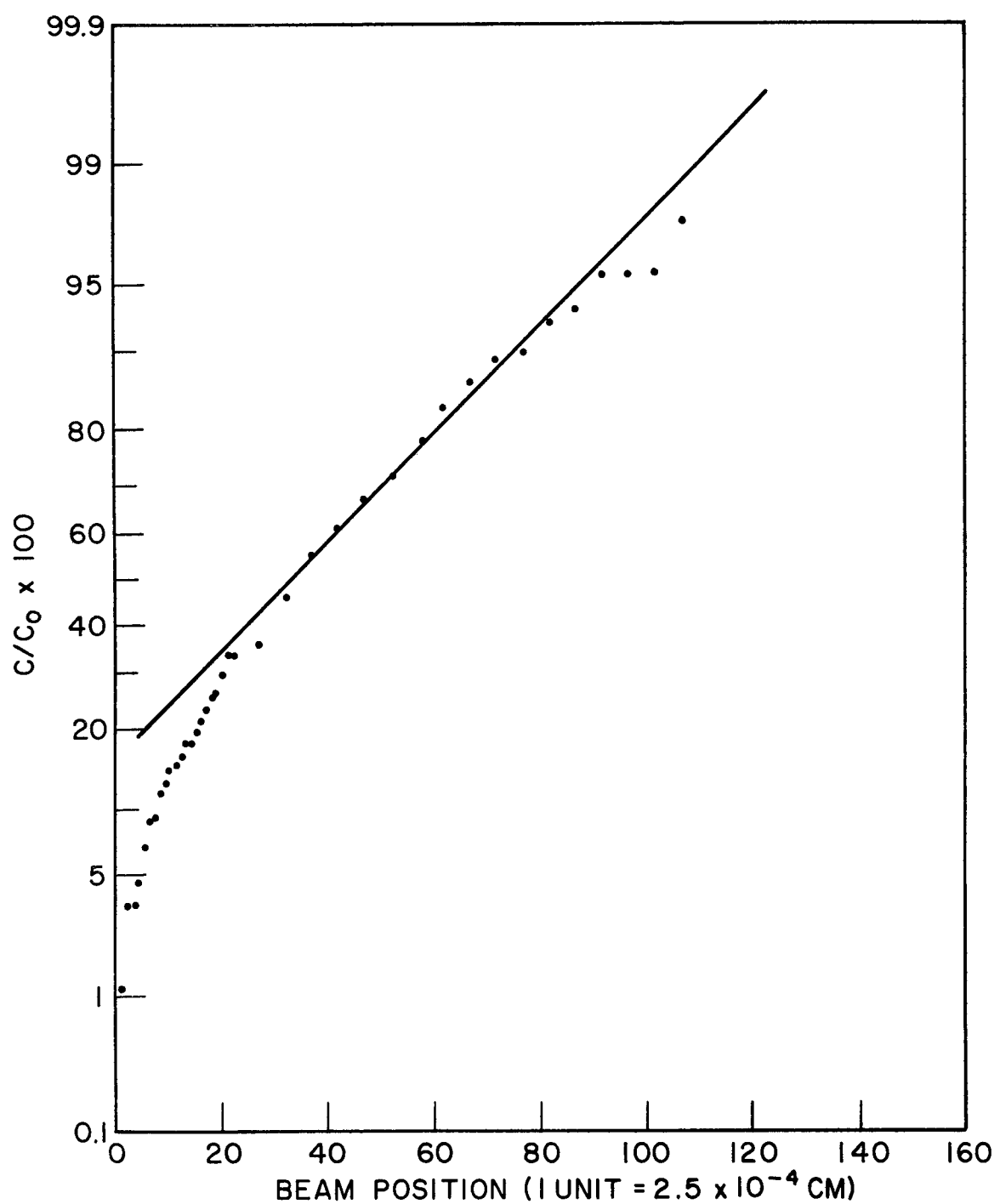


Figure A.2-22 - Probability plot of relative concentration, C/C_0 , versus penetration distance; 1500°C, 480 hr, 8.5% Ti, Scan 2.

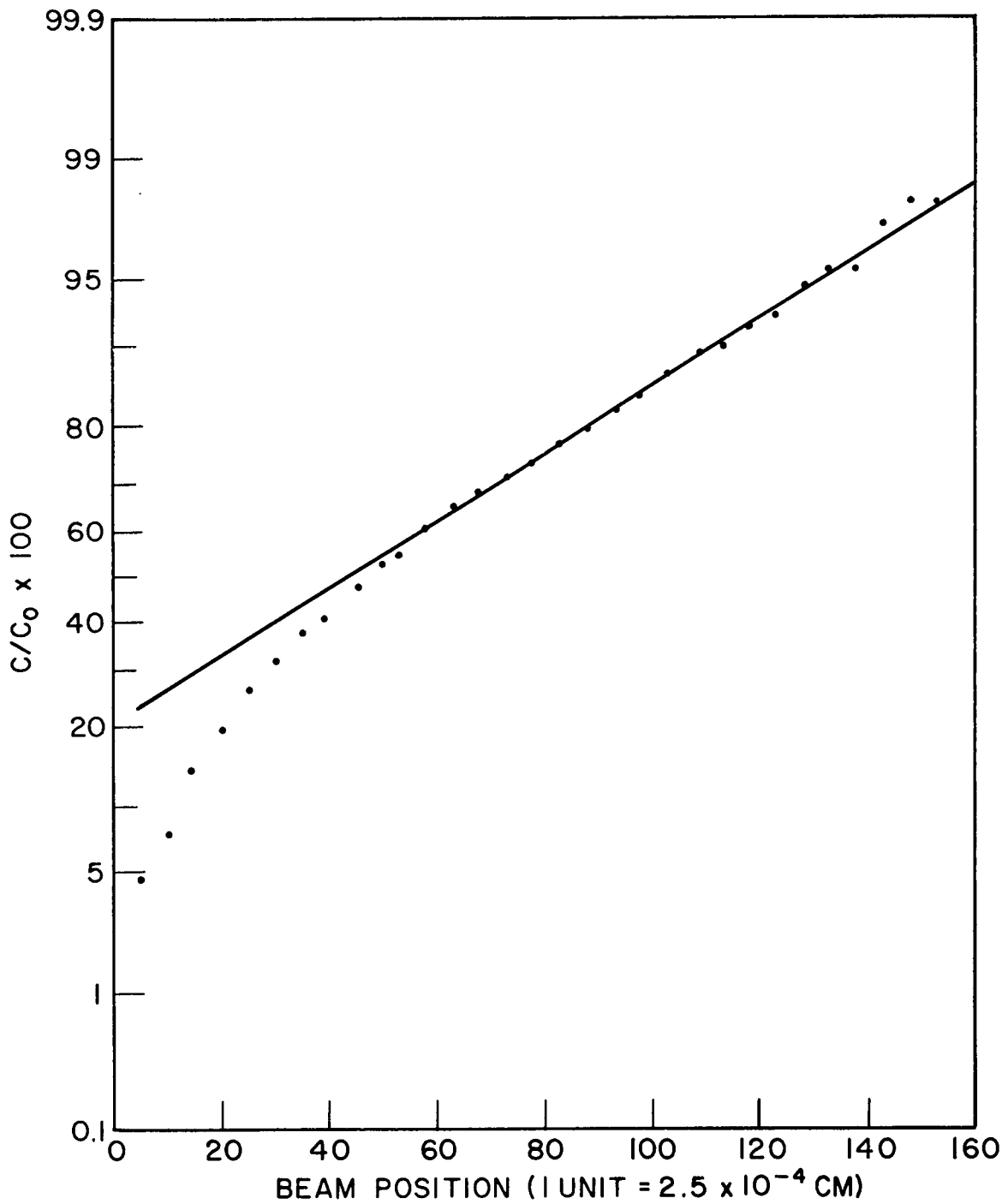


Figure A.2-23 - Probability plot of relative concentration, C/C_0 , versus penetration distance; 1500°C, 1000 hr, 8.5% Ti, Scan 1.

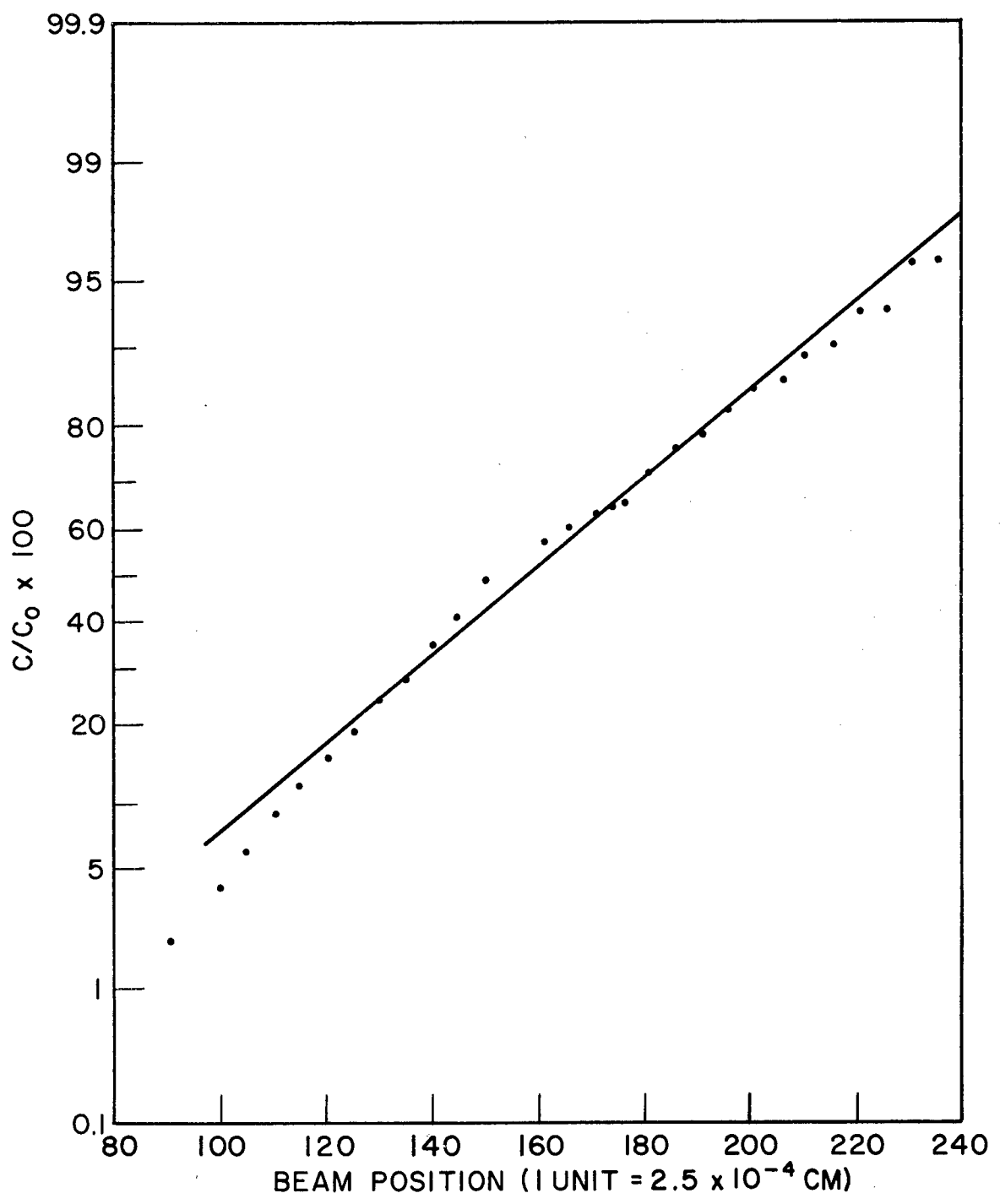


Figure A.2-24 - Probability plot of relative concentration, C/C_0 , versus penetration distance; 1500°C, 1000 hr, 8.5% Ti, Scan 2.

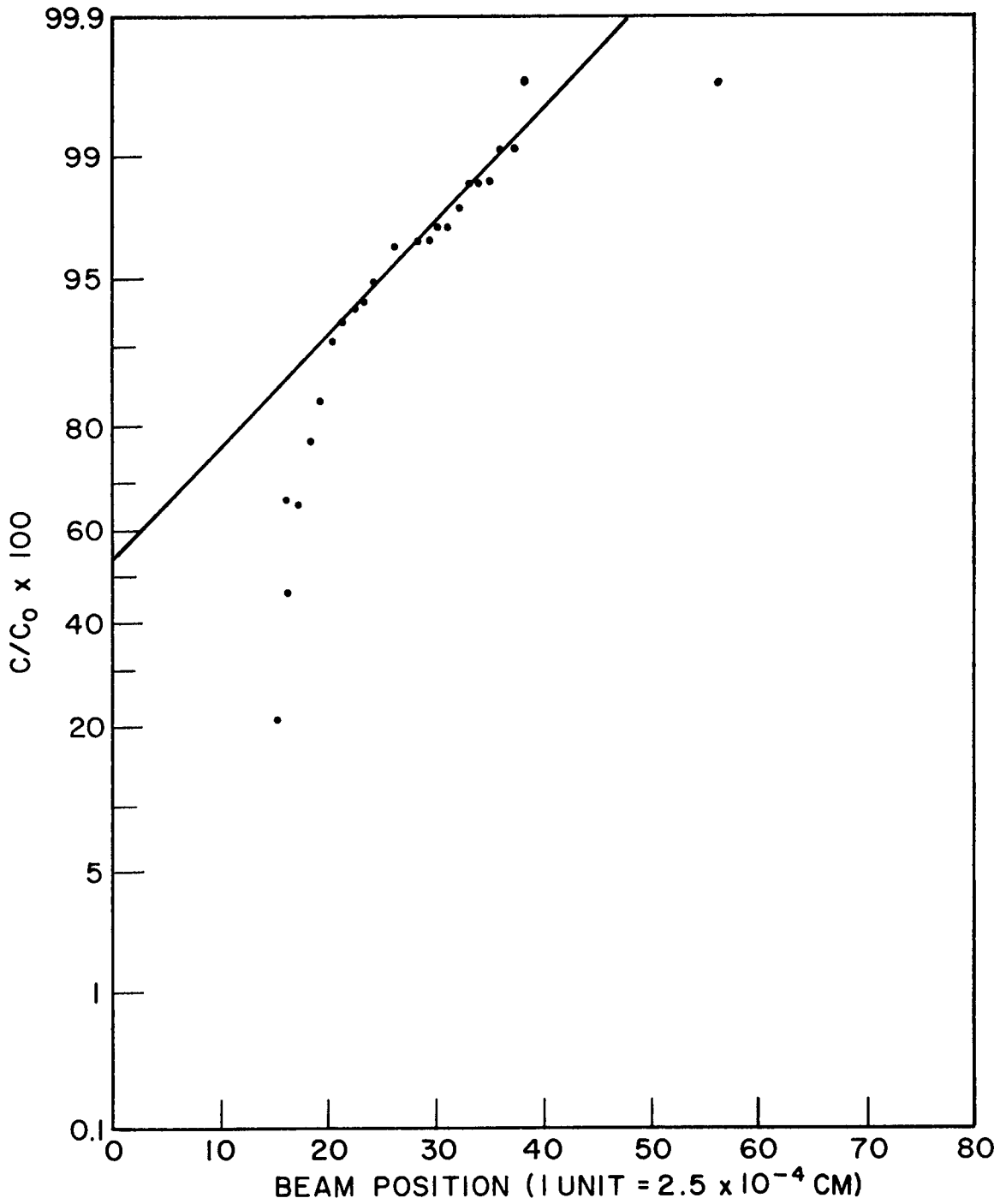


Figure A.2-25 - Probability plot of relative concentration, C/C_0 , versus penetration distance; 1500°C, 0.1 hr, 35% Ti, Scan 1.

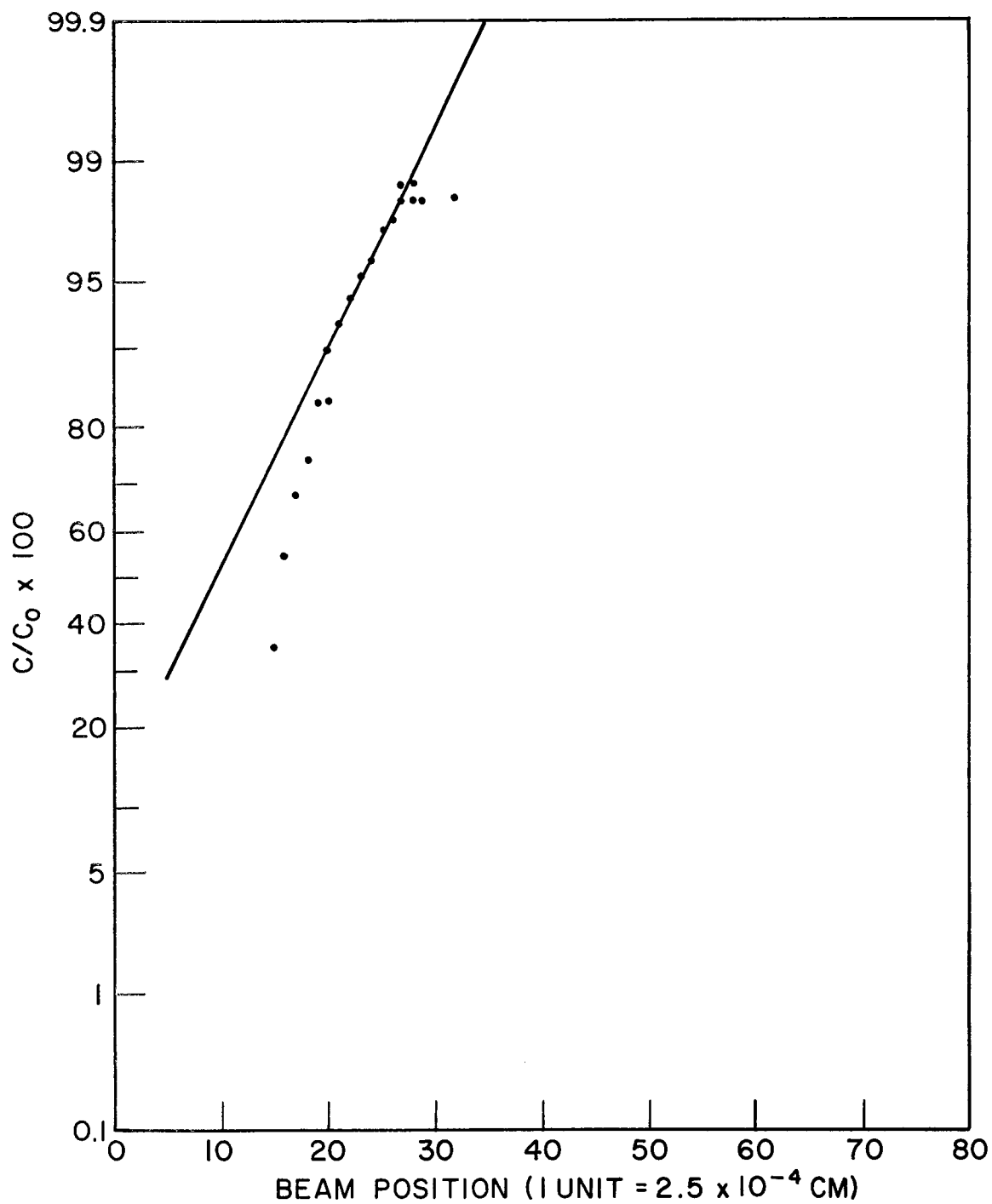


Figure A.2-26 - Probability plot of relative concentration, C/C_0 , versus penetration distance; 1500°C, 0.1 hr, 35% Ti, Scan 2.

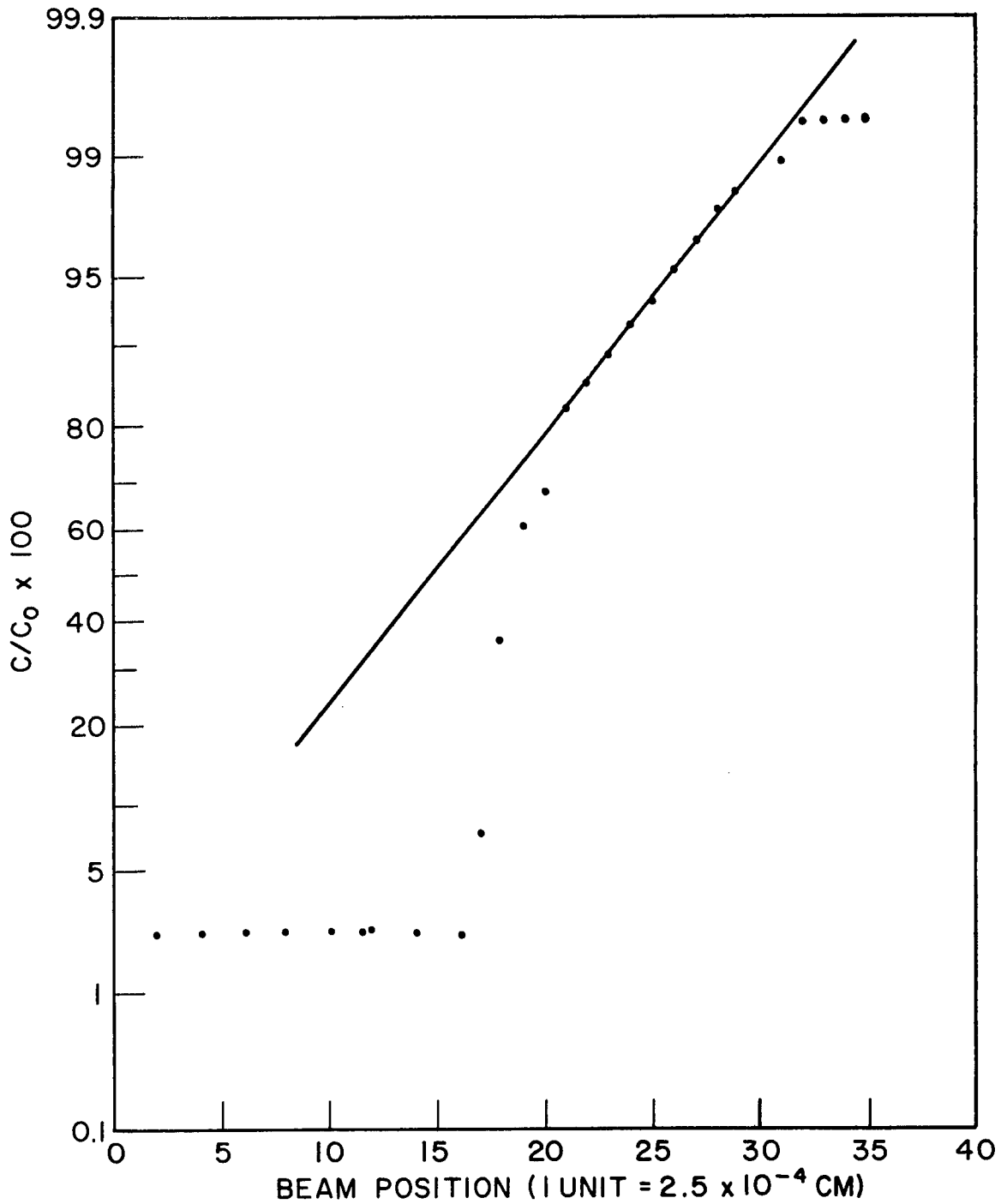


Figure A.2-27 - Probability plot of relative concentration, C/C_0 , versus penetration distance; 1500°C, 1.0 hr, 35% Ti, Scan 1.

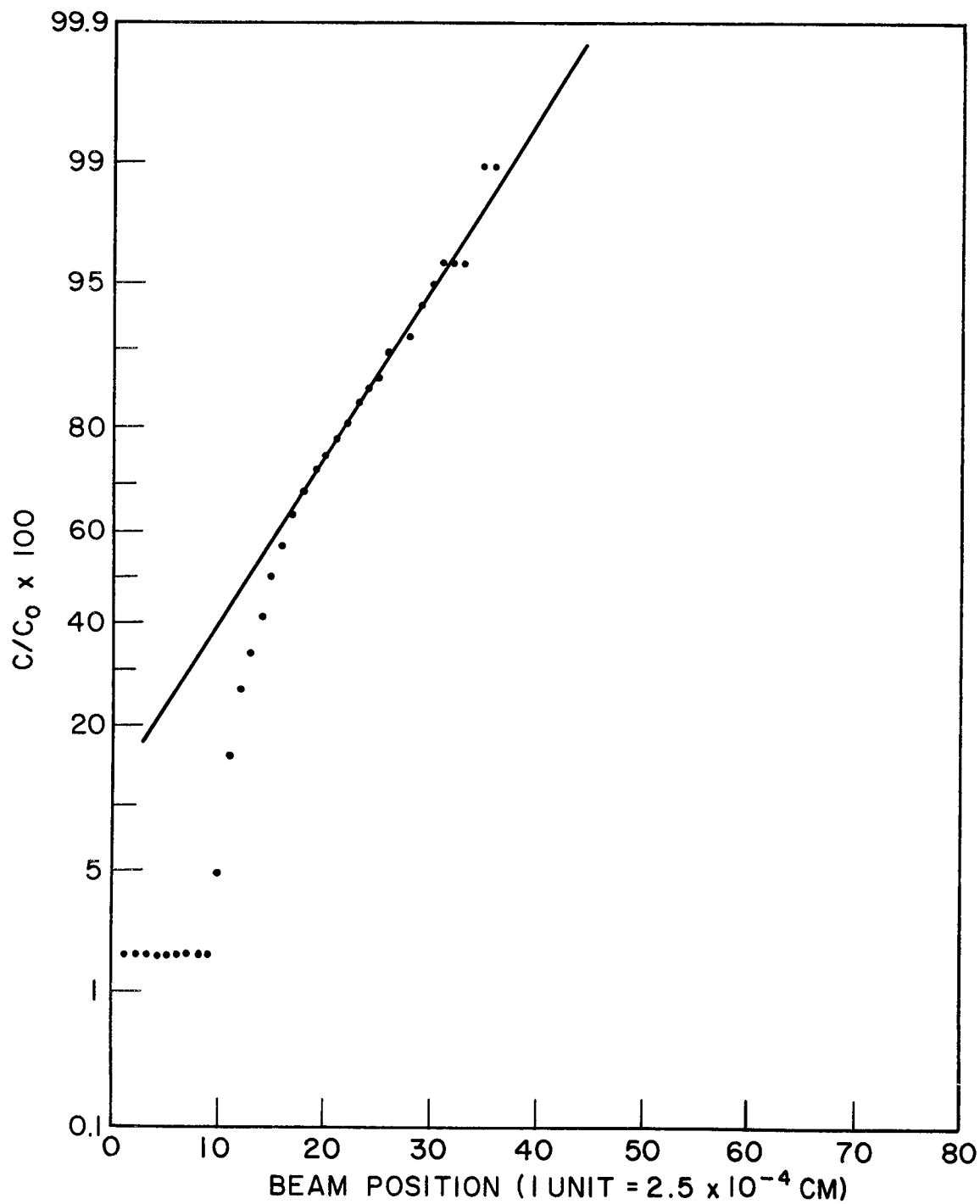


Figure A.2-30 - Probability plot of relative concentration, C/C_0 , versus penetration distance; 1500°C, 10 hr, 35% Ti, Scan 2.

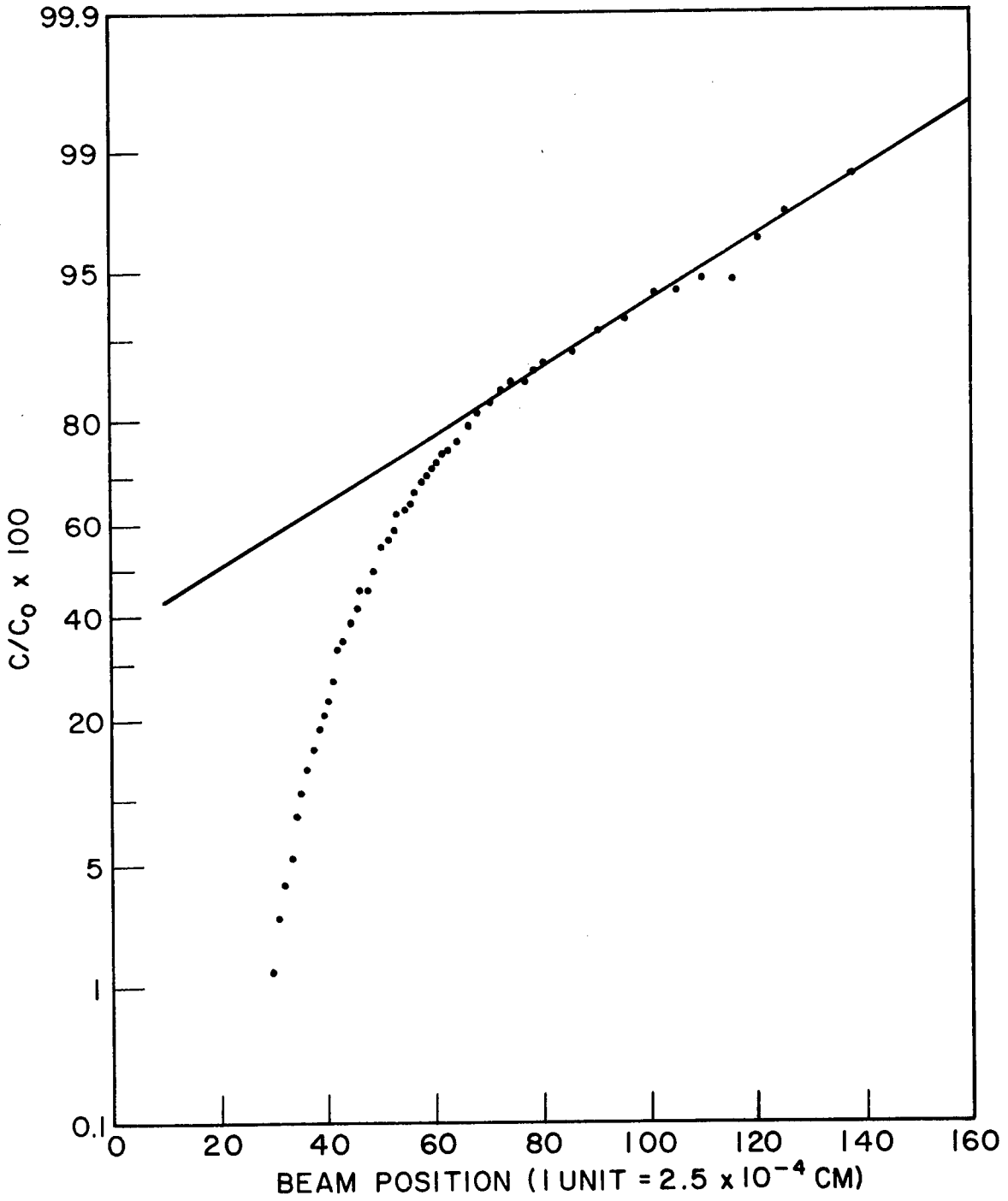


Figure A.2-31 - Probability plot of relative concentration, C/C_0 , versus penetration distance; 1500°C, 120 hr, 35% Ti, Scan 1.

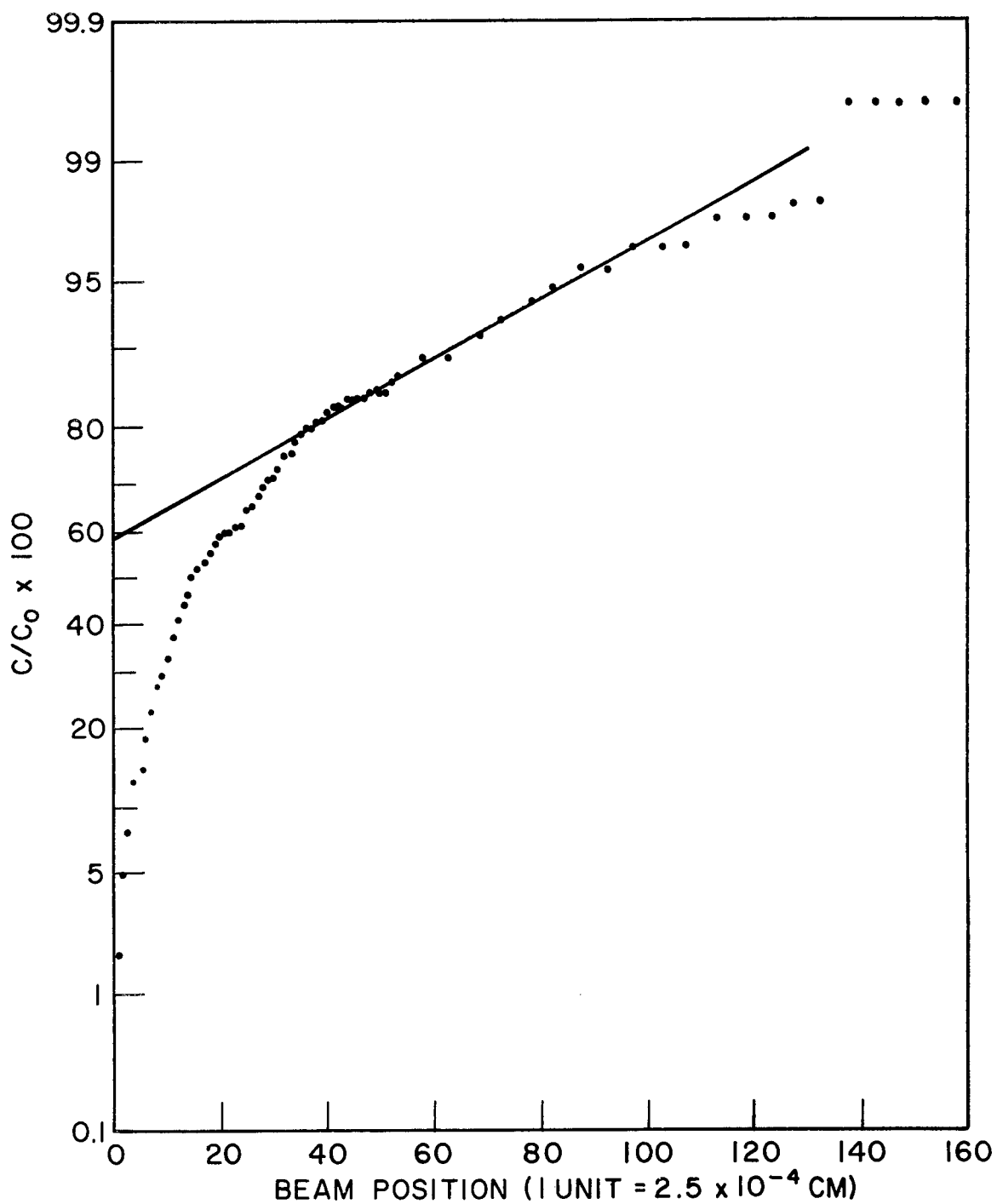


Figure A.2-32 - Probability plot of relative concentration, C/C_0 , versus penetration distance; 1500°C, 120 hr, 35% Ti, Scan 2.

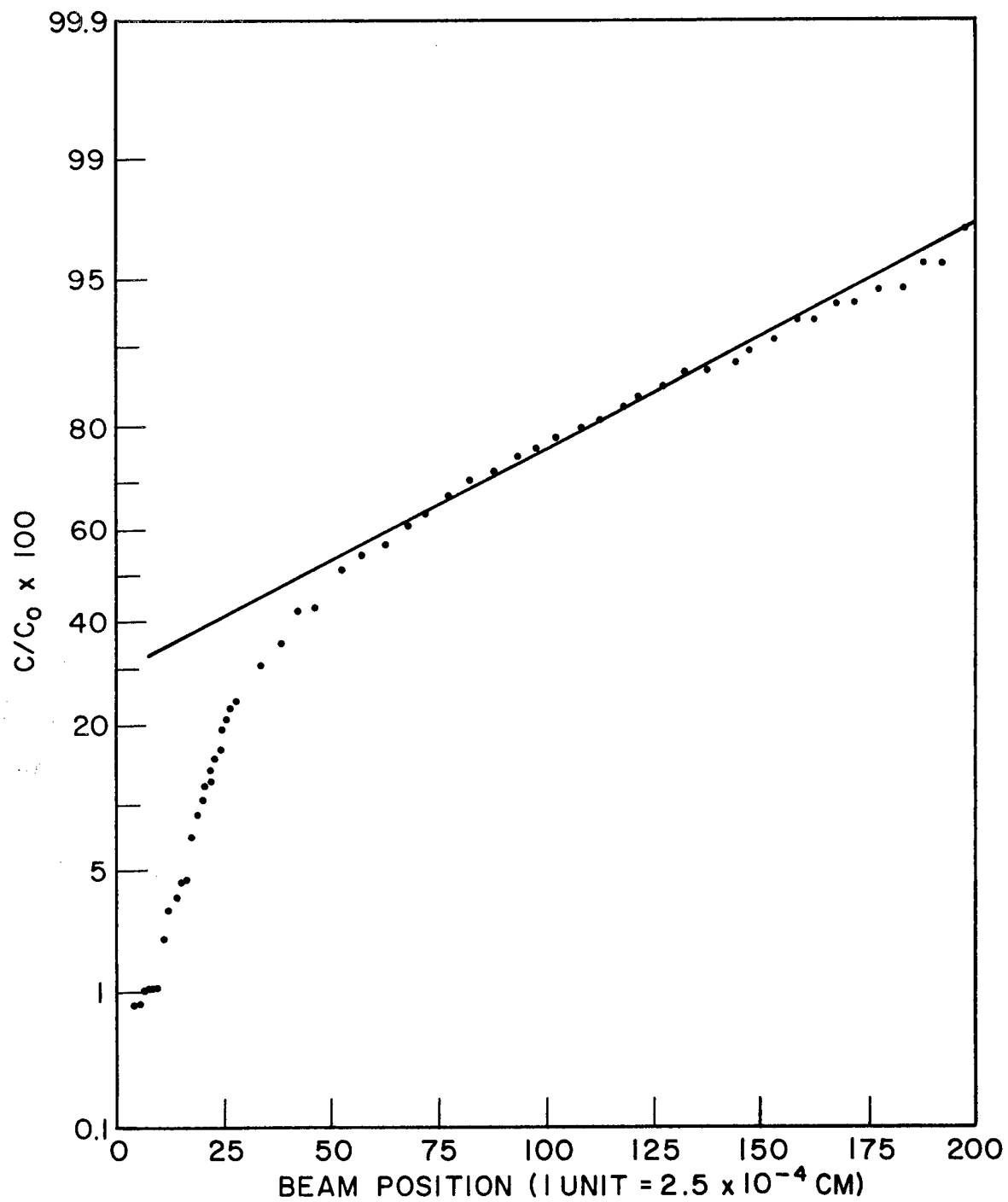


Figure A.2-33 - Probability plot of relative concentration, C/C_0 , versus penetration distance; 1500°C, 480 hr, 35% Ti, Scan 1.

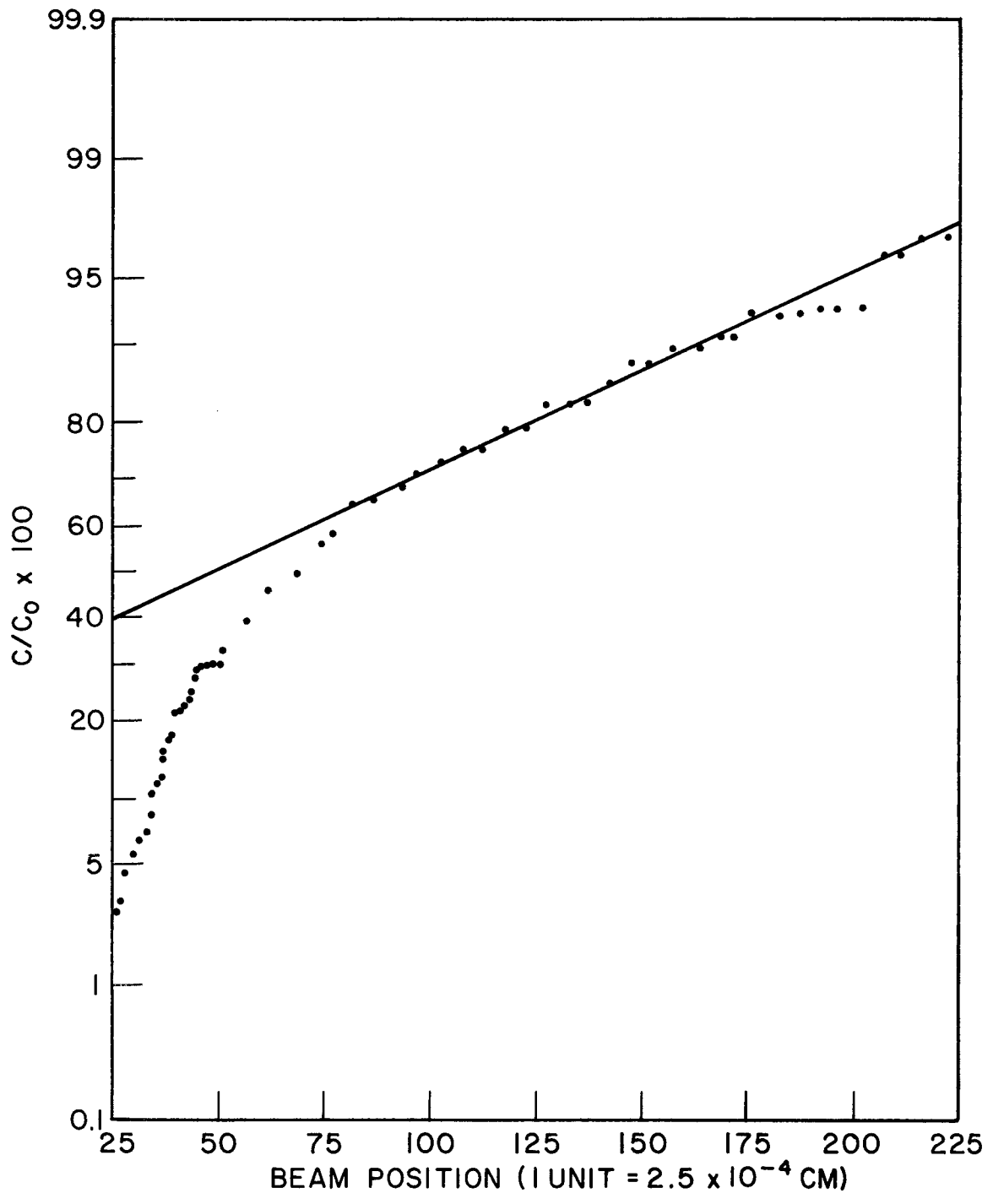


Figure A.2-34 - Probability plot of relative concentration, C/C_0 , versus penetration distance; 1500°C, 480 hr, 35% Ti, Scan 2.

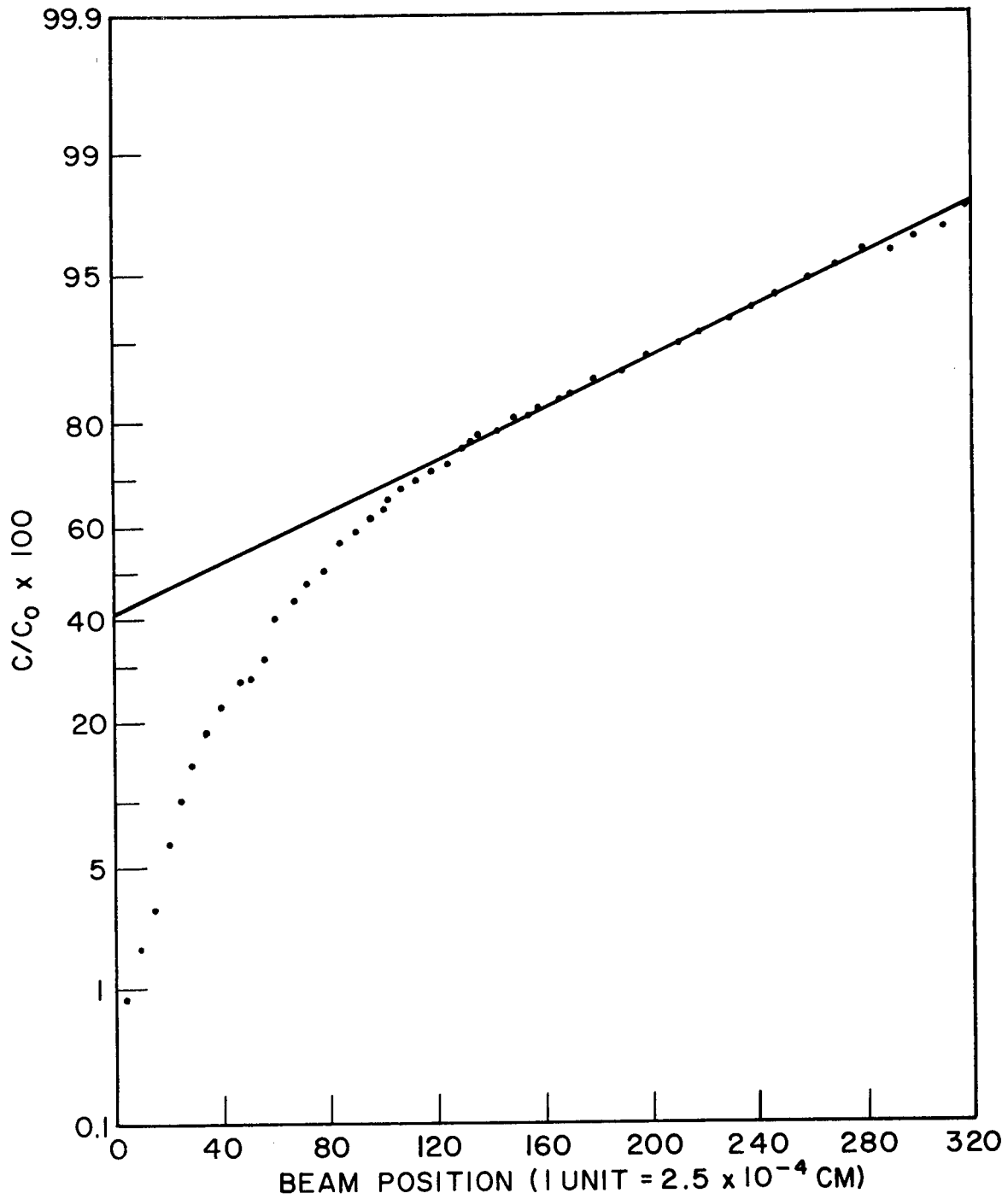


Figure A.2-35 - Probability plot of relative concentration, C/C_0 , versus penetration distance; 1500°C, 1000 hr, 35% Ti, Scan 1.

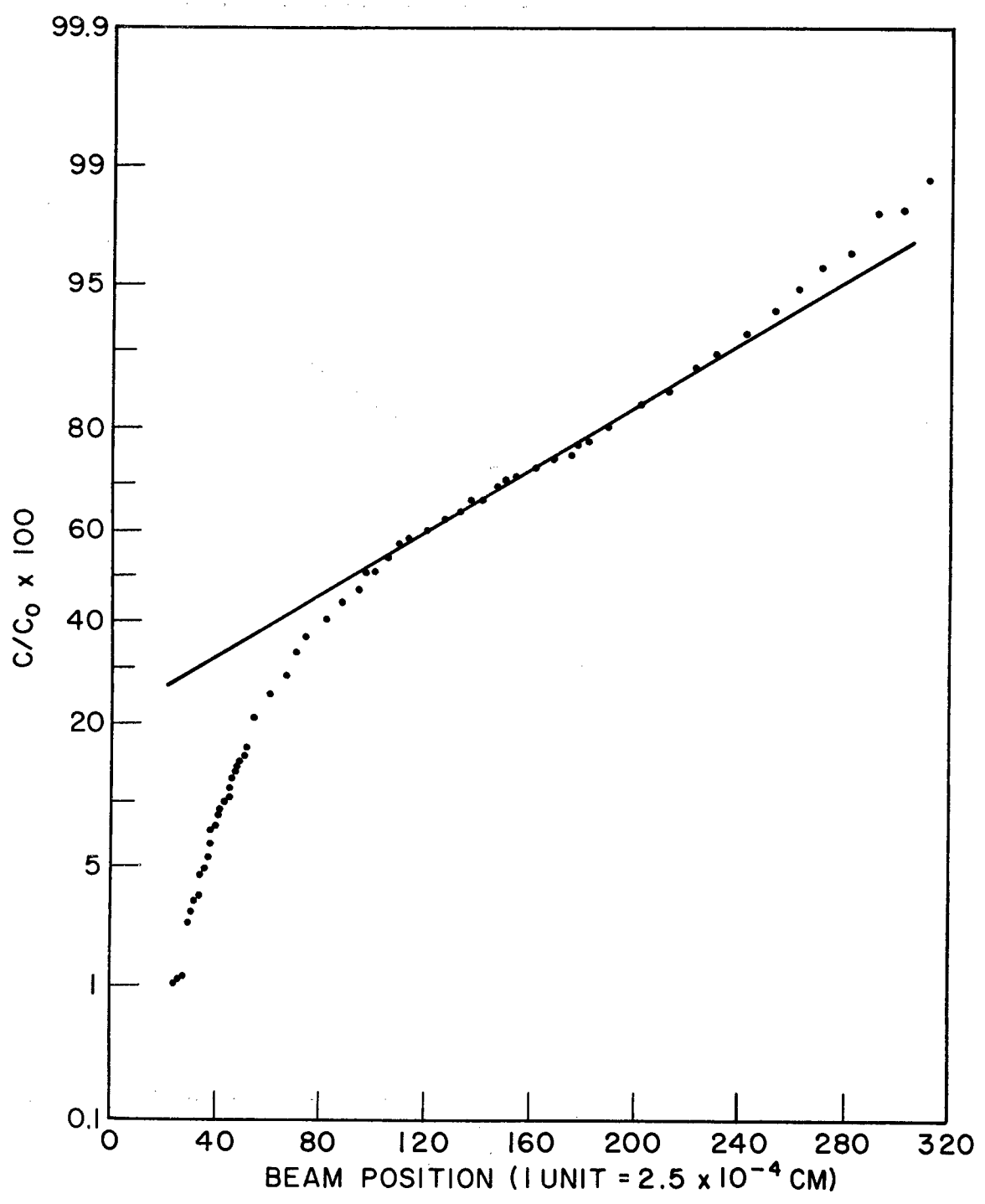


Figure A.2-36 - Probability plot of relative concentration, C/C_0 , versus penetration distance; 1500°C, 1000 hr, 35% Ti, Scan 2.

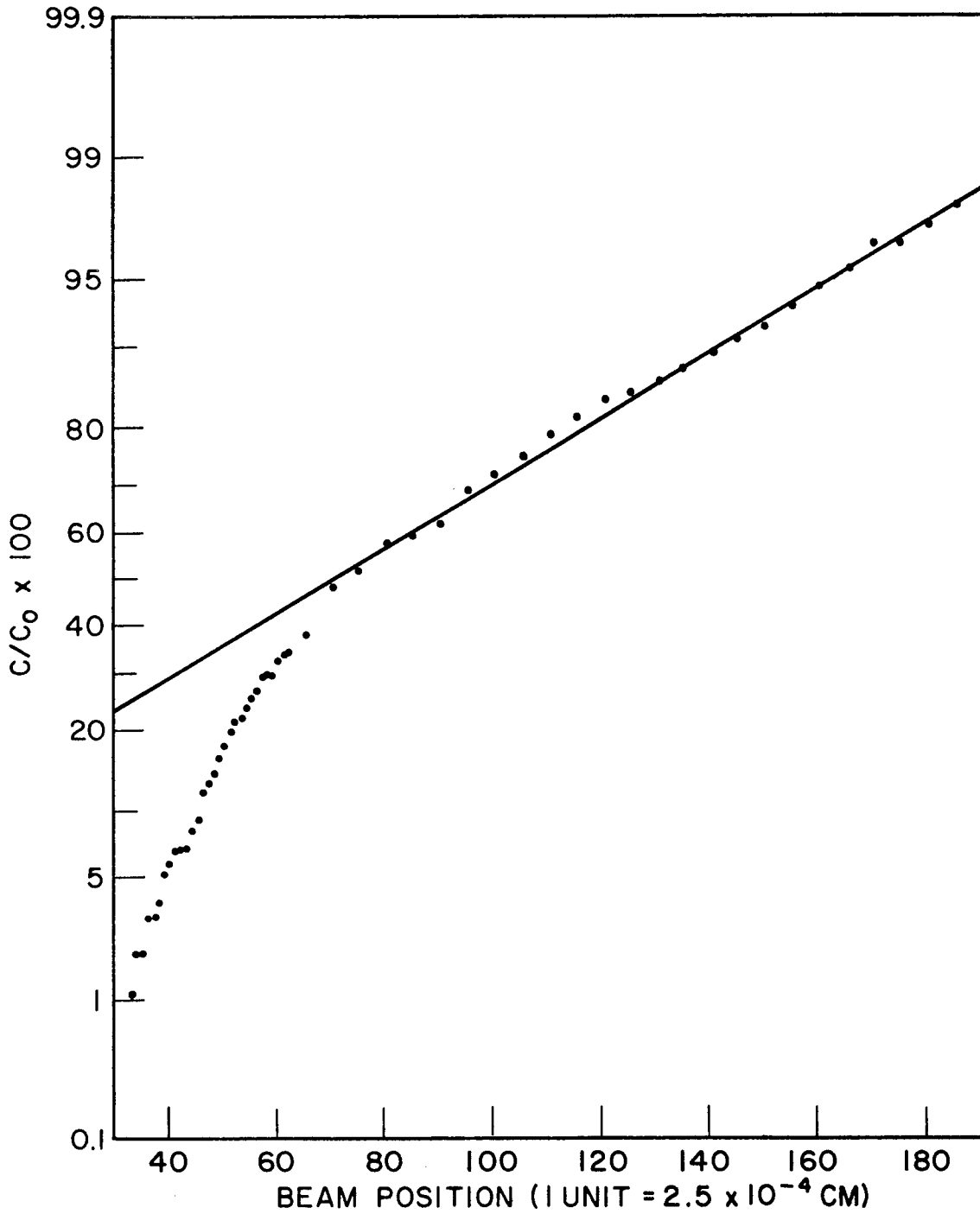


Figure A.2-37 - Probability plot of relative concentration, C/C_0 , versus penetration distance; 1800°C, 10 hr, 35% Ti, Scan 1.

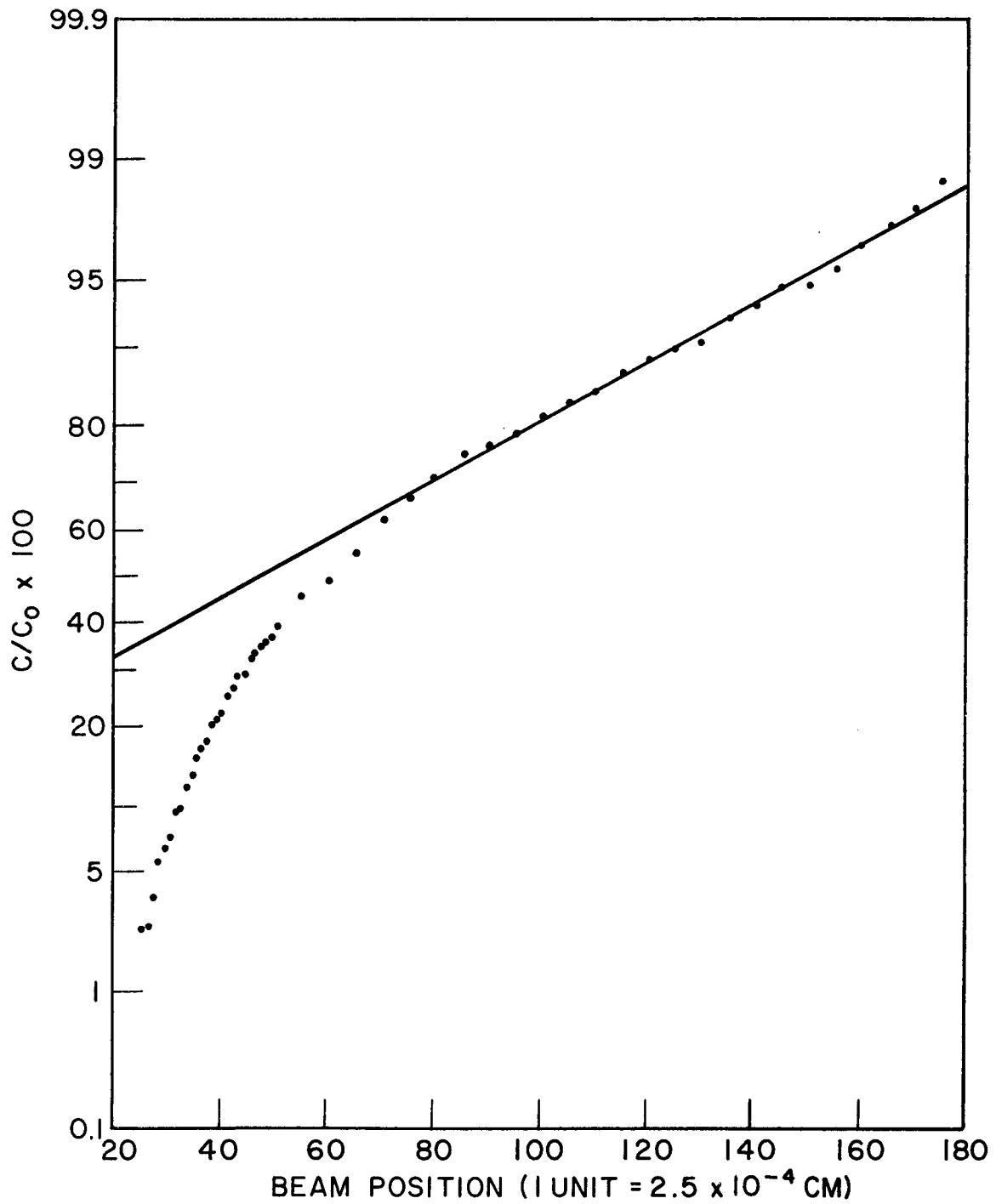


Figure A.2-38 - Probability plot of relative concentration, C/C_0 , versus penetration distance; 1800°C, 10 hr, 35% Ti, Scan 2.

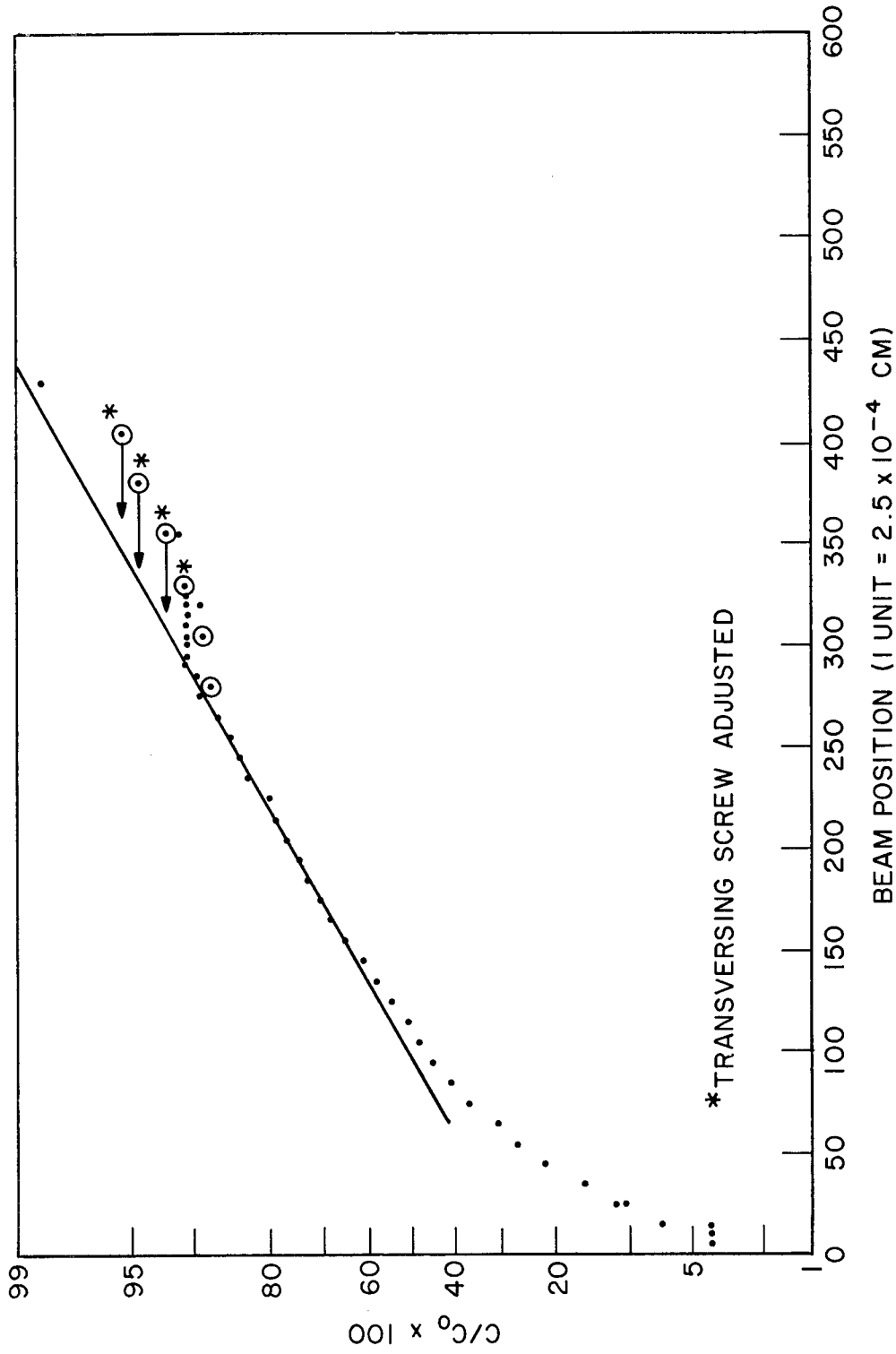


Figure A.2-39 - Probability plot of relative concentration, C/Co, versus penetration distance; 2000°C, 10 hr, 35% Ti, Scan 1.

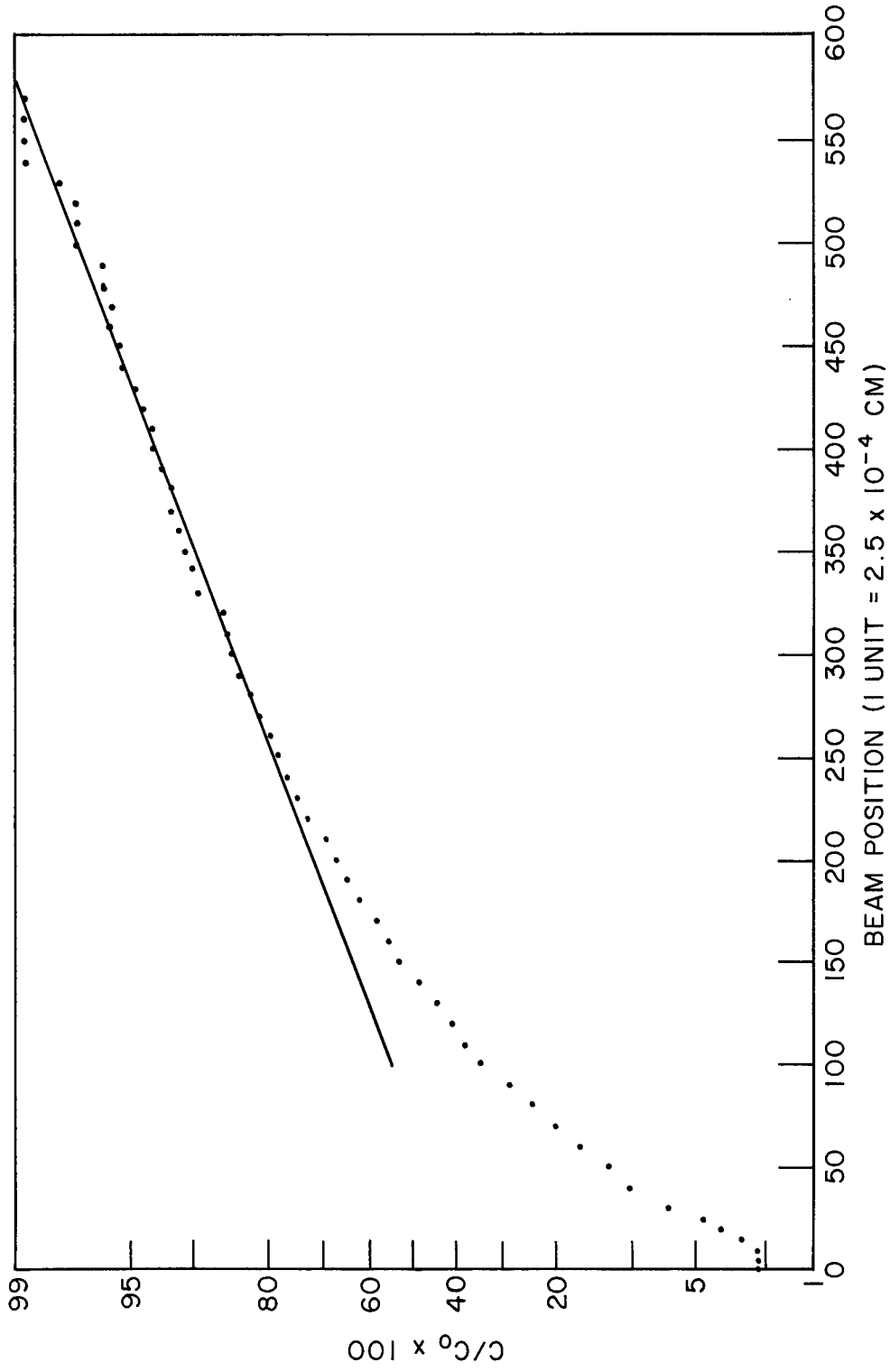


Figure A.2-40 - Probability plot of relative concentration, C/Co, versus penetration distance; 2000°C, 10 hr, 35% Ti, Scan 2.

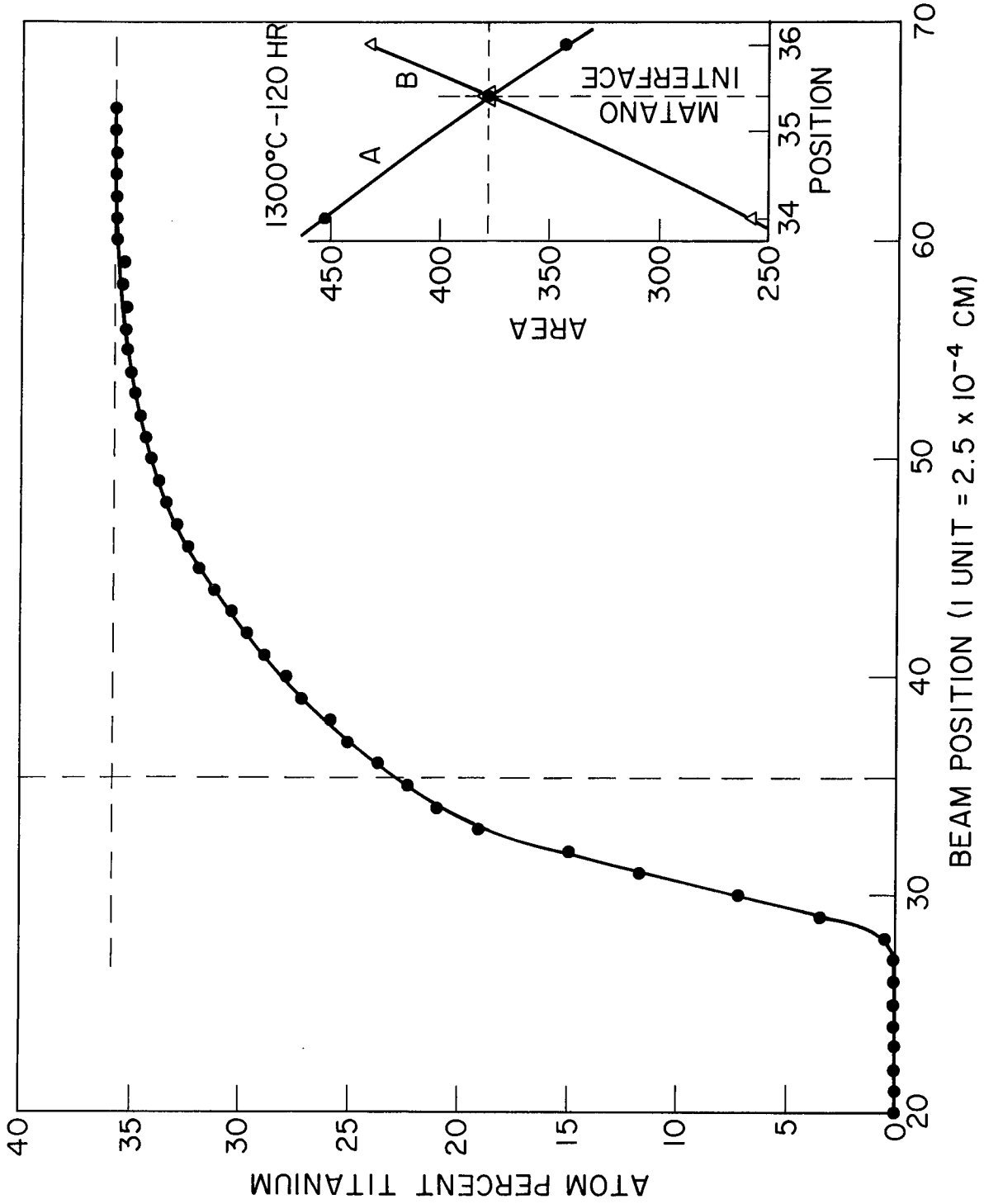


Figure A.2-41 - Linear plot of concentration versus penetration distance; 1300°C, 120 hr, 35% Ti.

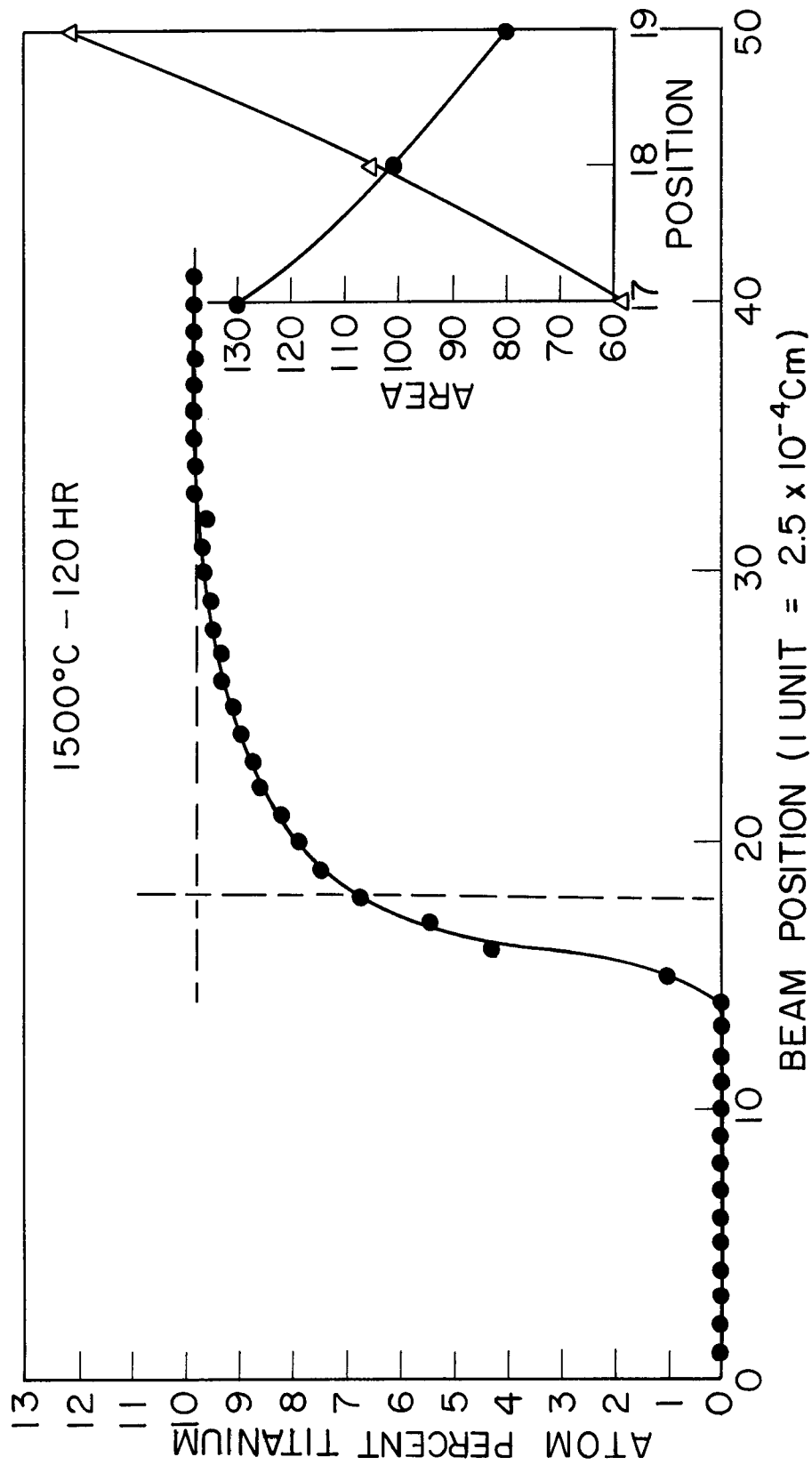


Figure A.2-42 - Linear plot of concentration versus penetration distance; 1300°C, 120 hr, 8.5% Ti.

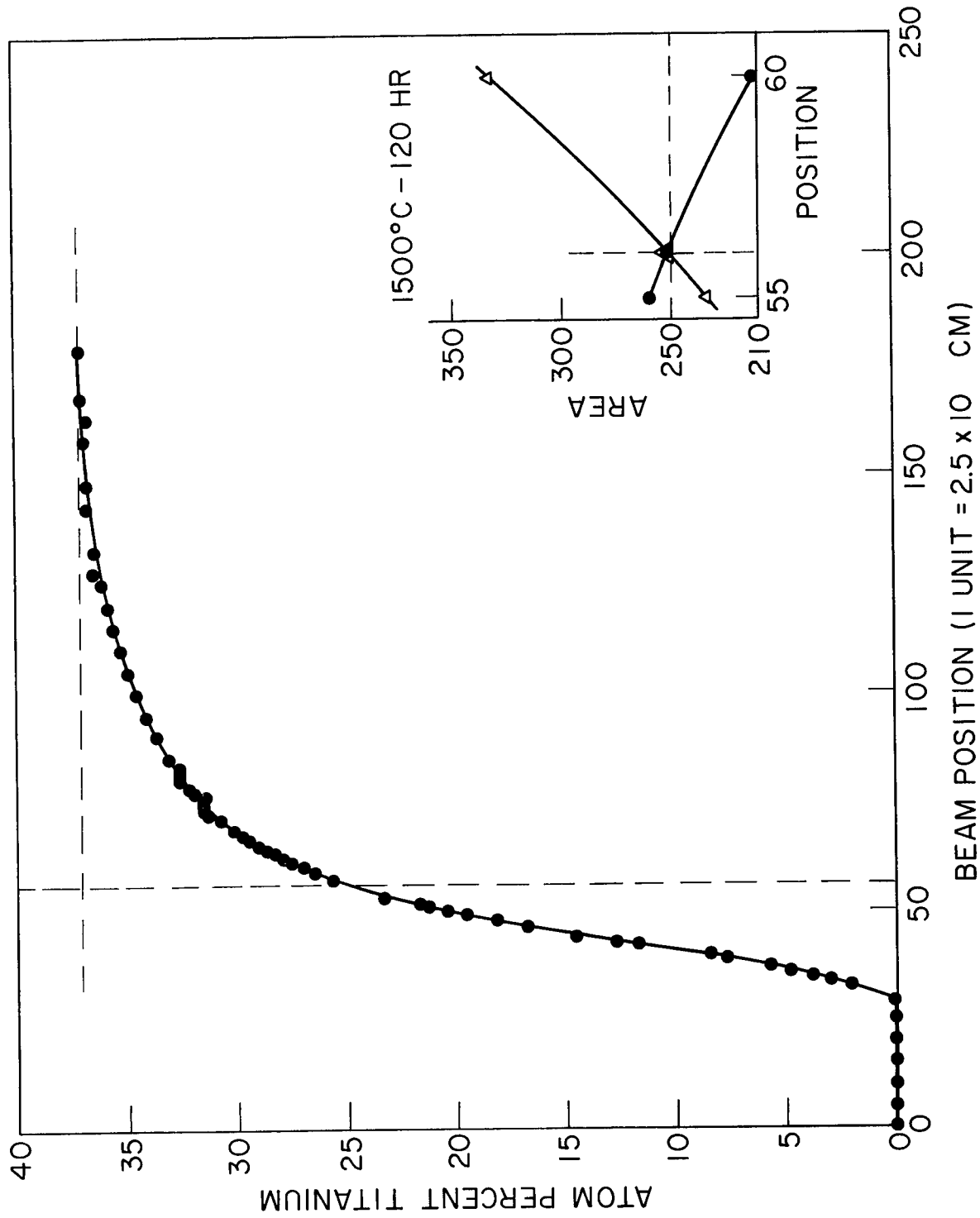


Figure A.2-44 - Linear plot of concentration versus penetration distance; 1500°C, 120 hr, 35% Ti.

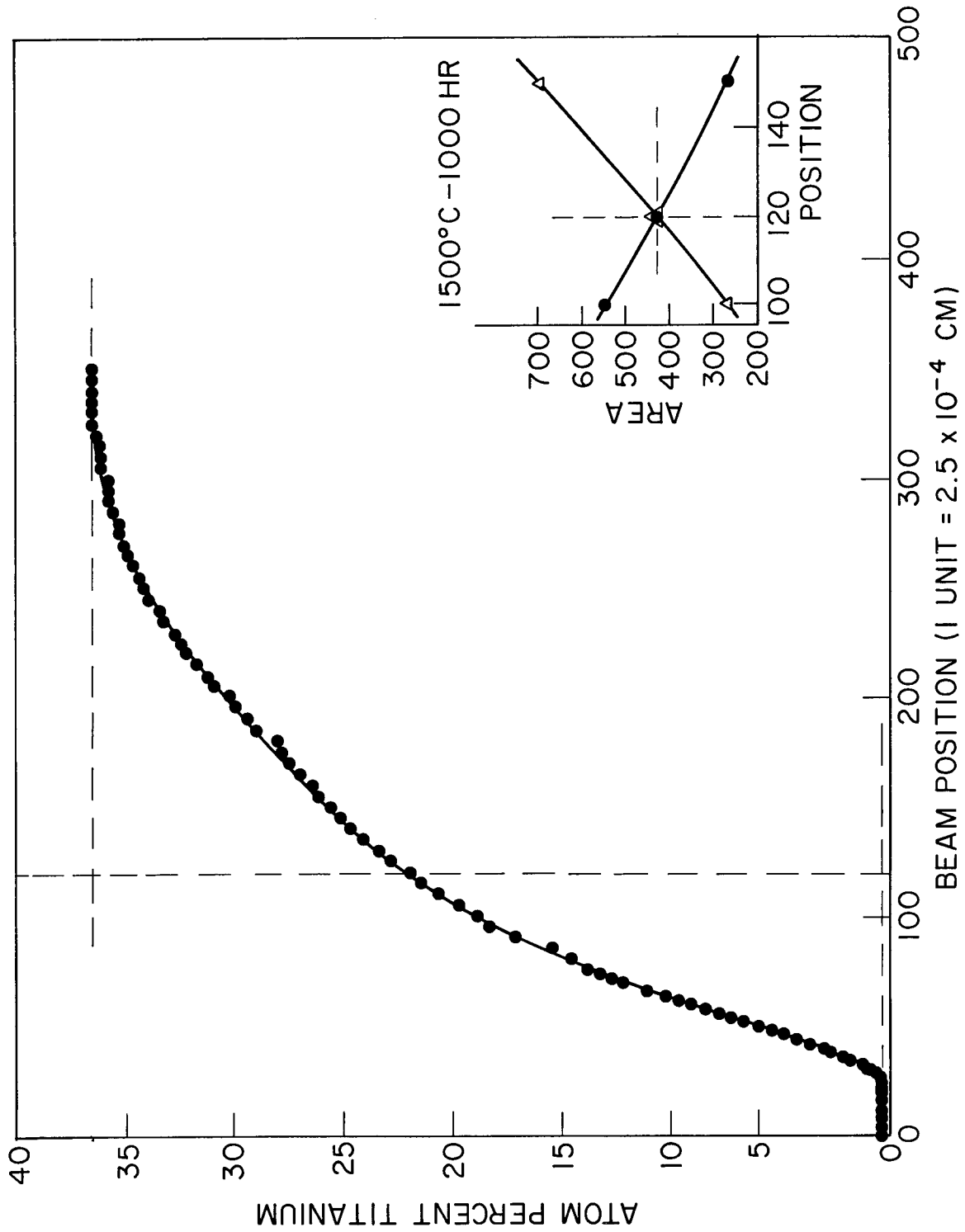


Figure A.2-45 - Linear plot of concentration versus penetration distance; 1500°C, 1000 hr, 35% Ti.

ATMOSPHERIC

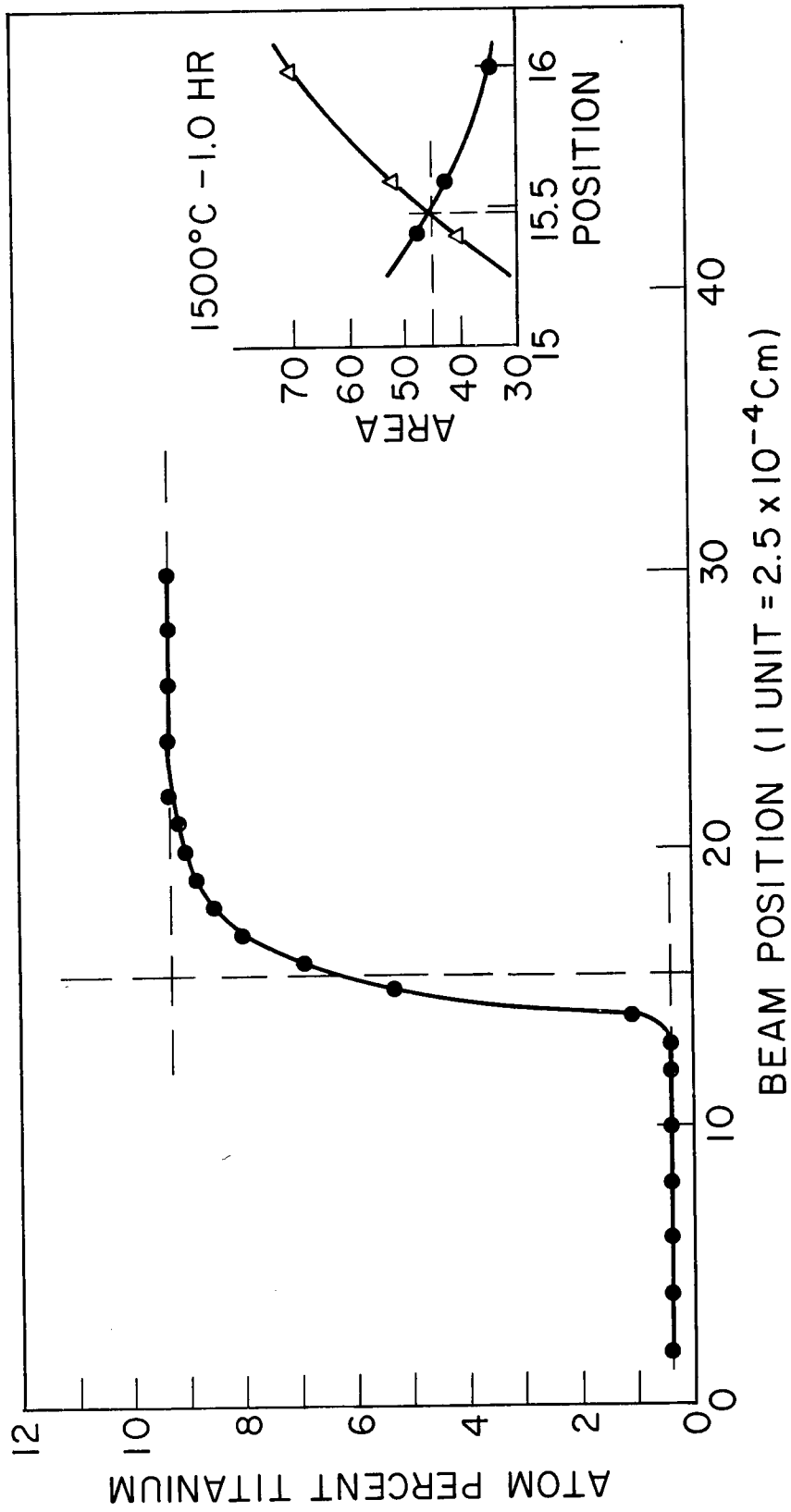


Figure A.2-46 - Linear plot of concentration versus penetration distance; 1500°C, 1.0 hr, 8.5% Ti.

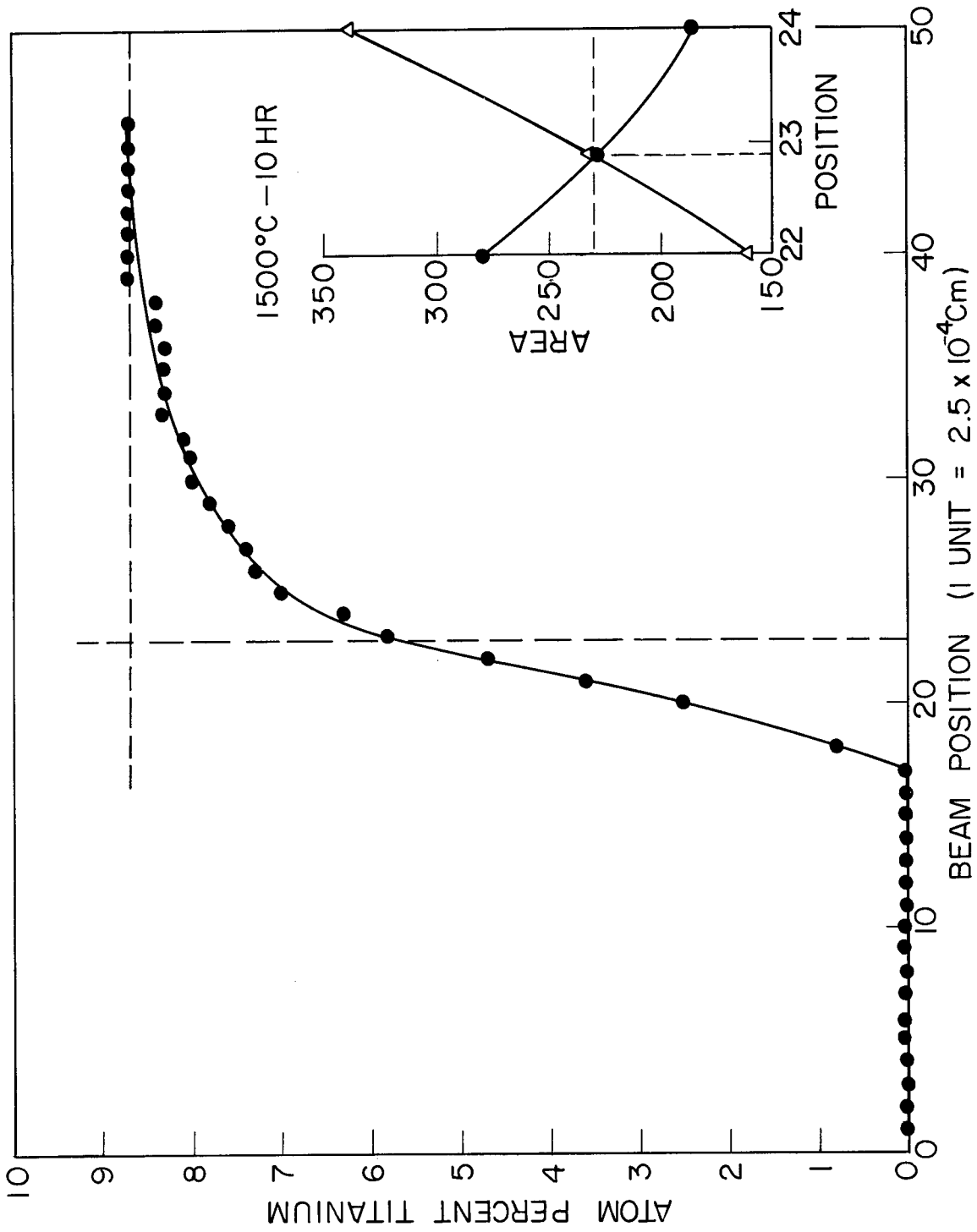


Figure A.2-47 - Linear plot of concentration versus penetration distance; 1500°C, 10 hr, 8.5% Ti.

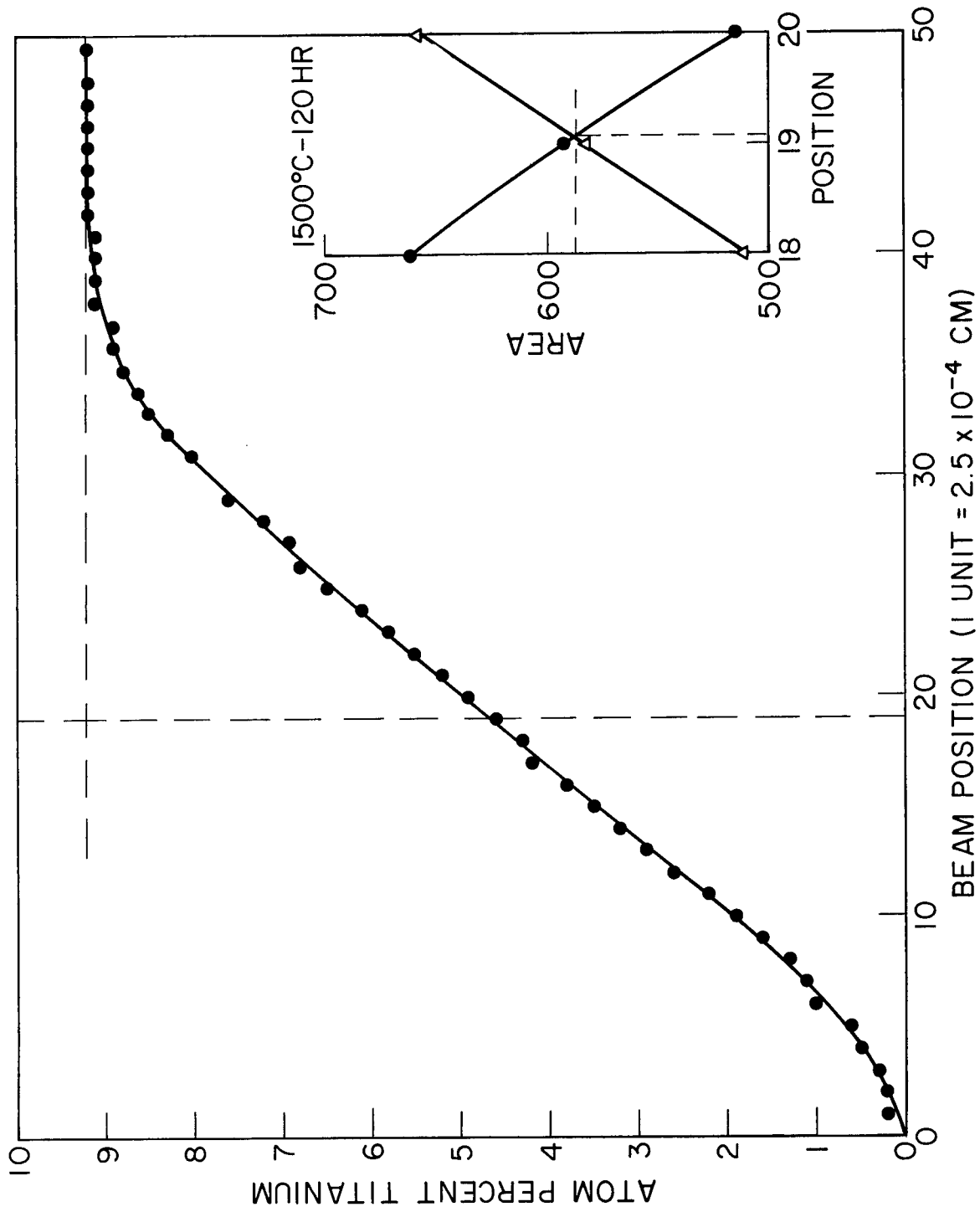


Figure A.2-48 - Linear plot of concentration versus penetration distance; 1500°C, 120 hr, 8.5% Ti.

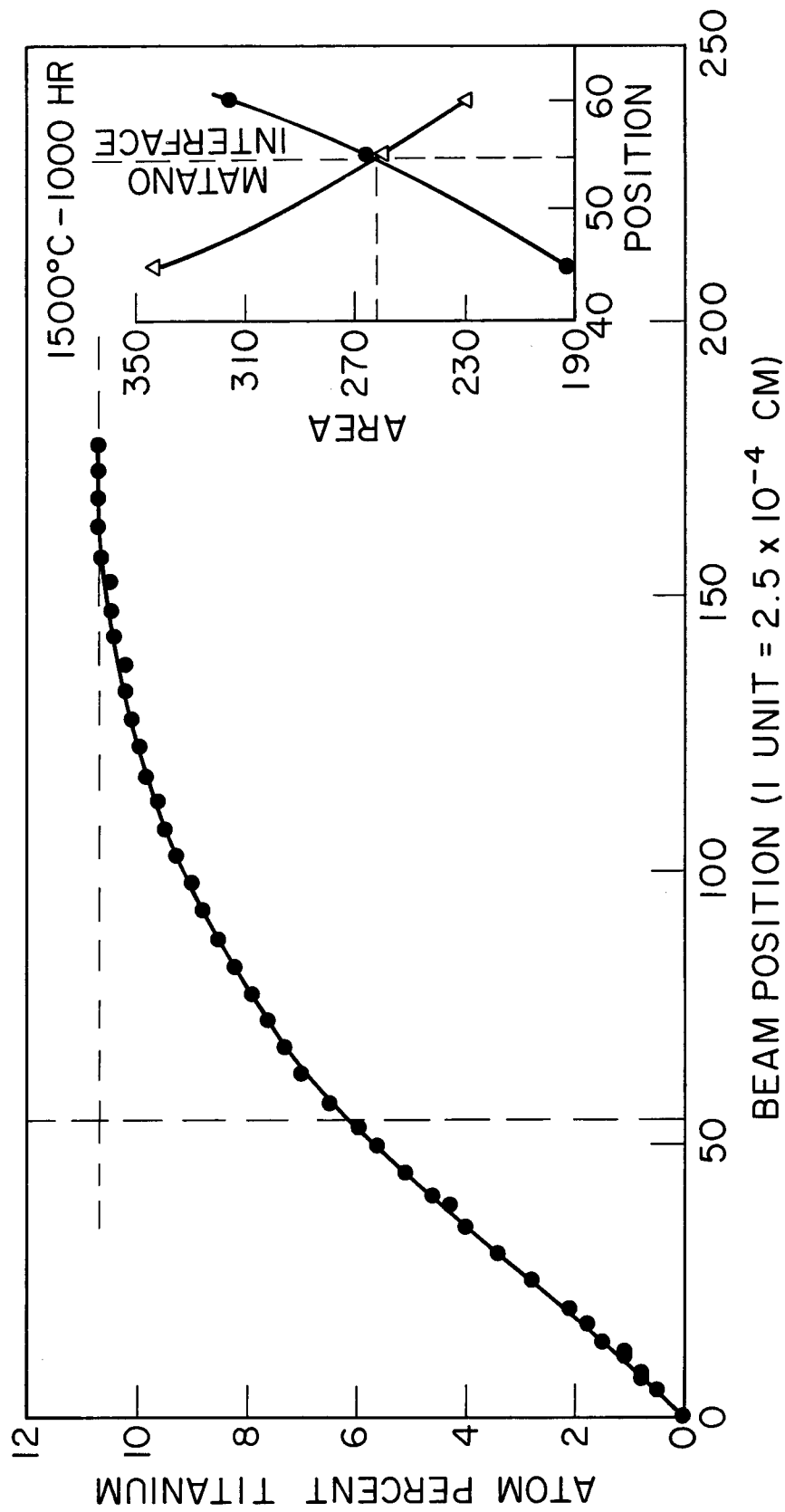


Figure A.2-49 - Linear plot of concentration versus penetration distance; 1500°C, 1000 hr, 8.5% Ti.

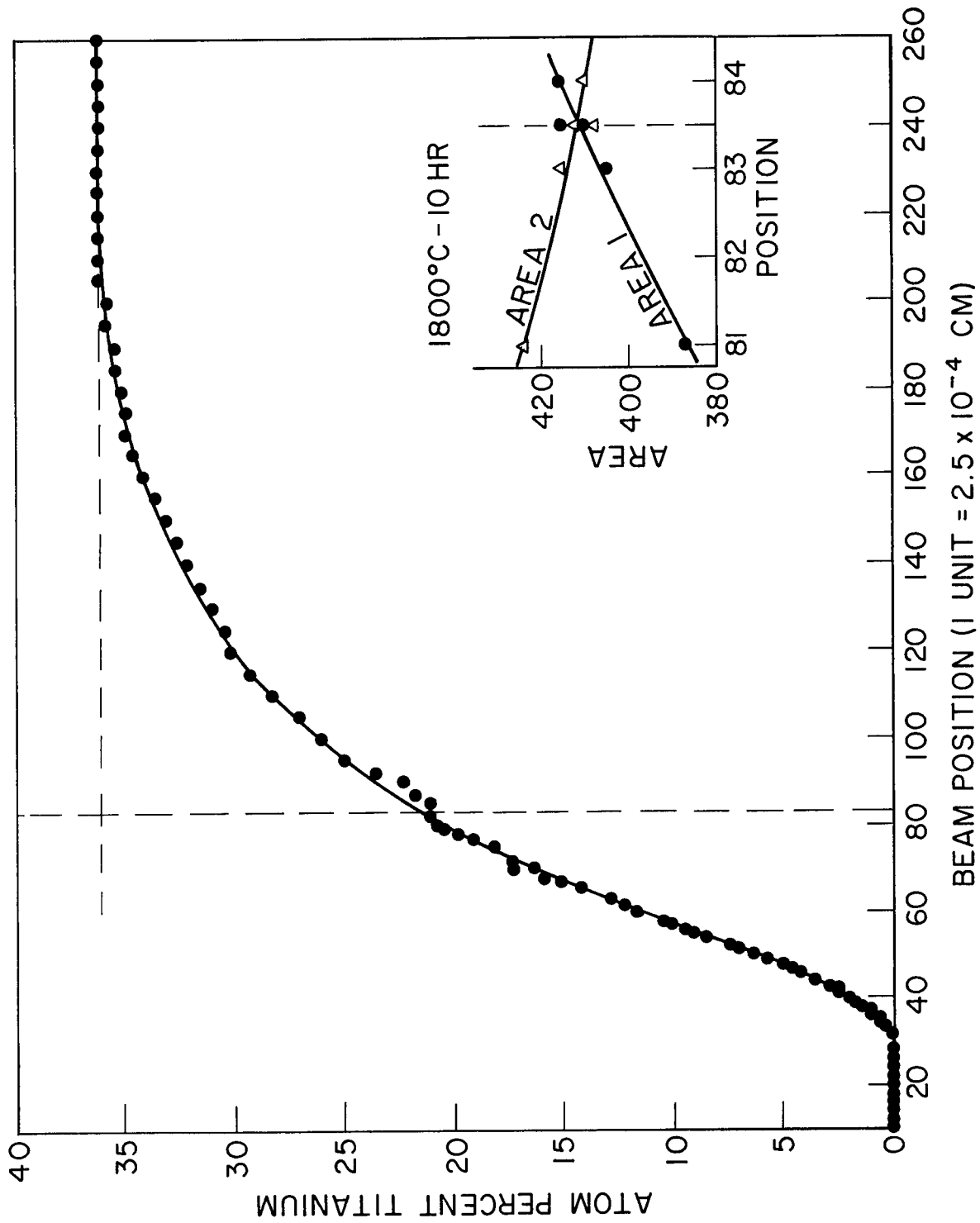


Figure A.2-50 - Linear plot of concentration versus penetration distance; 1800°C, 10 hr, 35% Ti.

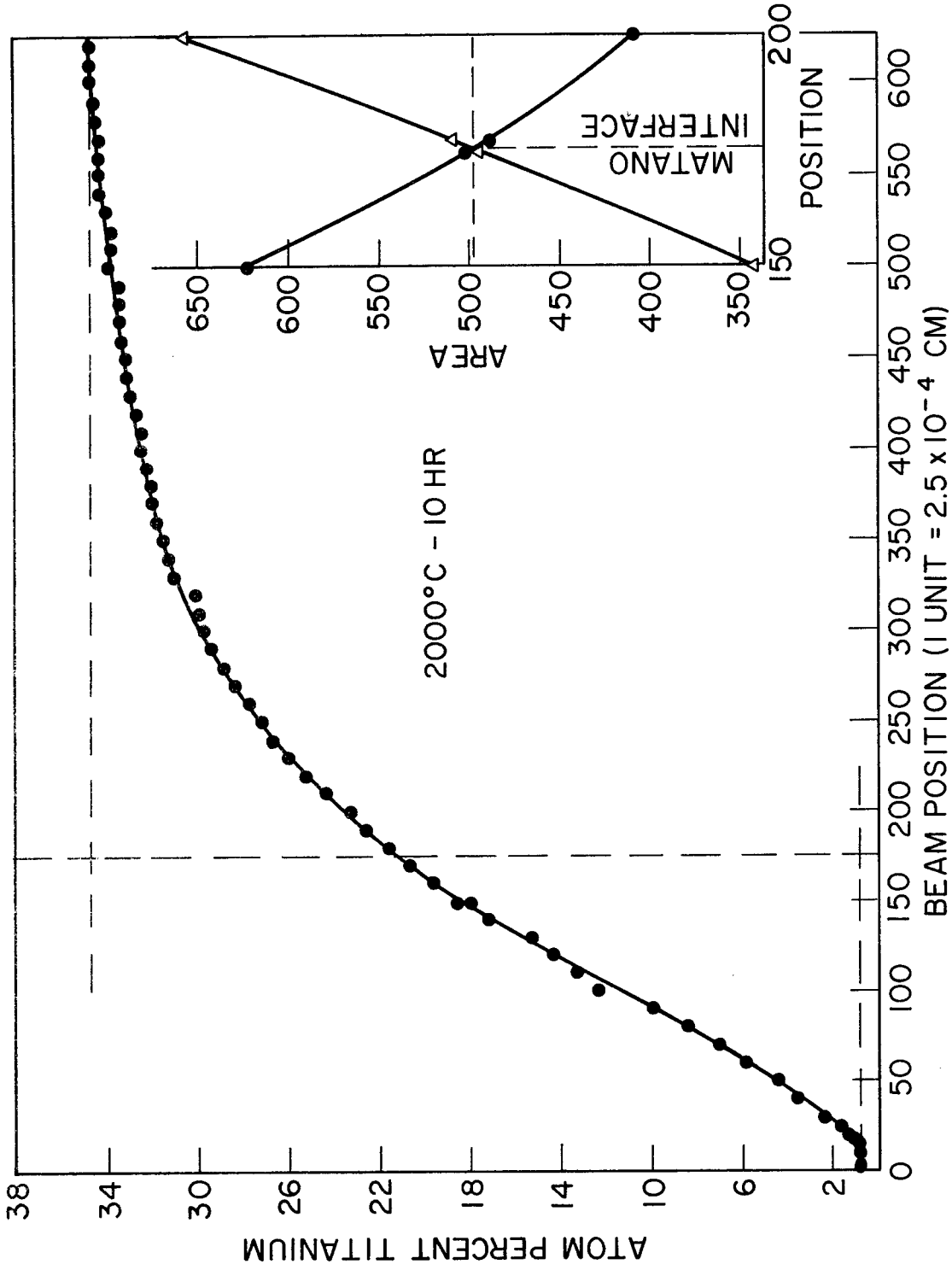


Figure A.2-51 - Linear plot of concentration versus penetration distance; 2000°C, 10 hr, 35% Ti.

APPENDIX 3

SAMPLE CALCULATIONS

A.3-1 Grube Solution

If the diffusion coefficient, D , is a constant and if the infinite boundary conditions, Eq. [A.1-9], apply, then the solution to the diffusion equation for non-steady conditions, Eq. [A.1-7], is given by Eq. [A.1-12] to be

$$C(x,t) = \frac{C_0}{2} \left[1 - \operatorname{erf} \left(\frac{x}{2\sqrt{Dt}} \right) \right] \quad [\text{A.1-12}]$$

or

$$C(x,t) = \frac{C_0}{2} \operatorname{erfc} \left(\frac{x}{2\sqrt{Dt}} \right).$$

The relationship between the error function and the integral of the normal curve of error ($\phi(x) = -\frac{1}{\sqrt{2\pi}} e^{-x^2/2}$) is such that if Eq. [A.1-12] holds, a plot of the data as C/C_0 vs. penetration distance on probability paper will have the form of a straight line. This fact is also discussed in the text (p.13) and in reference (15).

Consider the data of couple #33, scan 1, [35 a/o Ti, 1500°C, 10 hr.]. These data are given in Table 4, p.34 and are

plotted as C/C_0 vs distance on probability paper in Figure 13(a), p. 69. Now, recalling that if the Grube solution holds, the distance origin, $x = 0$, will be at $C/C_0 = 0.5$ for all $t > 0$, we take from the straight line portion of Figure 13(a),

$$\frac{C}{C_0} = 0.5, \quad x = 8.1$$

and

$$\frac{C}{C_0} = 0.9, \quad x = 22.0$$

or

$$\Delta x = 13.9.$$

Applying these data to Eq. [A.1-12], we get

$$\frac{2C(x,t)}{C_0} - 1 = -\operatorname{erf} \left(\frac{x}{2\sqrt{Dt}} \right) = -\operatorname{erf} (z)$$

or

$$2(0.9) - 1 = -\operatorname{erf} (z)$$

$$0.8 = -\operatorname{erf} (z)$$

From tables of the error function (2) we obtain

$$z = 0.905 = \frac{x}{2\sqrt{Dt}}$$

$$t = 10 \text{ hr.} = 3.6 \times 10^4 \text{ sec}$$

$$x = 13.9 \text{ probe units, correcting}$$

for thermal expansion

$$= 13.9 \times 2.522 \times 10^{-4} \text{ cm}$$

$$Dt = \frac{13.9 \times 2.522 \times 10^{-4}}{2 \times 0.905} = 19.42 \times 10^{-4} \text{ cm}^2$$

$$Dt = 377 \times 10^{-8} \text{ cm}^2$$

$$\underline{\underline{D = 1.05 \times 10^{-11} \text{ cm}^2/\text{sec.}}}$$

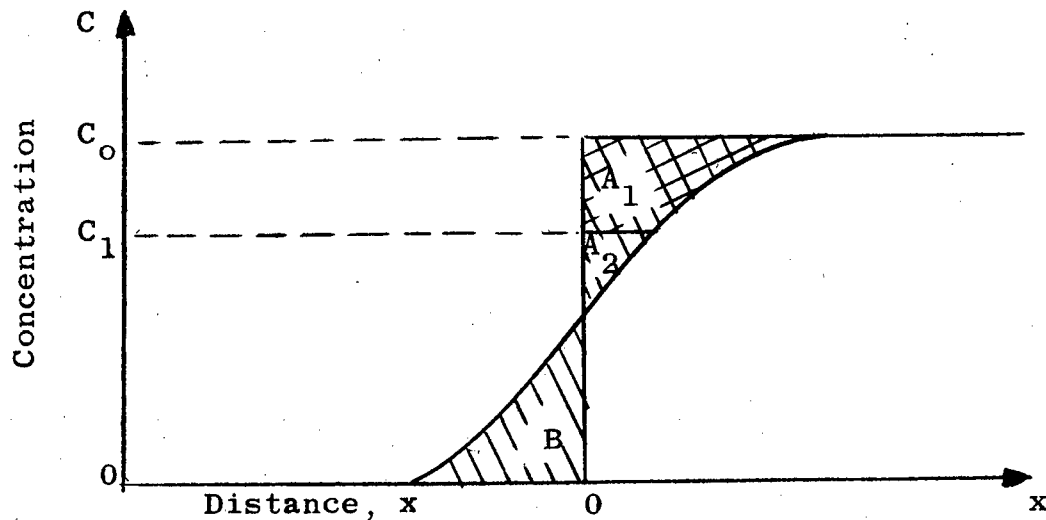
A.3-2 Boltzmann-Matano Method

If the diffusion coefficient is a single valued function of concentration, i.e., $D = D(C)$, and if the infinite boundary conditions, Eq. [A.1-9], apply, then the solution to the diffusion equation for non-steady conditions, Eq. [A.1-6], is given by Eq. [A.1-17] to be

$$D_{C_1} = - \frac{1}{2t} \frac{dx}{dC} \Big|_{C_1} \cdot \int_{C_0}^{C_1} x \, dC . \quad [A.1-17]$$

This relationship is developed in Appendix 1, and it is therefore only noted here that C_1 represents any concentration between 0 and C_0 at which one wishes to evaluate D .

Consider the data of couple #33, scan 1, [35 a/o Ti, 1500°C, 10 hr.]. The concentration-penetration curve for the penetration data of this couple is given in Figure 13(b) and is shown schematically below:



UNCLASSIFIED

The second condition of Matano, Eq. [A.1-18], is met if Area A equals Area B. Planimeter measurements of these areas on Figure 13(b) as a function of position are plotted in the lower right hand corner of Figure 13(b). The Matano interface is found to be at probe position 12.7. The equal areas are 318 planimeter units (pl).

Evaluating D at 30 a/o Ti:

The terms of Eq. [A.1-17] may be evaluated from Figure, 13(b),

$$\int_{C(30)}^{C_0} x \, dC = \text{Area } A_1 \text{ in the sketch} = 246 \text{ (pl)}$$

$$\left. \frac{dx}{dC} \right|_{C=30} = -1.45 \frac{\text{beam units}}{\text{a/o}} \left(\frac{u}{\text{a/o}} \right)$$

Also from planimeter measurement,

$$10 \text{ a/o} \times 10 \text{ beam units} = 393 \text{ planimeter units.}$$

Substituting,

$$D = \frac{1}{2 \times 3.6 \times 10^{-4}} \times 1.45 \times 246 \times \frac{100}{392} \times (2.5 \times 10^{-4})^2$$

$$= \text{sec}^{-1} \left(\frac{u}{\text{a/o}} \right) (\text{pl}) \frac{(u \cdot \text{a/o})}{(\text{pl})} \frac{\text{cm}^2}{u^2} = \frac{\text{cm}^2}{\text{sec}}$$

Correcting for thermal expansion,

$$D = 12.64 \times 10^{-4} \times (2.528 \times 10^{-4})^2 \frac{\text{cm}^2}{\text{sec}}$$

$$\underline{\underline{D = 8.08 \times 10^{-11} \text{ cm}^2/\text{sec}}}$$

A.3-3 The Effective Penetration During Welding

The effective penetration distance due to diffusion which takes place during the welding process may be computed by considering the value of D taken from the extrapolated $\log D$ vs $\frac{1}{T}$ plot.

The welding temperature is

$$T \cong 1100^{\circ}\text{C} \text{ (brightness)}$$

$$\cong 1195^{\circ}\text{C} \text{ (corrected)}$$

$$= 1468^{\circ}\text{K}_1;$$

$$\text{thus } \frac{1}{T} = 6.81 \times 10^{-4} \text{ } (^{\circ}\text{K})^{-1}.$$

The time of welding varied from 5 to 6 minutes,

$$t \cong 360 \text{ sec.}$$

From Figure 24 p. 83 at $\frac{1}{T} = 6.8 \times 10^{-4}$,

$$D = 5 \times 10^{-14} \text{ (0 a/o Ti) to } 2 \times 10^{-12} \text{ (30 a/o Ti),}$$

$\text{cm}^2/\text{sec.}$

For the smaller value,

$$Dt = 1.8 \times 10^{-11} \text{ (cm)}^2,$$

and for the larger,

$$Dt = 7.2 \times 10^{-9} \text{ cm}^2.$$

These values of Dt may be compared with measured values in Table 5, p. 36.

UNCLASSIFIED

APPENDIX 4

CONTAMINATION

The niobium-titanium alloy system is a continuous body-centered cubic (b.c.c.) solid solution from the transition temperature of titanium (882°C) to the solidus. A two-phase field extends from 882°C at 100% Ti to approximately 50% Ti at about 400°C, below which no further reaction takes place. Based on these equilibria, binary alloys of less than 50 a/o Ti would be single phase b.c.c. solid solutions at all temperatures below the solidus. However, the 8.5 a/o Ti and 35 a/o Ti alloys used in this study were found to contain a precipitate, both as received and after recrystallization.

Annealing at 1900°C in vacuum ($< 10^{-5}$ torr) by electron-beam bombardment or by induction heating of the as received 1/2-inch diameter rods successfully removed all traces of the second phase. Also, examination of the welded diffusion couples revealed no evidence of a second phase. However, diffusion anneals at 1300°-1500°C in vacuum for more than one day caused the precipitate to form again, Figure A.4-1(a,b). The hardness of the 8.5 a/o Ti alloy, Table A.4-1, further demonstrates the effect of the various annealing treatments.

TABLE A.4-1

Hardness of a Cb 8.5 a/o Ti Alloy after Various Anneal Conditions

<u>Condition</u>	<u>Hardness, VPHN 8.5 a/o Ti Alloy</u>
Recrystallized, 1500°C, 8 hr	252
Electron-Beam Anneal, 1900°C, 5 min	135
Induction Anneal, 1900°C, 1 min	130
Diffusion Couple, As Welded	130
After Diffusion Anneal	
(a) with Alumina	218
(b) all metal	130

A.4-1 Source of Contamination

Efforts to obtain positive identification of the precipitate were unsuccessful, but reduction in oxygen content of both alloys by the 1900°C anneals, while nitrogen content remained about the same, Table A.4-2, suggest that the precipitate might be a ternary oxide.

TABLE A.4-2

Gas Analysis (ppm)

Condition	8.5 a/o Ti		35 a/o Ti	
	O	N	O	N
As Received	130	57	453	65
Electron Beam Anneal (a)	170	--	150	--
Induction Anneal (b)	48	60	59	70
(a) 1900°C, ~5 min, 10 ⁻⁵ torr				
(b) 1900°C, ~1 hr, 10 ⁻⁶ torr				

At this point in the experimental program a second furnace became available for diffusion anneals. Couples annealed in it at the same temperature, time, and vacuum conditions as in the first furnace showed no precipitate.

The second furnace is an all-metal system and the specimen, wrapped in niobium foil, is supported in a tantalum "can" which is suspended inside the self-supporting tantalum resistance heater. The molybdenum wire heater of the first furnace is supported on an alumina core, and the specimens were placed on high purity, recrystallized, alumina disks within a tantalum "can" which in turn was suspended inside the alumina core.

The presence of alumina, although it should be inert to niobium, appears to have caused contamination of the NbTi alloys. To verify this supposition, alloy specimens were annealed by induction with the specimen suspended in the coil by tantalum wire and in a second all-metal tantalum resistance furnace. No precipitate was found. Furthermore, after removing the alumina from within the tantalum 'can' and with specimens wrapped in niobium foil, alloys annealed in the first furnace at 1300°C and below were also free of the precipitate.

A.4-2 Identity of Precipitate

Positive identification of the precipitate by x-ray techniques have not been successful. The quantity present is too small to produce measurable intensities and the precipitate

allotriomorphs are too small for micro x-ray techniques. However, specimens containing large precipitate allotriomorphs have been examined with the electron microprobe. Concentration data and photomicrographs indicating corresponding contamination spots are presented in Figures A.4-2 and A.4-3.

The distance between spots is 2.5×10^{-4} cm and from this the spot size is estimated to be 1 -1.5 microns in diameter. For spots which are identified as contained totally within or outside of a precipitate allotriomorph the maximum titanium and corresponding columbium compositions are given in Table A.4-3.

TABLE A.4-3

COMPOSITION (Atom Percent)

	8.5 a/o Ti Alloy		35 a/o Ti Alloy	
	Matrix	Precipitate	Matrix	Precipitate
Ti	0.2-2.0	57	16	80.3
Cb	100	4.8	86	4.5
Total	102	62	102	85

The solute (Ti) concentration in the matrix of both alloys has been considerably reduced. The precipitate concentration identifies the phase as one very rich in titanium. These data combined with the previous deduction that the precipitate is an oxide, suggest that the phase is primarily TiO. The broad composition range over which TiO exists (10) is in harmony with the variations in compositions of the precipitate observed in these microprobe examinations. Also, the precipitate

in the 8.5 a/o Ti alloy is itself two phase in some regions. This too is in accord with the reported peritectoid reaction at 925°C in the TiO phase field (10). It is therefore concluded that the precipitate formed in these Nb-Ti alloys is a non-stoichiometric ternary oxide of the form $Ti(Cb)O$.

APR 1965

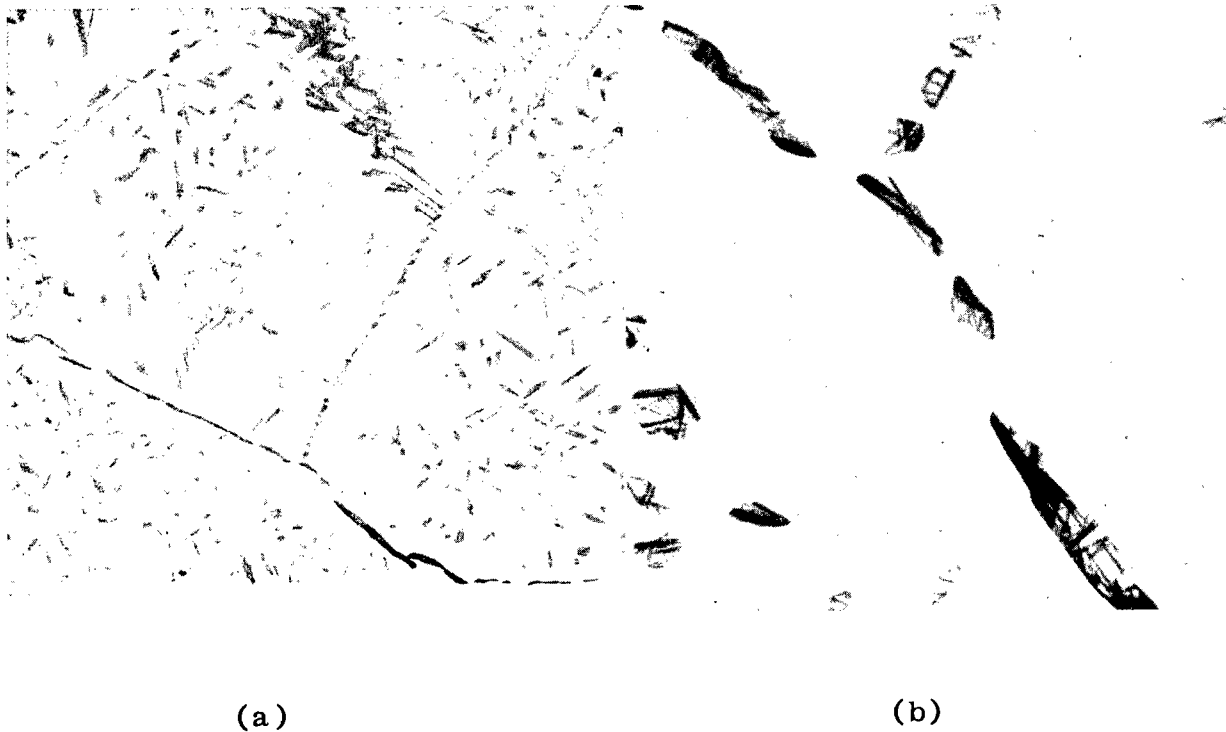
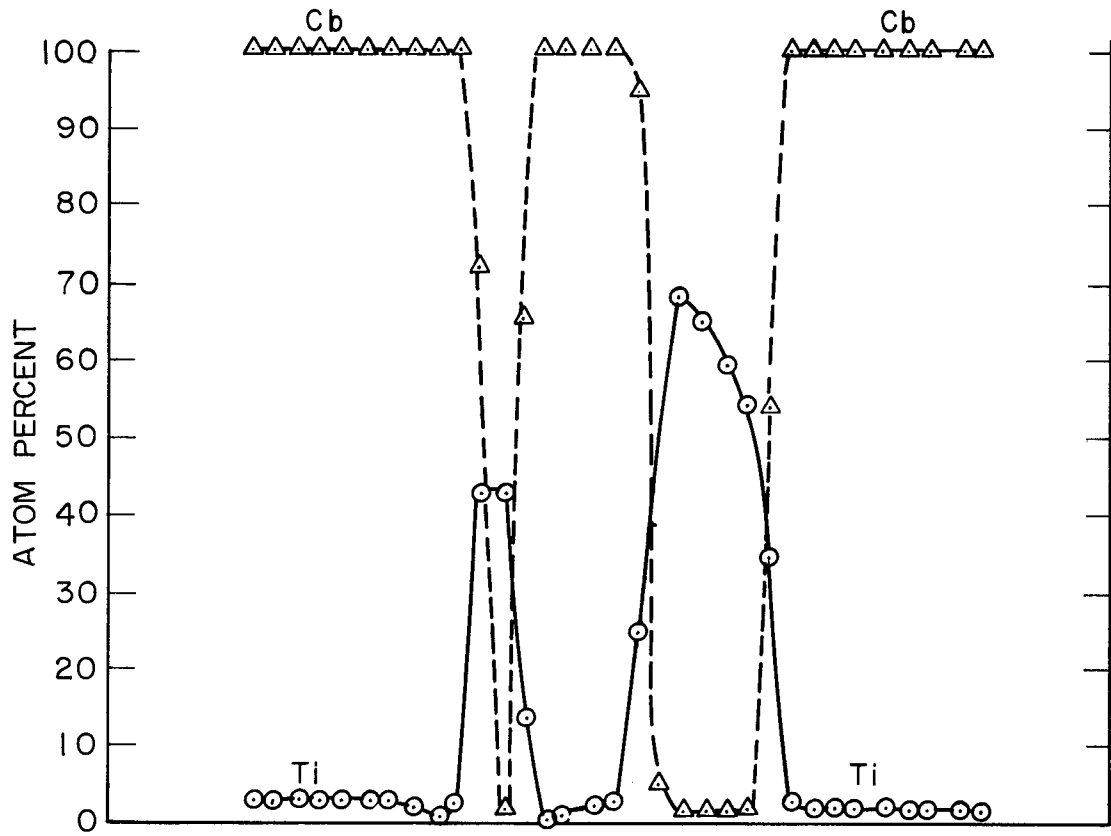
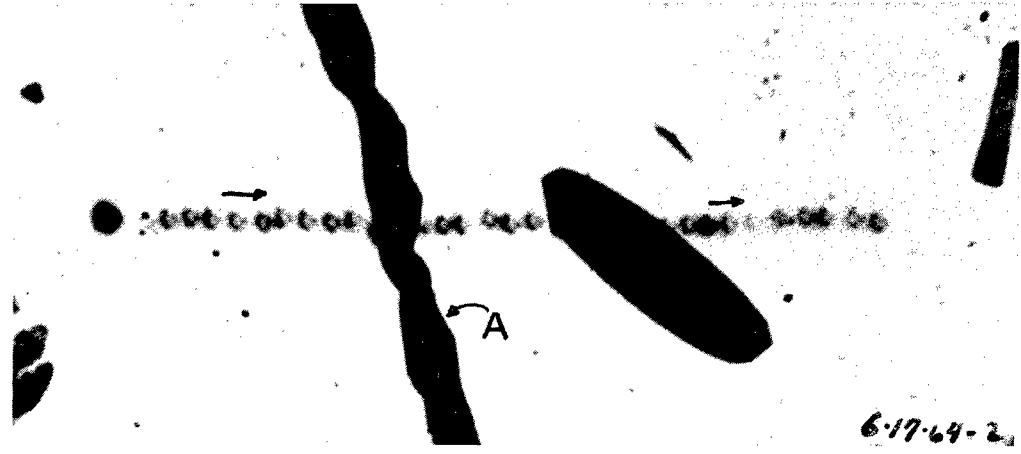


Figure A.4-1 - Photomicrographs showing the precipitate which developed in a Cb 8.5 a/o Ti alloy annealed at 1500°C for 8 hours in vacuum ($<10^{-5}$ torr) in the presence of alumina. The alloy had previously been annealed at 1900°C by electron-beam heating. Unetched. (a) X250, (b) X1500.

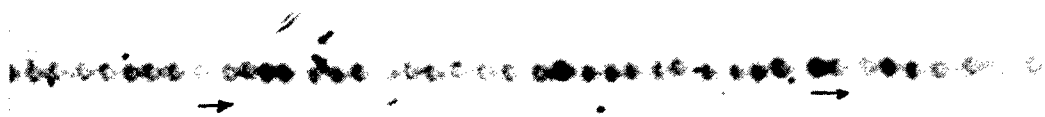
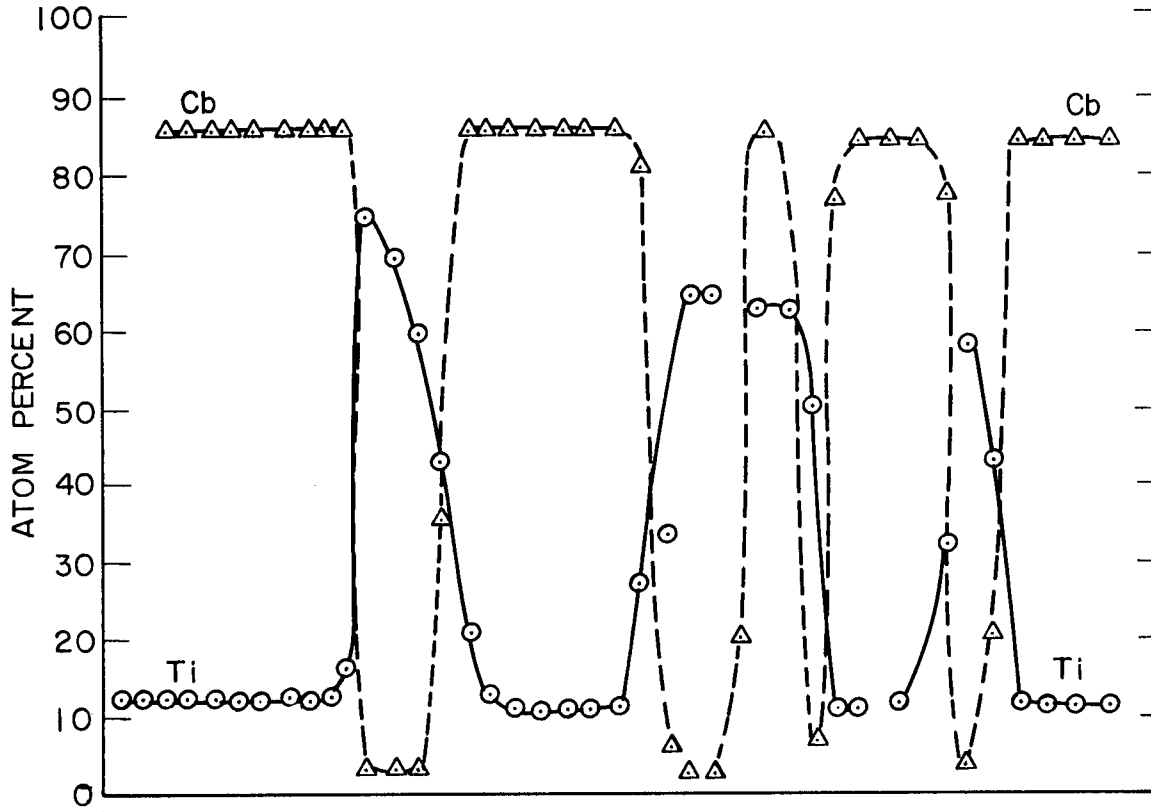


UNCLASSIFIED



6-17-69-2

Figure A.4-2 - Composition as measured by electron microprobe analysis of matrix and precipitate in an alloy of nominally Cb-8.3 a/o Ti. The precipitate at A is at a grain boundary. The precipitate formed in a previously single phase alloy during an anneal in vacuum (10^{-5} torr) at 1500°C for 888 hours in a furnace containing a hot alumina core. Distance between spots is nominally 2.5 microns. Arrows indicate direction of beam travel. Magnification is about 1500X.



6-17-64-4

Figure A.4-3 - Same as Figure A.4-2 except nominal composition is Cb-35 a/o Ti.

REFERENCES

1. Adolf Fick, "Uber Diffusion", POGG ANN 94 (1855) 59.
2. J. Crank, The Mathematics of Diffusion, Clarendon Press, Oxford, 1956.
3. L. S. Darken, "Formal Basis for Diffusion Theory", Atom Movements, ASM, Cleveland, 1951.
4. G. S. Hartley, Diffusion and Swelling of High Polymers, III", Trans Faraday Society 45 (1949) 820.
5. J. E. Reynolds, B. L. Averbach and Morris Cohen, "Self-Diffusion and Interdiffusion in Gold-Nickel Alloys", Acta Met 5 (1959) 29.
6. C. Matano, "On the Relation Between the Diffusion Coefficients and Concentration of Solid Metals (The Nickel-Copper System)", Japanese Journal of Physics, Transactions 8 (1933) 109.
7. C. S. Hartley and J. E. Steedly, Jr., "Diffusion in the Cu-Pt System", Diffusion II, New York Meeting, AIME, February 19, 1964. For abstract, see J. Metals 16 (1964) 107.
8. Ibid, private communication, 1 July 1964.
9. H. H. Woodbury, "Diffusion of Cd in CdS", Phys. Rev. 134 (1964) 492, footnote 12.
10. Max Hanson, Constitution of Binary Alloys, 2nd Edition McGraw-Hill, New York, 1958.
11. A. R. G. Brown, D. Clark, J. Eastabrook and K. S. Jepson, "The Titanium-Niobium System", Nature 201 (1964) 914.
12. R. A. Wolfe and H. W. Paxton, "Diffusion in b.c.c. Alloys", a report from Carnegie Institute of Technology to the Office of Naval Research, March 1, 1964. Also, R. A. Wolf, doctoral thesis, Carnegie Institute of Technology, 1964.
13. F. Seitz, "On the Theory of Vacancy Diffusion in Alloys", Phys. Rev. 74 (1948) 1513.

14. G. Grube and A. Jedele, "Die Diffusion der Metalle in Festen Zustand", Zeitz Fur Electro Chemie 38 (1932) 799.
15. W. A. Johnson, "Diffusion Experiments on a Gold-Silver Alloy by Chemical and Radioactive Tracer Methods", Trans. AIME 147 (1942) 331.
16. J. R. Cost and C. A. Wert, "Gas Metal Equilibrium and the Niobium-Nitrogen Solid Solution", University of Illinois, January 15, 1962, AF-OSR 2067.
17. L. S. Birks and E. J. Brooks, Rev. of Sci, Instr. 28 (1957) 9.
18. L.C.C. Da Silva and R. F. Mehl, "Interface and Marker Movements in Diffusion in Solid Solutions of Metals", J. Metals 3 (1951) 155.
19. W. Seith and T. Heumann, Diffusion of Metals, Exchange Reactions, Chapter 9, a translation by U. S. Joint Publication Research Service, New York of: Diffusion in Metallen: Platzwech-selreactionen, Wolfgang Seith and Theodore Heumann. Springer-Verlag, Berlin (1955).
20. A. S. Winkelman, C. S. Hartley and J. E. Steedly, Jr. "Diffusion in the Cb-Ti and Cb-Mo Systems", High Temperature Materials and Measurements, New York Meeting, AIME, February 20, 1964. For abstract see J. Metals 16 (1964) 118. Also same as reference 8.
21. R. F. Peart, D. Graham and D. H. Tomlin, "Tracer Diffusion in Niobium and Molybdenum", Acta Met 10 (1962) 519.
22. R. Resnick, L. S. Castleman and L. Seigle, "The Self-Diffusion in Niobium-III", USAEC Report SEP-252 (1959). Also, Trans Met Soc AIME 218 (1960) 307.
23. L. S. Birks, Electron Probe Microanalysis, Chapter 8, Interscience Publishers, New York, 1963.
24. R. A. Seebold and L. S. Birks, in private discussion with the author concerning experimental measurement of data such as that referred to in Table 10-1, p.162 of reference 23.
25. J. E. Steedly, private communication of results which will be presented to a "Conference on Diffusion in b.c.c. Materials" sponsored by the Oak Ridge National Laboratory Chapter, American Society for Metals, Gatlinburg, Tenn., September 15-18, 1964.

26. Seith and Heumann, op. cit., Chapter 6.
27. G. B. Gibbs, D. Graham, and D. H. Tomlin, "Diffusion in Titanium and Titanium-Niobium Alloys", Phil Mag 8, Ser. 8, #92 (1963) 1269.
28. J. J. Federer and T. S. Lundy, "Diffusion of Zr⁹⁵ and Cb⁹⁵ in b.c.c. Zirconium", Trans. Met. Soc. AIME 227 (1963) 592.
29. P. G. Shewmon, Diffusion in Solids, Chapter 6, McGraw-Hill, New York, 1963.
30. Robert L. Andelin, "Self Diffusion in Single-Crystal Tungsten and Diffusion of Rhenium Tracer in Single-Crystal Tungsten", Los Alamos Scientific Laboratory report LA 2880, March 1963.
31. L. Boltzmann, "Zur Integration der Diffusionsgleichung bei variabeln Diffusion Coefficienten", Wien. Ann., 53 (1894) 959.

DOCUMENT CONTROL DATA - R&D		
<i>(Security classification of title, body of abstract and indexing annotation must be entered when the overall report is classified)</i>		
1. ORIGINATING ACTIVITY <i>(Corporate author)</i> U.S. Naval Research Laboratory Washington, D.C. 20390		2a. REPORT SECURITY CLASSIFICATION Unclassified
		2b. GROUP
3. REPORT TITLE DIFFUSION IN COLUMBIUM RICH COLUMBIUM-TITANIUM ALLOYS WITH CONSIDERATION OF THE POSSIBILITY THAT THE DIFFUSION COEFFICIENT IS TIME DEPENDENT		
4. DESCRIPTIVE NOTES <i>(Type of report and inclusive dates)</i> A final report on one phase of the problem.		
5. AUTHOR(S) <i>(Last name, first name, initial)</i> Reuther, Theodore C., Jr.		
6. REPORT DATE December 14, 1964	7a. TOTAL NO. OF PAGES 176	7b. NO. OF REFS 31
8a. CONTRACT OR GRANT NO. NRL Problem M01-09	9a. ORIGINATOR'S REPORT NUMBER(S) NRL Report 6221	
b. PROJECT NO. RR 007-01-46-5407		
c.	9b. OTHER REPORT NO(S) <i>(Any other numbers that may be assigned this report)</i>	
d.		
10. AVAILABILITY/LIMITATION NOTICES Unlimited availability		
11. SUPPLEMENTARY NOTES	12. SPONSORING MILITARY ACTIVITY Dept. of the Navy (Office of Naval Research)	
13. ABSTRACT Interdiffusion has been studied in Cb vs. Cb 8.5 atom percent Ti and Cb vs. Cb 35 a/o Ti couples at temperatures of 1300° to 2000°C and for times of 0.1 to 1000 hours. The electron microprobe has been used to obtain the penetration curves. Marker displacement toward and the development of porosity within the alloy at 1800° and 2000°C demonstrate that a vacancy mechanism is operative in this b.c.c. alloy system. Porosity was also observed at 1500°C. At 1500°C for anneal times extending from 10 to 1000 hours for the more dilute alloy and from 10 to 120 hours for the 35 a/o Ti alloy, the interdiffusion coefficient D computed by the Boltzmann-Matano analysis is determined to be independent of time. The arrhenius plot for results extrapolated to 100 a/o Cb is a straight line and yields an activation energy of 110 k cal/g-atom. However, as composition is increased to 30 a/o Ti, an increase in the concentration dependent of D is observed with increasing temperature. This is manifest by curvature of the log D vs. 1/T plots with increasing titanium content.		

CLASSIFICATION

14. KEY WORDS	LINK A		LINK B		LINK C	
	ROLE	WT	ROLE	WT	ROLE	WT
Columbium-Titanium alloys Columbium Alloy Diffusion Diffusion coefficient Electron microprobe Porosity						

INSTRUCTIONS

1. **ORIGINATING ACTIVITY:** Enter the name and address of the contractor, subcontractor, grantee, Department of Defense activity or other organization (*corporate author*) issuing the report.

2a. **REPORT SECURITY CLASSIFICATION:** Enter the overall security classification of the report. Indicate whether "Restricted Data" is included. Marking is to be in accordance with appropriate security regulations.

2b. **GROUP:** Automatic downgrading is specified in DoD Directive 5200.10 and Armed Forces Industrial Manual. Enter the group number. Also, when applicable, show that optional markings have been used for Group 3 and Group 4 as authorized.

3. **REPORT TITLE:** Enter the complete report title in all capital letters. Titles in all cases should be unclassified. If a meaningful title cannot be selected without classification, show title classification in all capitals in parenthesis immediately following the title.

4. **DESCRIPTIVE NOTES:** If appropriate, enter the type of report, e.g., interim, progress, summary, annual, or final. Give the inclusive dates when a specific reporting period is covered.

5. **AUTHOR(S):** Enter the name(s) of author(s) as shown on or in the report. Enter last name, first name, middle initial. If military, show rank and branch of service. The name of the principal author is an absolute minimum requirement.

6. **REPORT DATE:** Enter the date of the report as day, month, year; or month, year. If more than one date appears on the report, use date of publication.

7a. **TOTAL NUMBER OF PAGES:** The total page count should follow normal pagination procedures, i.e., enter the number of pages containing information.

7b. **NUMBER OF REFERENCES:** Enter the total number of references cited in the report.

8a. **CONTRACT OR GRANT NUMBER:** If appropriate, enter the applicable number of the contract or grant under which the report was written.

8b, 8c, & 8d. **PROJECT NUMBER:** Enter the appropriate military department identification, such as project number, subproject number, system numbers, task number, etc.

9a. **ORIGINATOR'S REPORT NUMBER(S):** Enter the official report number by which the document will be identified and controlled by the originating activity. This number must be unique to this report.

9b. **OTHER REPORT NUMBER(S):** If the report has been assigned any other report numbers (*either by the originator or by the sponsor*), also enter this number(s).

10. **AVAILABILITY/LIMITATION NOTICES:** Enter any limitations on further dissemination of the report, other than those

imposed by security classification, using standard statements such as:

- (1) "Qualified requesters may obtain copies of this report from DDC "
- (2) "Foreign announcement and dissemination of this report by DDC is not authorized."
- (3) "U. S. Government agencies may obtain copies of this report directly from DDC. Other qualified DDC users shall request through _____."
- (4) "U. S. military agencies may obtain copies of this report directly from DDC. Other qualified users shall request through _____."
- (5) "All distribution of this report is controlled. Qualified DDC users shall request through _____."

If the report has been furnished to the Office of Technical Services, Department of Commerce, for sale to the public, indicate this fact and enter the price, if known.

11. **SUPPLEMENTARY NOTES:** Use for additional explanatory notes.
12. **SPONSORING MILITARY ACTIVITY:** Enter the name of the departmental project office or laboratory sponsoring (*paying for*) the research and development. Include address.
13. **ABSTRACT:** Enter an abstract giving a brief and factual summary of the document indicative of the report, even though it may also appear elsewhere in the body of the technical report. If additional space is required, a continuation sheet shall be attached.

It is highly desirable that the abstract of classified reports be unclassified. Each paragraph of the abstract shall end with an indication of the military security classification of the information in the paragraph, represented as (TS), (S), (C), or (U).

There is no limitation on the length of the abstract. However, the suggested length is from 150 to 225 words.

14. **KEY WORDS:** Key words are technically meaningful terms or short phrases that characterize a report and may be used as index entries for cataloging the report. Key words must be selected so that no security classification is required. Identifiers, such as equipment model designation, trade name, military project code name, geographic location, may be used as key words but will be followed by an indication of technical context. The assignment of links, roles, and weights is optional.